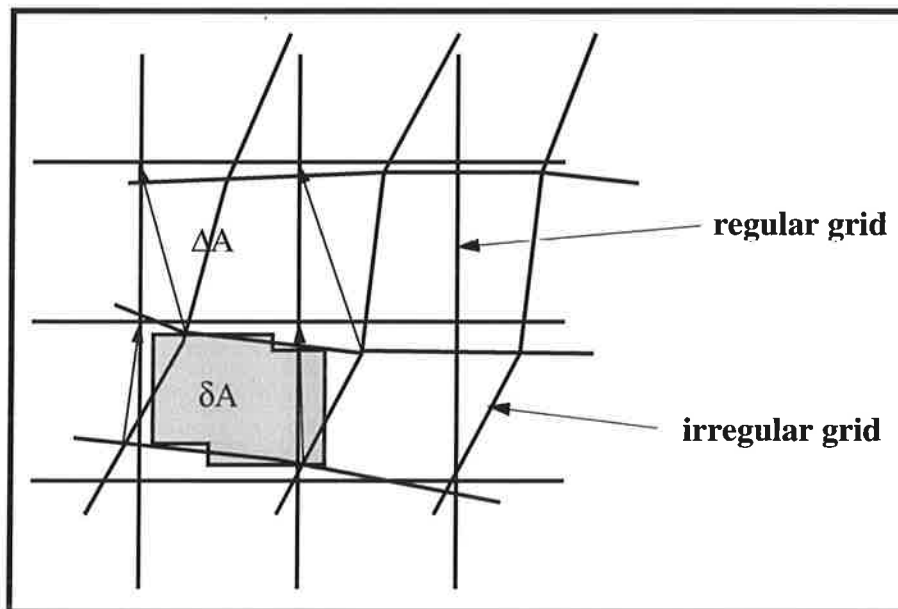




Max-Planck-Institut für Meteorologie

REPORT No. 265



MPI WORKSHOP
ON
CONSERVATIVE TRANSPORT SCHEMES
2-3 JUNE 1997

by
Bennert Machenhauer et al.

HAMBURG, July 1998

AUTHORS:

Bennert Machenhauer
Johan Feichter
Andreas Chlond
Markus Oik

Max-Planck-Institut für Meteorologie
Hamburg
Germany

Andreas Bott

Johannes Gutenberg-Universität
Mainz
Germany

Elias Valur Holm

ECMWF
Reading
U.K.

B.P. Leonard

The University of Akron
Akron, Ohio
USA

Shain-Jiann Lin

University of Maryland and Baltimore Country
Maryland, Virginia
USA

Phil Rasch

National Center for Atmospheric Research
Boulder, Colorado
USA

Sabine Brinkop
Robert Sausen

DLR
Oberpfaffenhofen
Germany

P. Braesicke
U. Langematz

Institut für Meteorologie
FU Berlin
Germany

MAX-PLANCK-INSTITUT
FÜR METEOROLOGIE
BUNDESSTRASSE 55
D-20146 HAMBURG
F.R. GERMANY

Tel.: +49 - (0)40 - 411 73 - 0
Telefax: +49 - (0)40 - 411 73 - 298
E-Mail: <name>@dkrz.de

CONTENTS

Background and Outcome of the Workshop..... 3

Extended Abstracts of Papers presented:

Johan Feichter, MPI, Hamburg

Performance of the NCAR semi-Lagrangian Transport Scheme in the MPI GCM.....5

Andreas Bott, Johannes Gutenberg-Universitaet Mainz:

The Area-preserving Flux-form Advection Algorithm..... 10

Andreas Chlond, MPI, Hamburg:

Locally Modified Version of Bott's Advection Scheme.....26

Elias Valur Holm, ECMWF, Reading:

A geometric approach to multidimensional advection:

improving efficiency using economization of power series.....37

B. P. Leonard, The University of Akron:

Bounded heigher-order schemes for convection-dominated transport.....48

Shain-Jiann Lin, Joint Center for Earch System Technology,

University of Maryland and Baltimore County and NASA-GSFC:

The Flux-Form Semi-Lagrangian Transport Scheme and its Applications

in Atmospheric Models..... .54

Phil Rasch, National Center for Atmospheric Research, Boulder:

Recent Developments in Transport Methods at NCAR.....65

Bennert Machenhauer and Markus Olk, MPI, Hamburg:

Design of a Semi-Implicit Cell-Integrated Semi-Lagrangian Model.....76

Sabine Brinkop and Robert Sausen:., DLR, Oberpfaffenhofen:

A Finite Difference Approximation for Convective Transports which maintains
Positive Tracer Concentrations.....86

P. Braesicke and U. Langematz, Institut fuer Meteorologie, FU Berlin:

Coupling of a Semi Lagrangian Transport Scheme to the Berlin TSM GCM.....93

Background and Outcome of the Workshop

A high accuracy of the numerical schemes used for advection of atmospheric constituents in climate models is important for reliable long term simulations. This is especially true for atmospheric variables with strong horizontal and/or vertical gradients. The horizontal spectral representation and advection used in previous versions of the ECHAM model for all the variables had serious problems for water vapor, liquid cloud water and short-lived chemical constituents which have sharp horizontal gradients. Large over- and undershoots could occur. The problem is most noticeable as regions of negative mixing ratios, but equally serious are the overshoots. Therefore, in the newest level 4 version of the ECHAM model it was decided to use a grid point representation and a three-dimensional shape-preserving semi-Lagrangian advection scheme (the Rasch-Williamson scheme) for such variables, but to keep the spectral representation and Eulerian advection for the remaining dynamical variables. The Rasch-Williamson advection scheme develops no over- or undershoots but has the draw-back, as all traditional semi-Lagrangian schemes, that it do not conserve the mass of the constituents advected (in the case of no sources and sinks). Therefore, a so called mass-fixer were introduce which keeps the mass before and after an advection time step constant for each constituent. However, eventually serious problems were experienced with tracers which show strong vertical concentration gradients, in particular near the surface or near the top of the model domain, but also in connection with the tropopause. In such cases the mass corrections needed was found to be large and could even be of the same order of magnitude as the mass itself. This could result in negative mixing ratios, which then when set to zero would produced an increase of total mass (Feichter, 1998 this volume). It has been realized that these problems were connected with difficulties in the formulation of consistent boundary conditions and an excessive inherent vertical diffusion in the scheme.

These problems and the desire to find remedies to alleviate or cure them were the reason for arranging the present workshop. Obviously, of interest were alternative schemes that in addition to being accurate and efficient were also conservative, i.e. conserved the mass of the constituents advected. Two such classes of methods have been developed and were represented at the workshop.

The first class is based on the use of the continuity equation on the flux form and consists of determining the fluxes through the sides of the grid cells in such a way that the mass is conserved. Each time step the total mass is redistributed in the grid cells using consistent fluxes in neighbor cells whereby the mass is automatically conserved. Several of the workshop participants has taken part in the recent development of this class of schemes and in the present proceedings is presented a three-dimensional version developed for the sphere as an alternative to the Rasch-Williamson scheme (Rasch, 1998 present report). It has recently been implemented in a version of the ECHAM4 model and is presently being tested. The draw-backs of the Rasch-Williamson scheme mentioned above seems largely to be removed with only a minor additional cost in computation time. Remaining error sources are, however, that in ECHAM4 the dynamical variables and especially the total air mass (or rather the logarithm of the surface pressure) are still represented and advected spectrally which is inconsistent with the application of the new flux-form grid point scheme used for the other variables. A mass fixer is still applied which

keeps the logarithm of the surface pressure constant implying that in effect the flux-form advected constituents are still mass fixed.

A second class of conservative transport schemes are the so called Cell-Integrated Semi-Lagrangian (CISL) schemes represented at the workshop by Machenhauer and Oik (1988, this report). In this class of schemes the mass advected into a grid cell is determined by an integration of mass over an upstream volume determined by backward constructed trajectories from the corners of the grid cell. Thus, each time step the total mass is just redistributed and therefore conserved. The Machenhauer-Oik version has been designed to cover also the dynamical variables, thus ensuring consistency and additional exact conservation of total air mass and other invariants as entropy, angular momentum and potential vorticity. Conceptually may the CISL schemes be considered similar to the mass-flux schemes. Only the fluxes through the cell walls are calculated differently. Both classes of schemes allow large time steps which, however, can be realized only when all model variables are advected by the same scheme and when the gravity wave terms in the equations are extrapolated in time in a stable way. So far has such a large time step CISL-system with a semi-implicit time stepping been designed and tested only for a one-dimensional shallow water model. On the globe has the CISL scheme been implemented and tested only for two-dimensional advection of a scalar. This seems however a major step toward a conservative three-dimensional cell-integrated fully semi-Lagrangian semi-implicit global climate model (Machenhauer and Oik, 1988, this report).

Such a development was discussed and recommended at the workshop. Generally were the opinion at the workshop that climate centers should devote more efforts in the development of climate models. Special emphasis should be on properties as conservation which are of particular importance in the long term integrations performed in climate modeling. Of course, also accuracy and efficiency are important in climate modeling. Different schemes should be tested and compared using the standard tests set up in Williamson et al. (1992)¹ for advection and shallow water equation dynamics on the sphere. The present efforts under WGNE auspices on the development of standard dynamical core tests needed to test and compare the basic dynamical cores of full GCMs were encouraged. Such common test cases will be very useful, especially if the special needs of testing of climate models are taken into account.

1. Williamson, D. L., J. B. Drake, J. J. Hack, and P. N. Swarztrauber. *Journal of Computational Physics*, 102 (1992), 211-224.

Performance of the NCAR Semi-Lagrangian Transport Scheme in the MPI GCM, ECHAM

Johann Feichter

Max-Planck-Institut for Meteorology, Hamburg

Atmospheric chemical constituents exert an influence on climate directly through their radiative properties, and indirectly through their impact on other radiatively active gases or through their ability to form aerosol particles. In order to estimate possible climate impact by increasing man-made pollutant concentrations in the atmosphere, the global atmospheric general circulation model ECHAM has been adapted for the transport of chemical constituents (ECHAM-CTM). Chemical species of importance have atmospheric residence times in the order of weeks, like ozone in the upper troposphere, or in the order of days, like nitrogen and sulfur species, or in the order of hours, like cloud water. Simulation of the spatial and temporal distribution of tracers which show strong horizontal and vertical gradients requires accurate numerical advection.

The spectral approach as used in the ECHAM model to transport the dynamical variables has serious deficiencies in representing the advection of water vapour, liquid water and short-lived tracers. Grid-point fields reconstructed from the spectral representation of a positive definite grid-point field are truncated and contain areas of over- and undershoot. The problem is most noticeable as regions of negative mixing ratios. Less noticeable, but equally serious, are regions of overshoot. Therefore a shape-preserving semi-Lagrangian advection scheme (Williamson and Rasch, 1989; Rasch and Williamson, 1990; Williamson, 1990) has been implemented in ECHAM for the transport of water vapour, liquid water and tracers. However, a representation of some prognostic variables like temperature, pressure and wind, in the spectral space, and of some variables in the grid space introduces inconsistencies. For example we have to transform the spectral pressure fields to grid-point fields in order to calculate the chemical species mass budgets. Truncation errors due to this transformation make it impossible to fix the mass exactly. But these errors are relatively small and uncertainties in the global air mass are in the order of 0.01 %.

Semi-Lagrangian methods have the benefit of high accuracy and relaxed stability criteria which allow larger time steps, but they are generally not mass-conserving. To overcome this drawback Williamson and Rasch introduced a mass fixer which keeps the mass before and after the advection constant. This mass fixer works well for small errors in the mass conservation, however, we experienced serious problems simulating tracers which shows strong vertical concentration gradients near to the surface or near to the top of the model domain. In these particular cases, the mass increased significantly and the application of the mass fixer produced unrealistic tracer distributions. When the mass correction is of the same order as the global mass itself the mass fixer produces sometimes negative mixing-ratios. These negative mixing-ratios are set to zero producing again an increase of mass.

To demonstrate the properties of the mass fixer we did two experiments. Both experiments were initialised by assuming a uniform initial mixing ratio in single model layer and a zero mixing ratio everywhere else, the first at the surface and the second at the 70 hPa level. No sources and sinks have been assumed. In Figure 1 we show the temporal evolution of the global mean tracer mass of these two experiments. The upper graph shows the increase of tracer mass if we do not apply the mass fixer. In particular the species initialised at the surface shows a strong increase of mass of about 100% after 15 days of integration. If we apply the mass fixer the increase of mass

amounts only to 0.6% after two month of integration which is acceptable. But it is questionable whether we can trust tracer distributions in cases when the mass flux tendencies are in the same order as the advective tendencies.

In order to study the sensitivity of tracer distribution against changes in the advection scheme we did two experiments, one with advective transport of cloud water and one without this transport. We choose cloud water because this species has certainly the greatest impact on the climate system. These experiments have been performed with ECHAM4-T30 applying a new cloud microphysical scheme from Lohmann and Roeckner (1996). According to Roeckner (pers. comm.) transport accounts only to about 10% of the cloud water tendency. In spite of this small contribution of transport to the cloud water tendencies the effect of neglecting the advective transport is surprisingly high. In Table 1 we present the the annual and global mean cloud forcings, the cloud cover and the liquid water and ice water content of clouds of both experiments. Note, that the cloud microphysics has been tuned based on simulations neglecting advective transport of cloud water. Including the advective transport enhances particularly the short- and long-wave cloud forcing. These forcings are not surprisingly quite sensitive to changes in cloud top heights and temperatures. This emphasizes the importance of an accurate advection scheme, in particular for a realistic simulation of cloud processes.

Global averages	No advective transport	With advective transport
SCF [W/m^2]	-47	-55
LCF [W/m^2]	30	37.7
CC	62	74.6
LWP [g/m^2]	68	70.2
IWP [g/m^2]	26	29.5

Table 1. Annual and global mean short-wave and long-wave cloud forcing, cloud cover and cloud liquid and ice water content (Lohmann, pers. comm.).

The performance of the model in terms of real tracer simulations has to be tested regarding the whole ensemble of transport processes. Hence we did tracer experiments to test the CTM with regard to the transport of gases and aerosols within the troposphere (CFCl_3 , Radon-222), stratosphere to troposphere exchange (C-14 , SF_6) and wet scavenging of aerosol particles (Lead-210, Beryllium-7). We show in Figure 2 results of a Radon-222 experiment together with observations at Bermuda in the Atlantic Ocean. Radon-222 is a rare gas with natural continental sources and a exponential life-time of 5.5 days. Due to its relatively short life-time it exhibits a strong contrast between continental and remote marine regions. During winter westerlies dominate the weather in Bermuda and Radon concentrations reflect synoptic transport from North America. Observations in Figure 2 represent hourly averages, model results 4-hourly instantaneous mixing ratios during January 1993. The mixing-ratios vary strongly with lowest values less than 100 mBq/SCM, maxima are greater than 2000 mBq/SCM. The agreement between the model results and the observa-

tions is excellent. Even if the calculated and the observed amplitudes show some differences, the arrival time of radon pollution events is captured very well. This emphasizes that the advection scheme works generally quite well. Obviously problems arise with the semi-Lagrangian advection scheme only if very strong vertical gradients occur at the top and the bottom of the model domain.

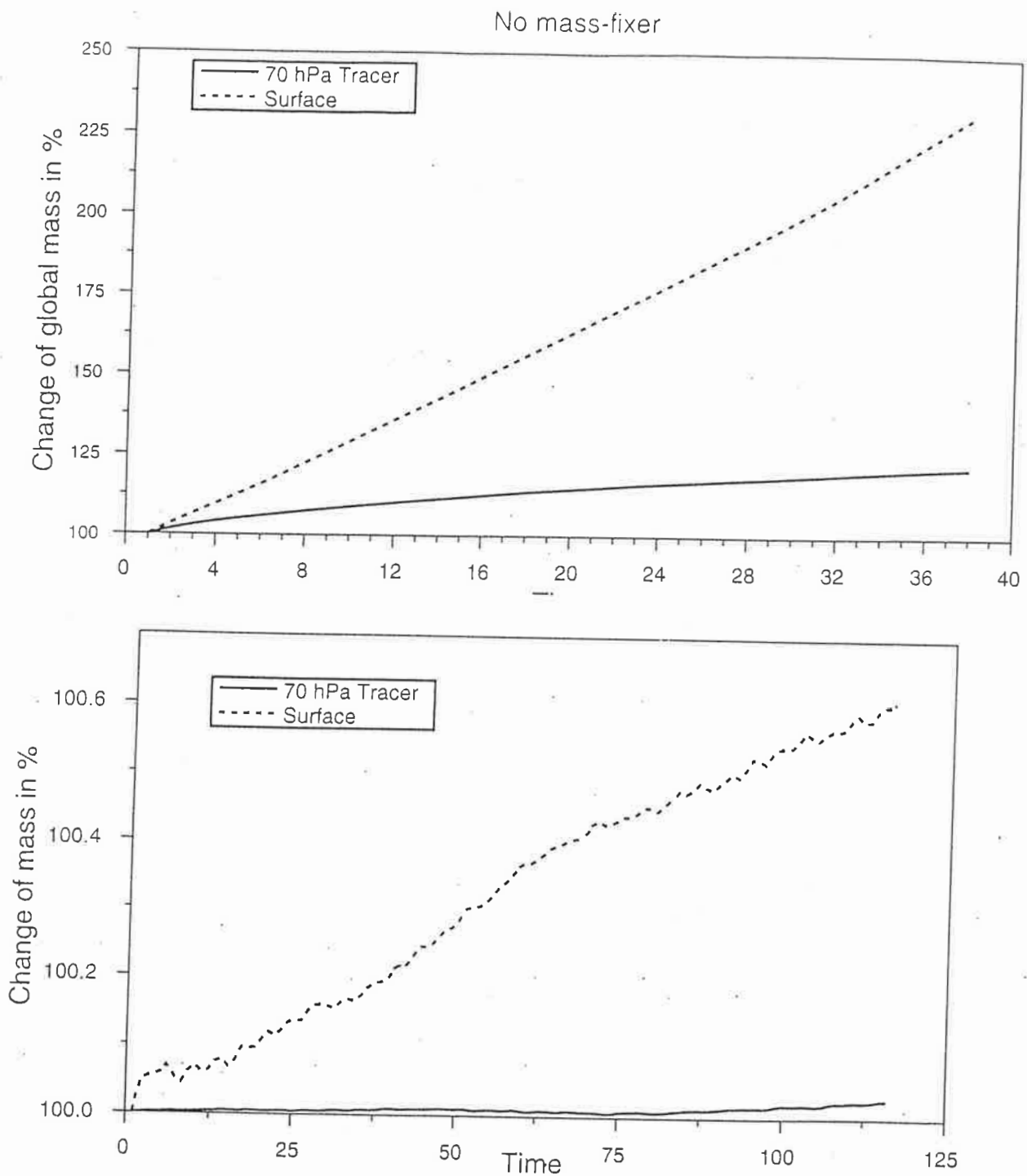


Figure 1. Change in global tracer mass during the model integration. The x-axis gives the number of the 12-hourly output intervals. The upper graph represents results of a simulation neglecting the mass fixer, the lower graph a simulation including the mass fixer.

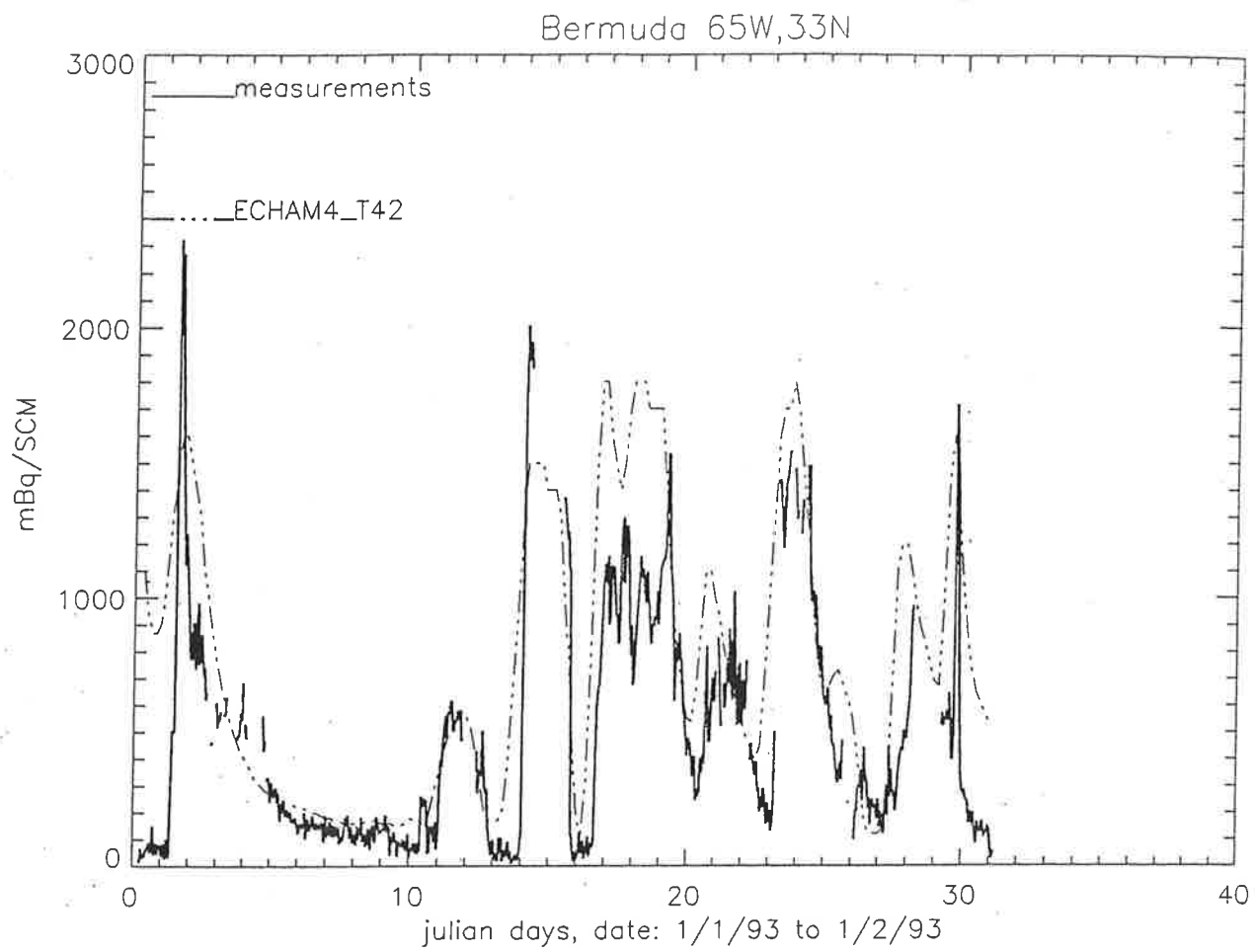


Figure 2. Model simulations and observations of Radon-222 at Bermuda.

The Area-Preserving Flux-Form

Advection Algorithm

Andreas Bott

Institut für Physik der Atmosphäre
Johannes Gutenberg-Universität Mainz

Workshop Hamburg, 2-3 June 1997

THE AREA-PRESERVING FLUX-FORM ADVECTION ALGORITHM

Andreas Bott

Johannes Gutenberg-Universitaet Mainz

D-55099 Mainz, Germany

The area-preserving flux-form advection algorithm (APF) of Bott (1989a,b) is a method for the numerical solution of the scalar transport equation. The main advantages of the method are: 1) Positive definiteness, 2) low numerical diffusion and 3) low computational effort. The scheme is based on the evaluation of the advective fluxes by means of higher order polynomials. Usually 4th order polynomials yield a good compromise between numerical accuracy and efficiency of APF. Positive definiteness of the method is obtained by nonlinear renormalization of the advective fluxes.

In Bott (1992, 1993) APF is extended to monotonicity (MAPF). For this the nonlinear positive definite flux limiters of the original approach are replaced by new monotone flux limiters. The monotone fluxes are derived for one-dimensional constant transport velocities. The deformation occurring in divergent flow fields is accounted for by adding to the monotone advection fluxes a correction term which has been derived from the deformation of the upstream method. The final algorithm is applicable to arbitrary multi-dimensional transport problems. However, due to the use of the time splitting method, MAPF is strictly monotone only in uniform flow fields.

Numerical results of different one- and two-dimensional advection experiments demonstrate that the monotone flux limitation is an attractive alternative to the positive definite algorithm. In MAPF amplitude and phase speed errors are somewhat larger as compared to APF. The computational effort of the monotone version is not much larger than that of the positive definite scheme. Thus, it is concluded that for many applications of atmospheric modeling the monotone area-preserving flux-form advection algorithm is an accurate and numerically efficient method for the solution of the transport equation.

Numerical Solution of the Transport Equation

Problems

- Numerical diffusion
- Positive definiteness
- Computational effort
- Monotonicity

Area-Preserving Flux-Form Advection Algorithm (APF)

(Bott, A., 1989: *Mon. Wea. Rev.*, **117**, 1006–1015)

(Bott, A., 1989: *Mon. Wea. Rev.*, **117**, 2633–2636)

- Low numerical diffusion
- Positive definiteness
- Low computational effort
- No monotonicity

Monotone Area-Preserving Flux-Form Advection Algorithm (MAPF)

(Bott, A., 1992: *Mon. Wea. Rev.*, **120**, 2592–2602)

(Bott, A., 1993: *Mon. Wea. Rev.*, **121**, 2637–2641)

- Low numerical diffusion
- Positive definiteness
- Low computational effort
- Monotonicity

Transport Equation

$$\frac{\partial \psi}{\partial t} = -\nabla \cdot (\mathbf{v}\psi)$$

One-dimensional case with constant grid spacing Δx

$$\frac{\partial \psi}{\partial t} = -\frac{\partial}{\partial x}(u\psi)$$

Positive velocity field

$$u \geq 0$$

Courant number

$$c_{j+1/2}^n = \frac{\Delta t}{\Delta x} u_{j+1/2}^n$$

Courant-Friedrich-Levy (CFL) criterion

$$\left| c_{j+1/2}^n \right| \leq 1$$

Discrete flux form

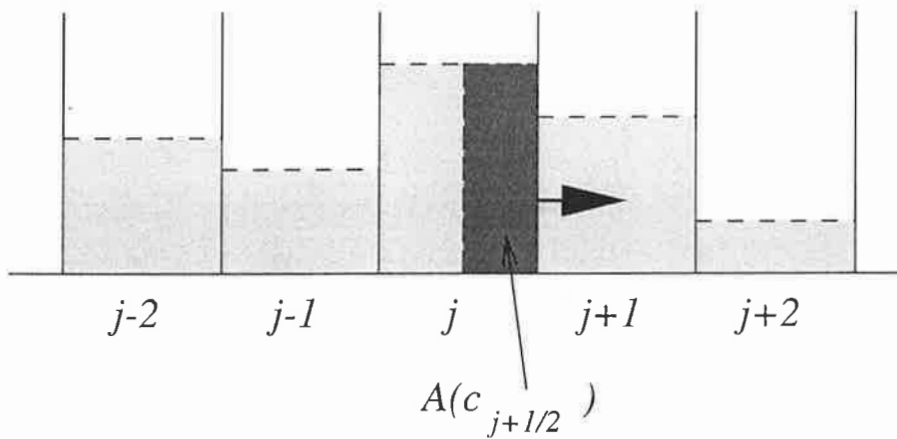
$$\psi_j^{n+1} = \psi_j^n - \frac{\Delta t}{\Delta x} \left(F_{j+1/2}^n - F_{j-1/2}^n \right)$$

Upstream Solution

Advective ψ -flux at $j + 1/2$

$$F_{j+1/2} = \frac{A(c_{j+1/2})}{\Delta t}$$

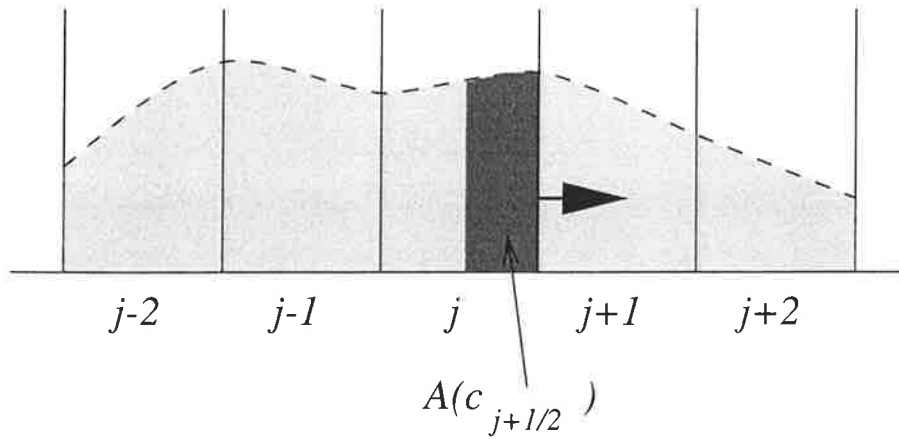
$$A(c_{j+1/2}) = c_{j+1/2} \Delta x \psi_j$$



Constant ψ -distribution in each grid box

- Large numerical diffusion
- Positive definiteness
- Low computational effort
- Monotonicity

Concept of Polynomial Fitting



$$\psi_{j,l}(x') = \sum_{k=0}^l a_{j,k} x'^k$$

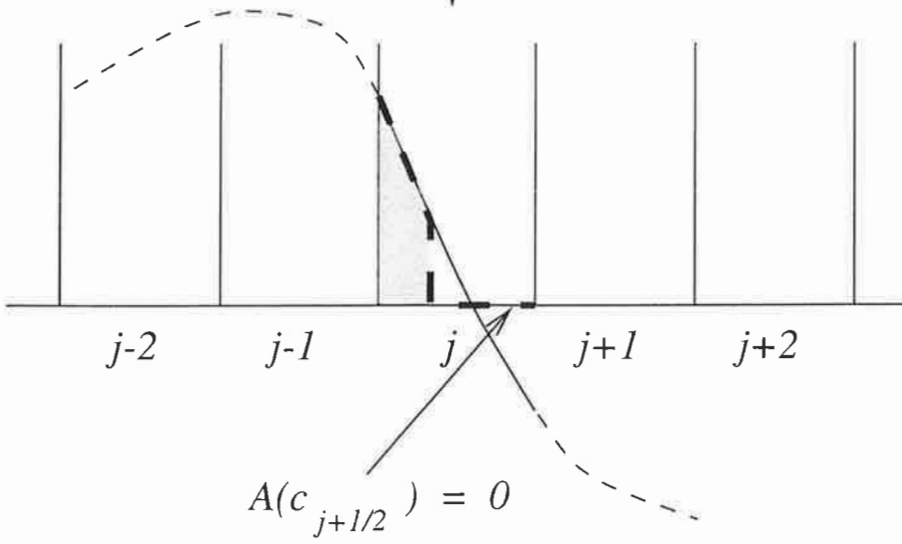
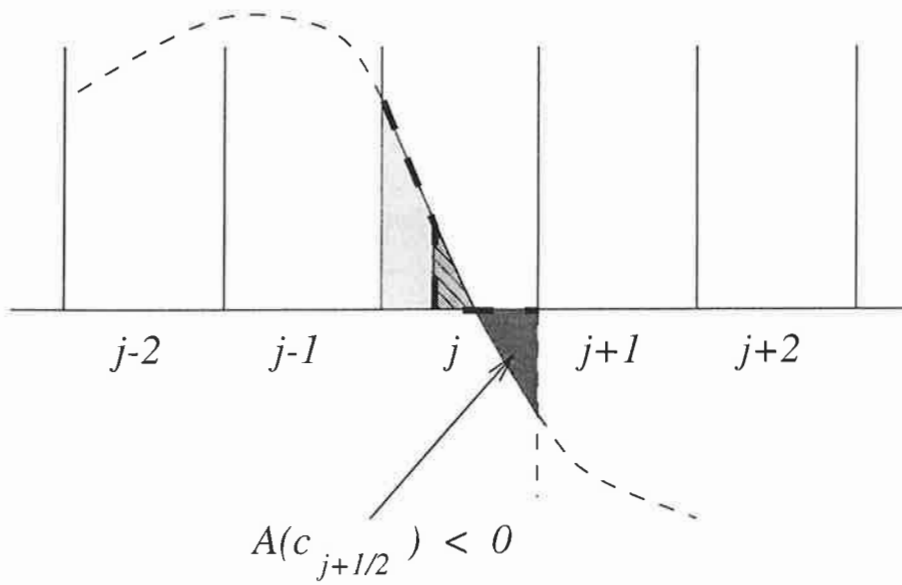
$$A(c_{j+1/2}) = \Delta x I_l(c_{j+1/2})$$

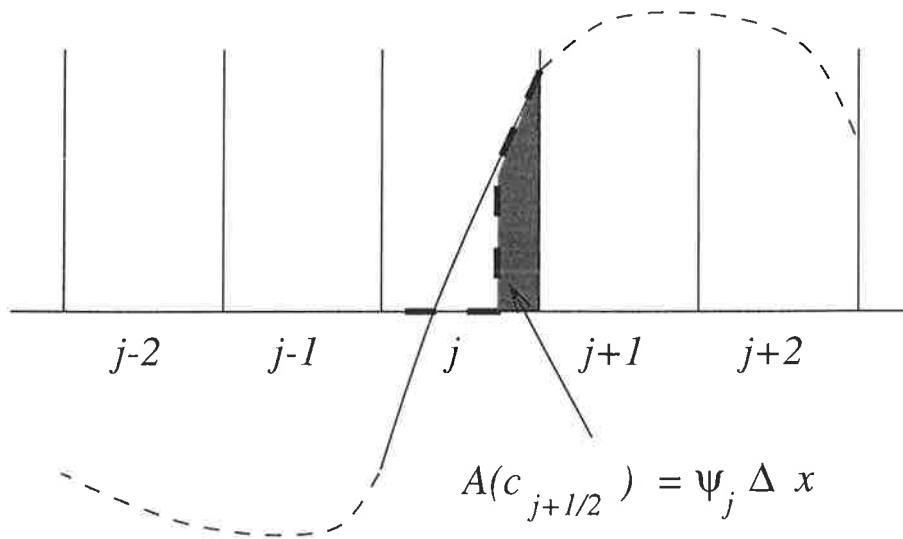
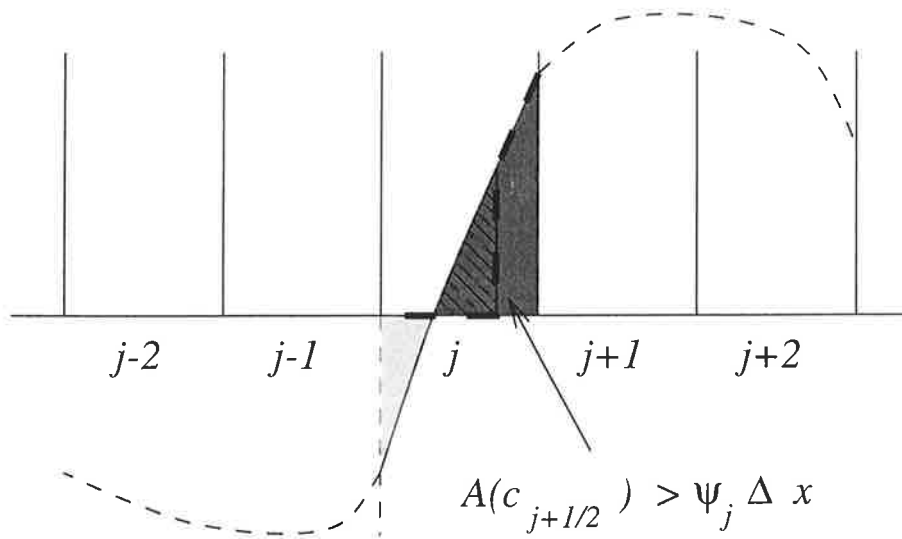
$$I_l(c_{j+1/2}) = \int_{1/2-c_{j+1/2}}^{1/2} \psi_{j,l}(x') dx'$$

Area preserving polynomial fitting

For $c_{j+1/2} = 1 \longrightarrow I_l(c_{j+1/2}) = \psi_j$

Positive Definite Flux Limitation

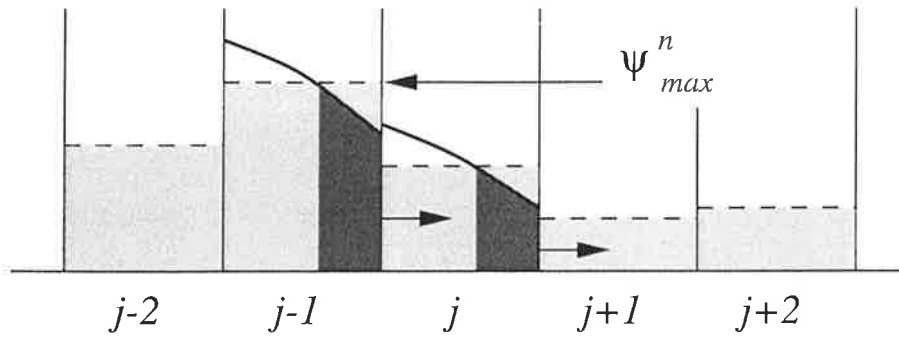




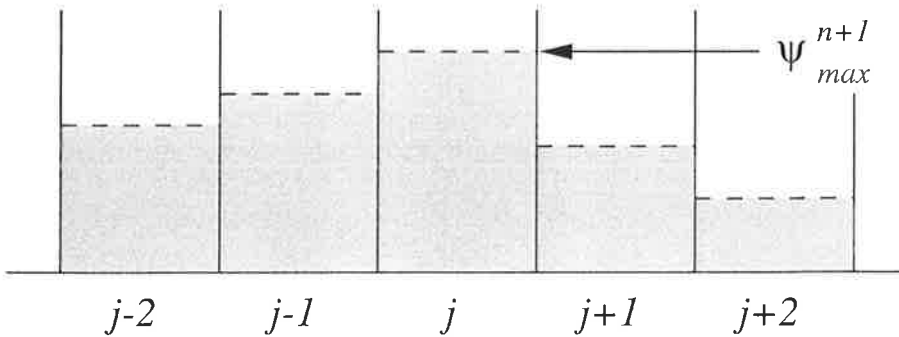
Monotone Flux Limitation

($u = \text{const}$)

Timestep n:



Timestep n+1:



Problems:

$$\psi_{max}^{n+1} > \psi_{max}^n \quad \text{or analogously} \quad \psi_{min}^{n+1} < \psi_{min}^n$$

Monotonicity of the scheme is ensured if:

$$\min(\psi_{j-1}^n, \psi_j^n) \leq \psi_j^{n+1} \leq \max(\psi_{j-1}^n, \psi_j^n) \quad u \geq 0$$

$$\min(\psi_{j+1}^n, \psi_j^n) \leq \psi_j^{n+1} \leq \max(\psi_{j+1}^n, \psi_j^n) \quad u < 0$$

Definitions:

$$F_{j+1/2}^+ = \alpha \int_{1/2-c_j^+}^{1/2} \psi_{j,l}^n(x') dx'$$

$$F_{j-1/2}^- = \alpha \int_{-1/2}^{-1/2+c_{j-1}^-} \psi_{j,l}^n(x') dx'$$

$$\alpha = \Delta x / \Delta t \quad c_j^\pm = \pm(c_{j+1/2}^n \pm |c_{j+1/2}^n|) / 2$$

$$\longrightarrow F_{j+1/2}^+ = 0 \quad \text{if} \quad u \leq 0 \quad F_{j-1/2}^- = 0 \quad \text{if} \quad u \geq 0$$

$$F_{j+1/2} = F_{j+1/2}^+ - F_{j+1/2}^-$$

$$\psi_j^{n+1} = \psi_j^n - \frac{1}{\alpha} \left[F_{j+1/2}^+ - F_{j-1/2}^+ \right] \quad u \geq 0$$

$$\psi_j^{n+1} = \psi_j^n - \frac{1}{\alpha} \left[F_{j-1/2}^- - F_{j+1/2}^- \right] \quad u < 0$$

Monotone Flux Limiters

$$\underline{u \geq 0:}$$

$$\begin{aligned} \alpha [\psi_j^n - \max(\psi_{j-1}^n, \psi_j^n)] + F_{j-1/2}^+ &\leq F_{j+1/2}^+ \\ &\leq \alpha [\psi_j^n - \min(\psi_{j-1}^n, \psi_j^n)] + F_{j-1/2}^+ \end{aligned}$$

$$\underline{u \leq 0:}$$

$$\begin{aligned} \alpha [\psi_j^n - \max(\psi_{j+1}^n, \psi_j^n)] + F_{j+1/2}^- &\leq F_{j-1/2}^- \\ &\leq \alpha [\psi_j^n - \min(\psi_{j+1}^n, \psi_j^n)] + F_{j+1/2}^- \end{aligned}$$

$$0 \leq F_{j+1/2}^+ \leq \alpha \psi_j^n \quad 0 \leq F_{j-1/2}^- \leq \alpha \psi_j^n$$

\implies

No flux in the opposite flow direction	$(F_{j\pm 1/2}^\pm < 0)$
Outflux not larger than total ψ-content	$(F_{j\pm 1/2}^\pm > \alpha \psi_j^n)$

The outgoing monotone fluxes of each gridbox depend on the values of the incoming monotone fluxes.

Procedure:

For positive velocities $F_{j+1/2}^+$ is calculated by starting in grid box $j = 2$ and increasing j up to the right boundary $j = m$ of the numerical grid mesh.

$F_{3/2}^+$ of grid box $j = 1$ is determined from the original positive definite approach of the advection scheme.

For negative velocities the procedure is vice versa, i. e. the calculation of $F_{j-1/2}^-$ starts at $j = m - 1$, and j is decreased to $j = 1$.

The outgoing flux $F_{m-1/2}^-$ of grid box $j = m$ is again taken from APF.

Divergent flow

Upstream solution:

$$\begin{aligned} F_{j+1/2}^+ &= \alpha c_j^+ \psi_j^n \\ &= \alpha \left(c_{j-1}^+ \psi_j^n + D_{j+1/2}^+ \right) \end{aligned}$$

$$\begin{aligned} F_{j-1/2}^- &= \alpha c_{j-1}^- \psi_j^n \\ &= \alpha \left(c_j^- \psi_j^n + D_{j-1/2}^- \right) \end{aligned}$$

Deformation terms:

$$D_{j+1/2}^+ = \psi_j^n (c_j^+ - c_{j-1}^+)$$

$$D_{j-1/2}^- = \psi_j^n (c_{j-1}^- - c_j^-)$$

Procedure:

The upstream fluxes $\alpha c_{j-1}^+ \psi_j^n$ and $\alpha c_j^- \psi_j^n$ are replaced by the corresponding monotone fluxes of the present approach.

The deformation terms are added.

The resulting fluxes are restricted to:

$$0 \leq F_{j+1/2}^+ \leq \alpha \psi_j^n$$

$$0 \leq F_{j-1/2}^- \leq \alpha \psi_j^n$$

Conclusions

Due to the more rigorous flux limiters, MAPF produces somewhat larger phase and amplitude errors than APF.

In applications with moderate spatial gradients of the transport quantities, APF and MAPF yield very good results, because APF produces very little over- and undershooting, and in MAPF the numerical diffusion is not too large.

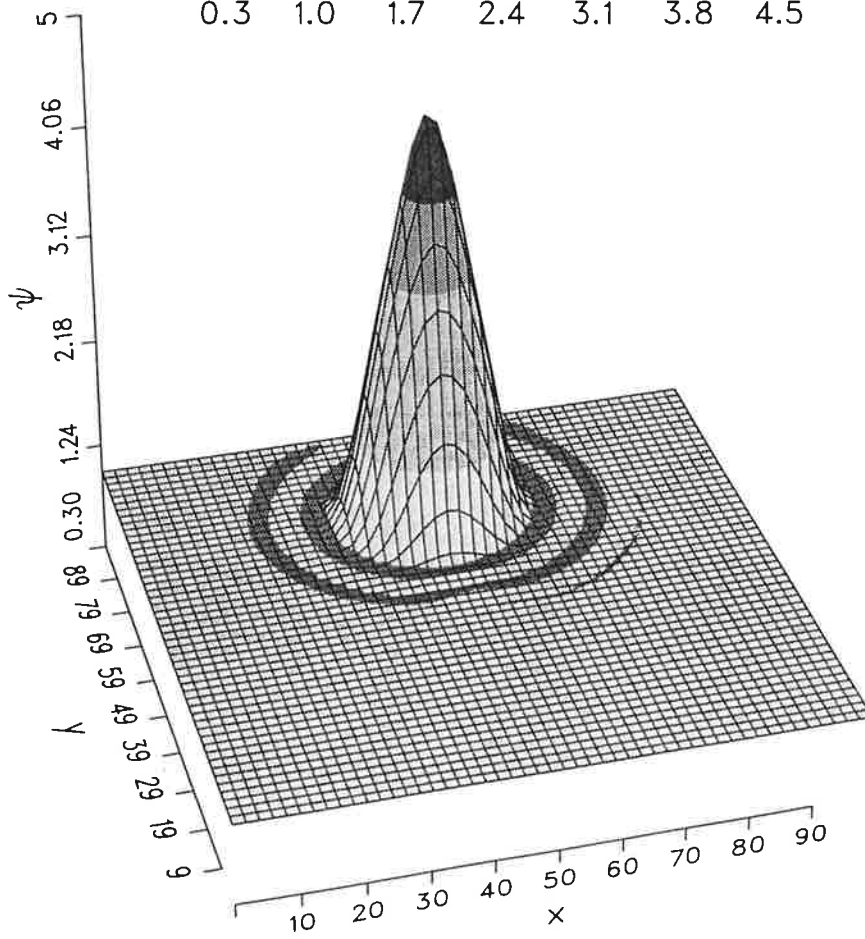
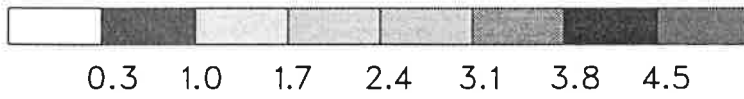
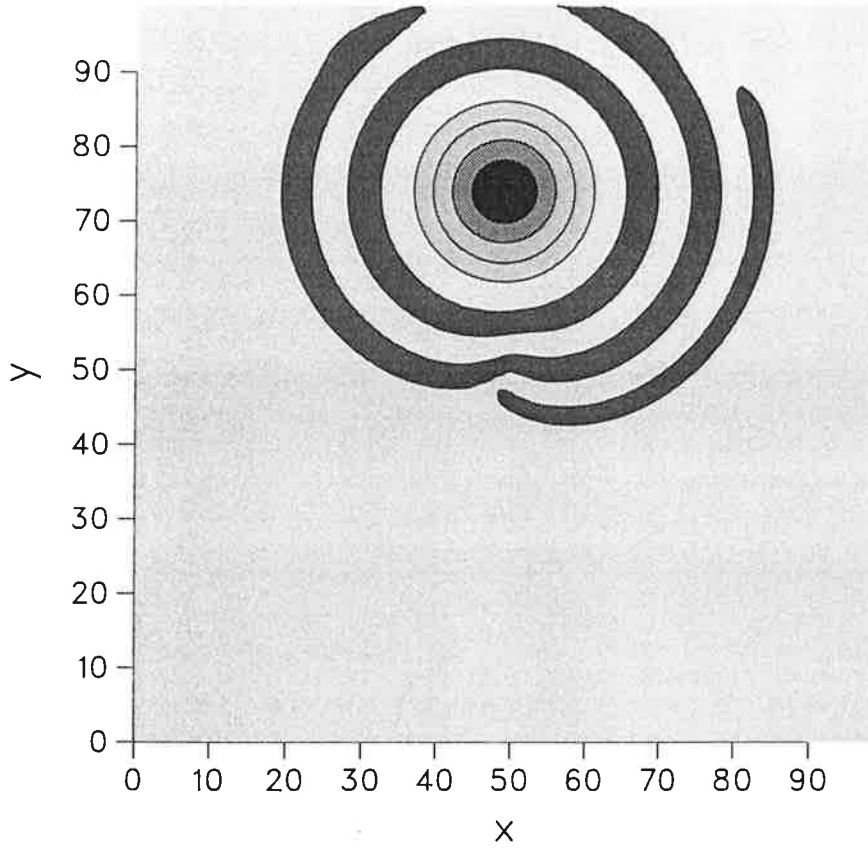
In uniform flow fields with strong spatial gradients MAPF is clearly superior to APF, because the ripples evolving in APF are too large.

In both model versions the largest numerical diffusion is produced during the first advective steps, i. e. when the discontinuities of the initial distributions are smoothed by the polynomials. In the long term run the algorithms are distinctly better.

In multidimensional applications MAPF is strictly monotone only, if the flow fields are uniform. Under typical atmospheric conditions, however, the numerical instabilities of MAPF are still so small that it may also be applied in the general case of arbitrary transport velocities.

ψ

min = 0.96 max = 4.5



Locally Modified Version of Bott's Advection Scheme

***Andreas Chlond
Max-Planck-Institut für Meteorologie
Hamburg, FRG***

1. Introduction

Advective processes are of central importance in geophysical fluid dynamics and their treatment is crucial in numerical modelling of the transport of trace constituents in atmospheric models. However, the numerical handling of advection is plagued with difficulties. For instance, problems may arise when the transport of positive definite scalar quantities, such as moisture, liquid water content and chemical concentrations, is treated, since unphysically negative constituent values may be generated and/or strong spatial gradients can be smeared out or ripples can be produced in their vicinity by the numerical scheme. During the past decades, a wide variety of finite difference methods have been suggested for the numerical solution of the advection equation and several intercomparisons have been published (e.g. see Woodward and Colella, 1984; Rood, 1987; and Müller, 1992 for reviews).

Here we present a simple and effective self-adjusting hybrid technique to develop a new conservative and monotonic advection scheme that exhibits very low numerical diffusion of resolvable scales. The proposed scheme combines Bott's area preserving flux form algorithm with an area preserving exponential interpolating scheme, the use of either at any particular location being automatically controlled by the local ratio of the nodal values involved in the approximation process.

2. Method

Recently, Bott (1989a, b) presented an upstream biased Eulerian finite volume advection scheme. Bott's flux scheme has several attractive properties: the method is mass conservative, positive definite, has small phase and amplitude errors and is computationally very efficient. However, the simulation of sharply varying gradients - especially in situations with non zero background values of the transported quantity - can result in unphysical oscillations, which although localized could cause difficulties in non-linear problems. To eliminate this deficiency of the scheme and to insure monotonicity we use a variant of Harten and Zwas' (1972) self-adjusting hybrid technique. The basic idea is to identify regions where monotonicity might be violated and then keep the rippling from occurring. This goal is achieved by combining Bott's accurate scheme, which is used in the smooth regions of the transported quantity, with the exponential scheme which is used in regions of sharp gradients (hence, the name hybrid is indicative of a combination of two different methods). The exponential upwinding interpolation concept is

based on previous work of Spalding (1972). In this approach piecewise exponential profiles are used to express the variation of a transported quantity between the grid points. Since the exponential interpolation functions are monotonic by construction no specific flux limiters have to be employed to avoid spurious oscillations near sharp gradients. Thus, we propose to construct the hybrid scheme using a combination of the unlimited Bott-scheme and the exponential scheme. The use of either of these two schemes at any particular location is controlled by a switch which automatically (i.e. self-adjusting) switches from one scheme to the other. The Bott scheme is used in the bulk of the domain in regions with smooth gradients; when the local curvature of the advected variable exceeds a preset value, however, the algorithm automatically switches to exponential upwinding. As a result, the hybrid scheme is also appropriate to address problems with sharp gradients and the scheme produces solutions which are found to be very close to those of the Bott-scheme, but displaying no over- or undershoots. An elaborate description of the scheme is given in Chlond (1994).

3. *Numerical results*

In this section numerical results will be presented to examine the performance of the newly proposed combined flux scheme algorithm. The results obtained with the combined scheme will be compared with Bott's (1989a, b) scheme (version l = 4), abbreviated) and with the exponential scheme, which will serve as references.

3.1. *One-dimensional experiments*

We first consider one-dimensional advection in a constant velocity field. The calculations are performed in a 64-point periodic domain with $\Delta x = 1$. The three types of test problems that are used to evaluate the accuracy of a numerical scheme are the Gaussian function, the square wave function and the triangular function which are superimposed on a constant background value of $\psi_B = 100$. Each of these functions helps to illustrate some strengths and limitations of a numerical method. The numerical results presented below are obtained with constant Courant numbers of $C = 0.1$, $C = 0.4$ and $C = 0.8$ after $N_T = 1920$, $N_T = 480$ and $N_T = 240$ iterations, respectively, corresponding to three revolutions around the 64-point periodic domain.

Figure 1 depicts the analytical solution as well as the numerical results of the advection of a Gaussian distribution, which are obtained with Bott's scheme (a), the exponential scheme (b) and with the combined scheme (c) (background values have been removed in this Figure and in the following). For the combined scheme tests one piece of additional information is included in this and in the following Figures: diamonds on the abscissa mark those points at which the "automatic switch" detects a "danger zone" and hence at which the exponential scheme has been activated. Obviously, Bott's scheme and the combined scheme yield a good agreement with the analytical solution and produce low amplitude and phase

errors. Thus, this experiment provides a demonstration of each schemes' ability to transport well-resolved, smoothly varying functions over large distances. In contrast, the exponential scheme is slightly diffusive and slowly diminishes the amplitude of the Gaussian distribution.

The second example is the advection of the square wave function. This function reveals a numerical method's capability to handle Gibb's oscillations that arise in the vicinity of discontinuities. As shown in Figure 2a, Bott's scheme generates dispersive ripples which distort the distribution. The exponential scheme (Figure 2b) broadens the distribution, but, as a result of monotonicity, exhibits no spurious oscillations, i.e. it generates diffusive rather than dispersive errors. The combined scheme, which has activated the exponential interpolation only in the vicinity of the points of discontinuity of the square wave function, produces the best results because it is considerable less diffusive than the exponential scheme and, moreover, it does not introduce wiggles.

The third test is the advection of a triangular distribution which should illustrate a numerical methods' capacity to treat sharp peaks and extremum points. As it is seen in Figure 3a, Bott's scheme performs quite well. Dispersive errors are still present but are much smaller in amplitude than for the case of the square wave. Again, the exponential scheme (Figure 3b) broadens the distribution somewhat but otherwise advects it quite accurately. In Figure 3c the same problem has been solved using the combined scheme. In this situation, no phase errors and dispersive ripples are visible and the numerical solution is almost identical to the exact solution, except at the lower corner points and in the vicinity of the extremum.

3.2. *Two dimensional rotational flow field test*

In this section we present results of several two dimensional rotational flow field tests , in which a prescribed distribution undergoes solid-body rotation counter-clockwise around a 100 x 100 zone grid with $x = y = 1$. The integrations are carried out with a time step of $t = 0.1$ so that 628 time steps will effect one complete revolution about the central point. The maximum Courant number in the domain is 0.7. As initial conditions we use two different test functions: the cone and the cube which are superimposed upon a constant background value of $\psi_B = 100$.

In the first experiment the cone is initialized with a base radius of 15 x and a maximum height of $\psi_{MAX} = 3.87$ at $(x, y) = (50, 75)$. Figure 4 shows (a) the initial distribution and the final distribution after six full rotations (3768 time steps) obtained with Bott's flux scheme (b) and with the combined flux scheme (c). As expected, both schemes exhibit very good shape preserving characteristics. Bott's scheme leaves the maximum amplitude of the cone nearly unchanged but creates new extrema in the distribution at the base of the cone. In contrast, the combined scheme produces no over- and undershootings but reduces the maximum slightly with ψ_{MAX}^n finally reaching 93.5% of ψ_{MAX} .

A more severe test problem is the rotation of a cube of unit height with lateral lengths of 20 centered at $(x, y) = (30, 70)$, (see Figure 6a). Figure 5 presents a comparison of the results of the two schemes for six full rotations of the cube. Bott's scheme generates dispersive errors which severely distort the distribution. In contrast, the combined scheme preserves the shape of the cube very well but tends to broaden the distribution somewhat. However, no oscillations occur neither at the base nor at the top of the cube.

4. *Conclusions*

A simple and effective self-adjusting hybrid technique has been introduced to construct a new conservative and monotonic advection scheme which is computationally very efficient. In principle the scheme combines Bott's (1989a, b) area preserving flux form algorithm, which is used in smooth regions of the flow, with an area preserving exponential interpolating scheme, which is used in regions where monotonicity might be violated.

Using standard linear advection test, we evaluated the accuracy of the combined scheme relative to Bott's scheme. The comparative test calculations presented demonstrate the combined schemes ability to accurately transport well-resolved, smoothly varying functions over large distances. Furthermore, the combined scheme is also well suited to address problems with sharp gradients and returns solutions which are virtually as good as those predicted by Bott's scheme in respect of capturing step gradients, but without the deficiency of the latter to produce physically unrealistic and often serious spurious oscillations.

References

- Bott, A. (1989a): A positive definite advection scheme obtained by non-linear renormalization of the advective fluxes. *Mon. Wea. Rev.*, 117, 1006-1015.
- Bott, A. (1989b): Reply. *Mon. Wea. Rev.*, 117, 2633-2636.
- Chlond, A. (1994): Locally modified version of Bott's advection scheme. *Mon. Wea. Rev.*, 122, 111-125.
- Harten, A., and G. Zwas (1972): Self-adjusting hybrid schemes for shock computations. *J. Comput. Phys.*, 9, 568-583.
- Müller, R. (1992): The performance of classical versus modern finite-volume advection schemes for atmospheric modelling in a one-dimensional test-bed. *Mon. Wea. Rev.*, 120, 1407-1415.
- Rood, R.B. (1987): Numerical advection algorithms and their role in atmospheric transport and chemistry models. *Rev. Geophys.*, 25, 71-100.
- Spalding, D.B. (1972): A novel finite-difference formulation for differential expressions involving both first and second derivatives. *Int. J. Num. Methods Eng.*, 4, 551.
- Woodward, P.R., and P. Colella (1984): The numerical simulation of two-dimensional fluid flow with strong shocks. *J. Comput. Phys.*, 54, 115-173.

Figure Captions

Figure 1: Solution of the one-dimensional linear advection equation in which a Gaussian distribution superimposed upon a constant background field of $\psi_B = 100$ is advected to the right in a 64-point grid with periodic boundaries. Shown are the analytical solution (full line) along with numerical solutions (dashed lines) obtained with Bott's flux scheme (version $l = 4$, abbreviated) (a), with the exponential scheme (b) and with the combined flux scheme (c) after three revolutions for Courant numbers $C = 0.8$, $C = 0.4$ and $C = 0.1$, corresponding to 240, 480 and 1920 time steps, respectively. Background field has been removed. Diamonds on the abszissa in (c) mark those points at which the exponential scheme has been activated.

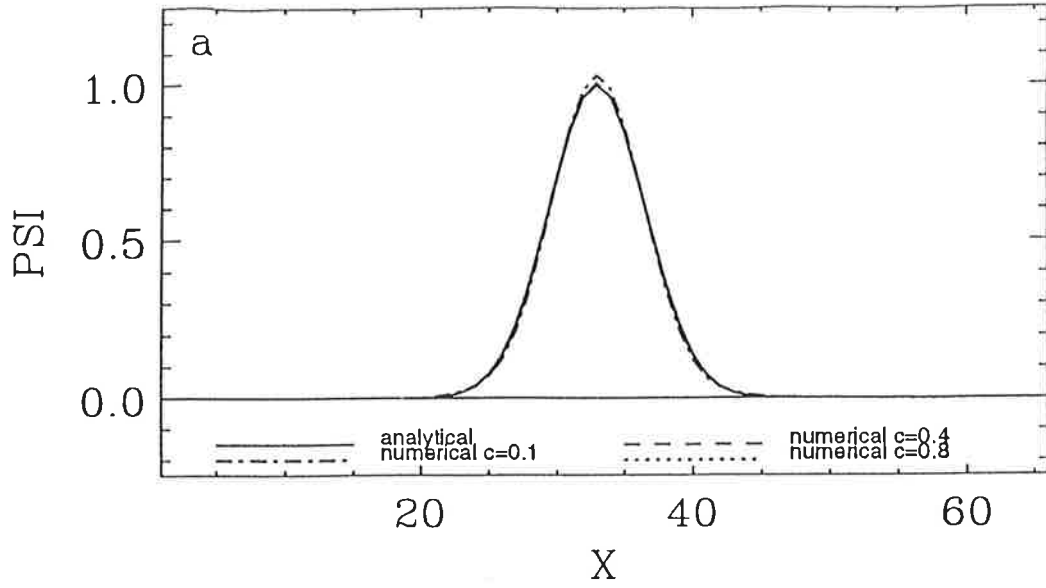
Figure 2: As in Figure 1, except for the square wave.

Figure 3: As in Figure 1, except for a triangular wave.

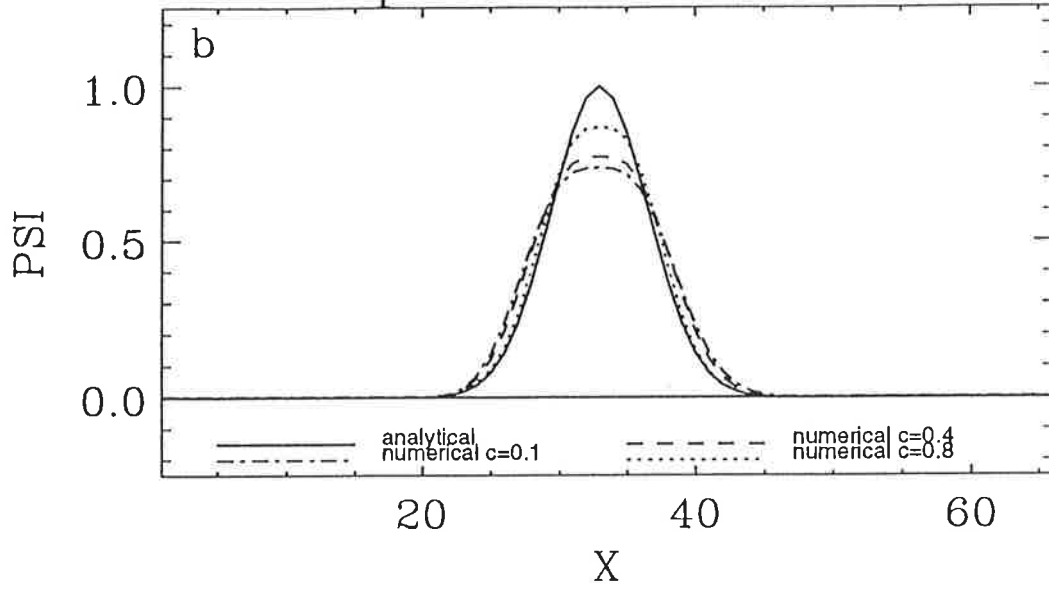
Figure 4: Solution of the two-dimensional linear advection equation in which a cone superimposed upon a constant background field of $\psi_B = 100$ undergoes solid body rotation counterclockwise in a 100×100 zone grid with cyclic boundary conditions. Shown are the initial condition (a) along with numerical solutions obtained with Bott's flux scheme (version $l = 4$, abbreviated) (b) and with the combined scheme after six full rotations, corresponding to 3768 time steps. The maximum Courant number is 0.7. Background field has been removed.

Figure 5: As Figure 4, except for a cube.

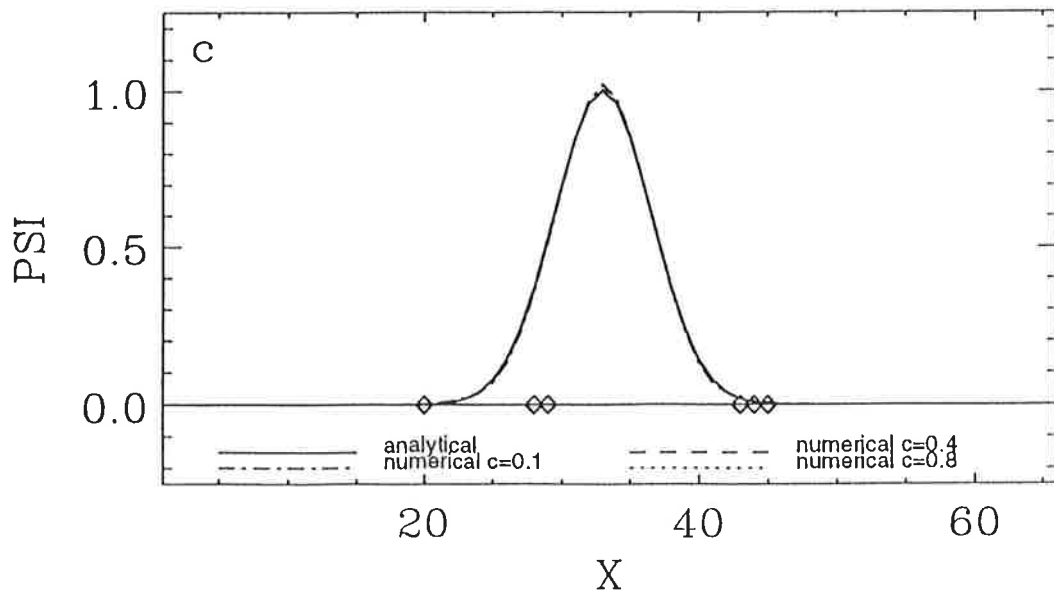
Bott-Scheme



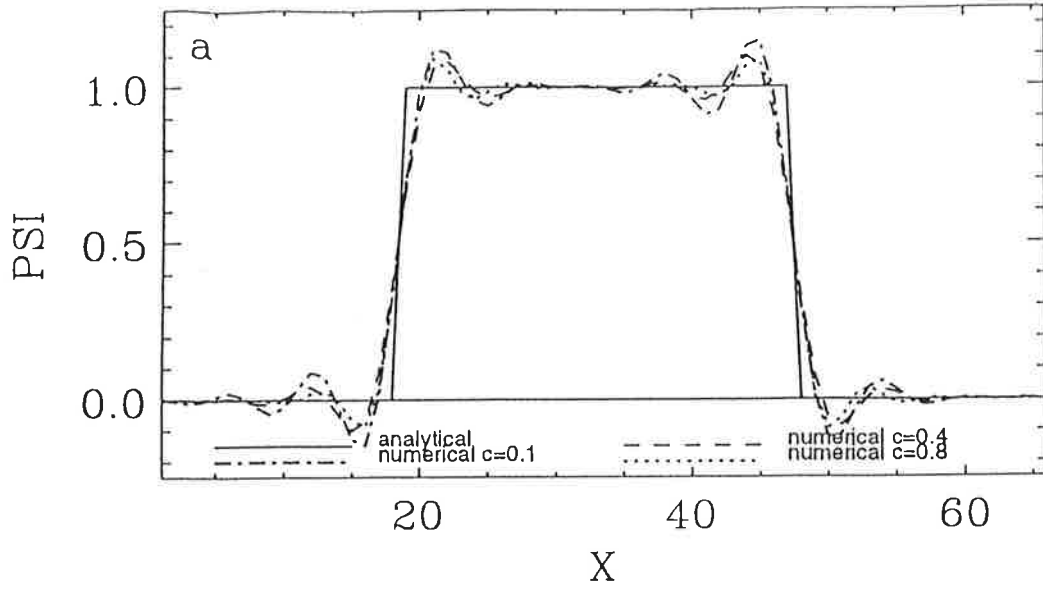
Exponential-Scheme



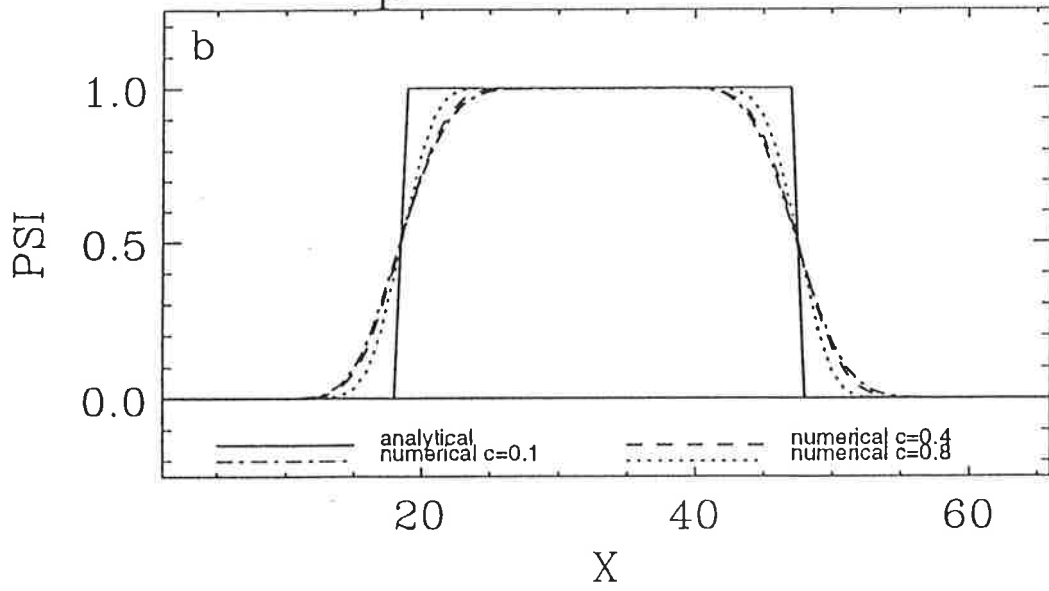
Combined-Scheme



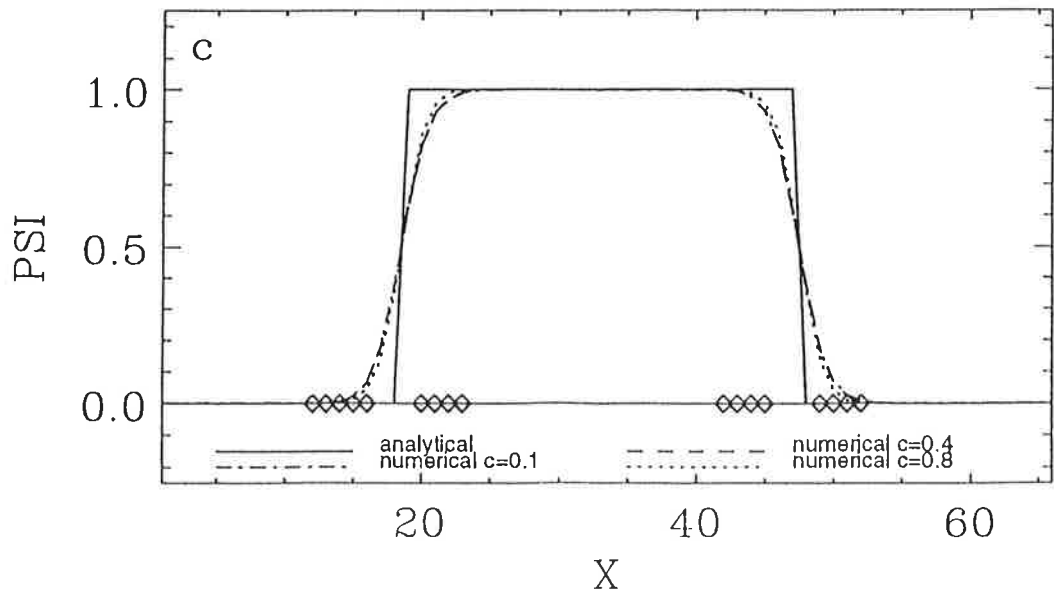
Bott-Scheme



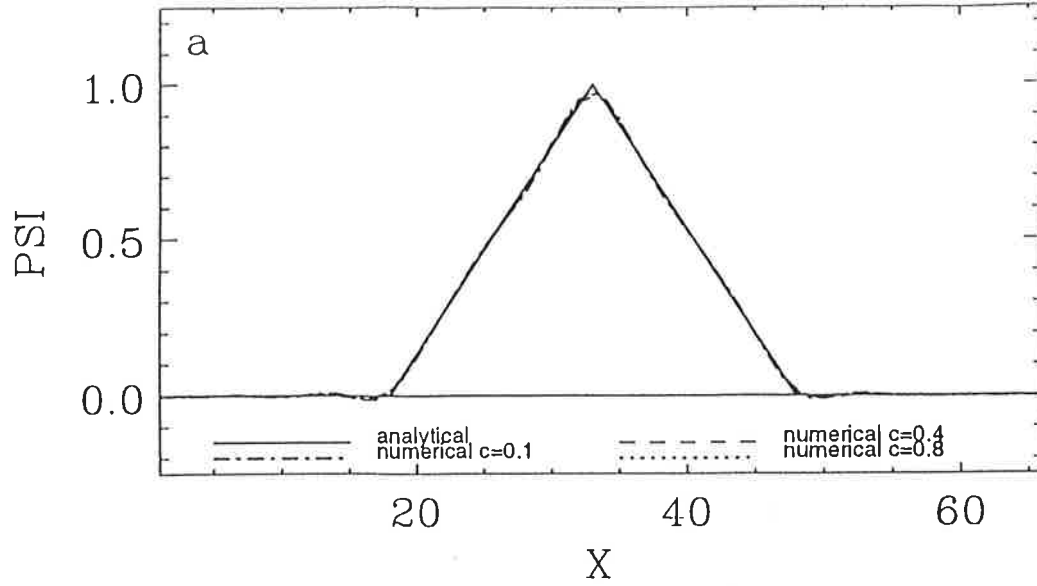
Exponential-Scheme



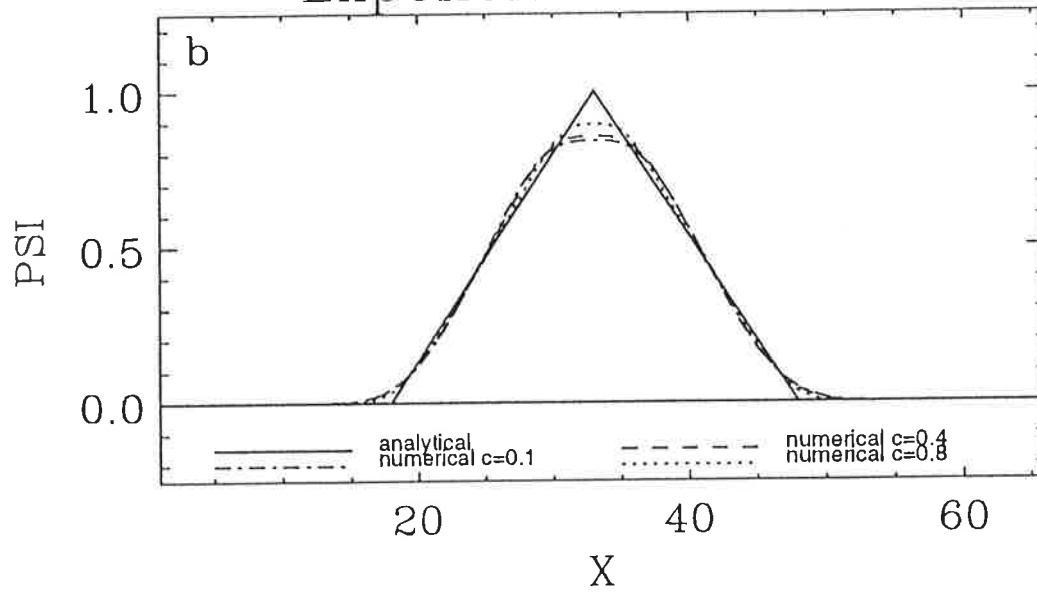
Combined-Scheme



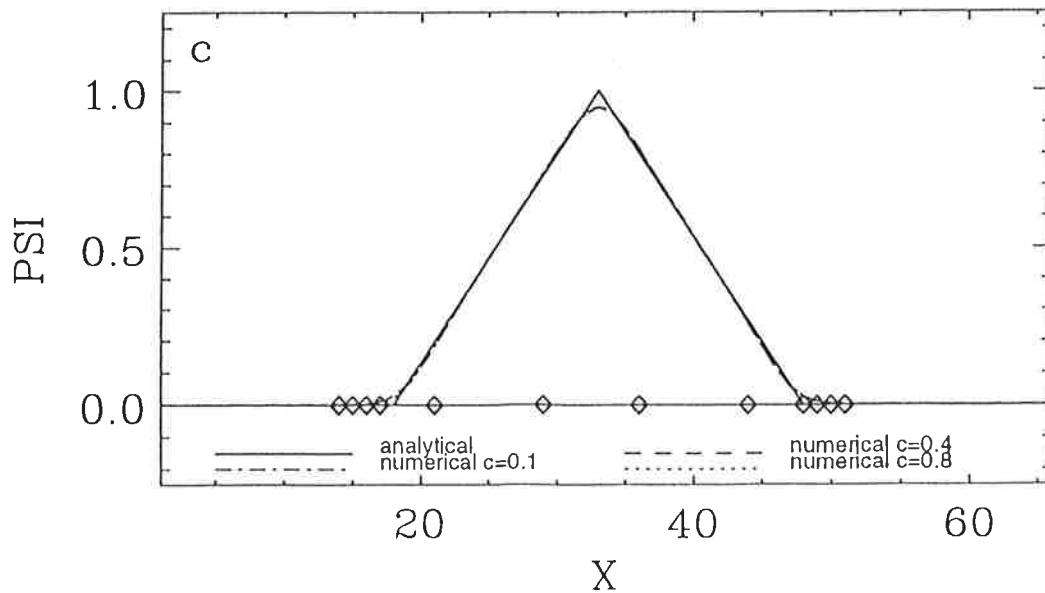
Bott-Scheme

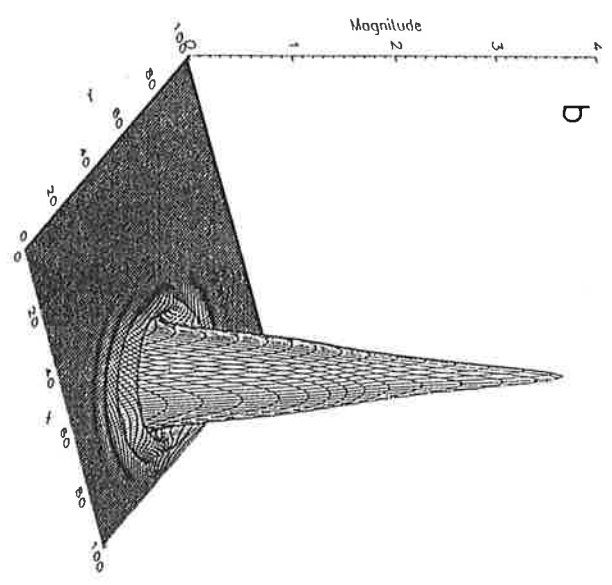
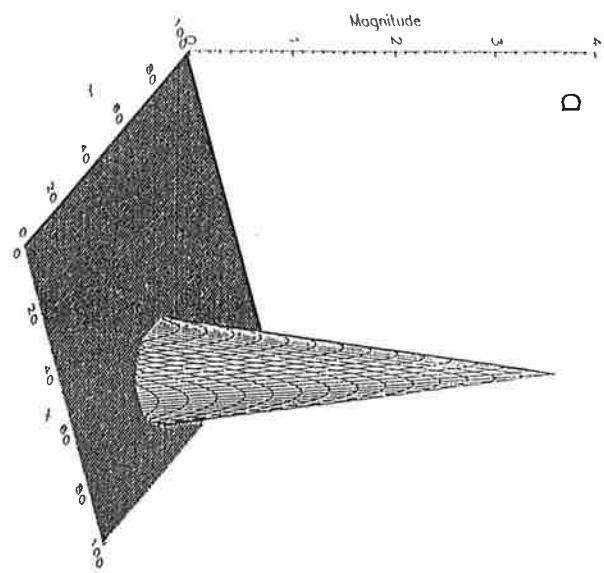
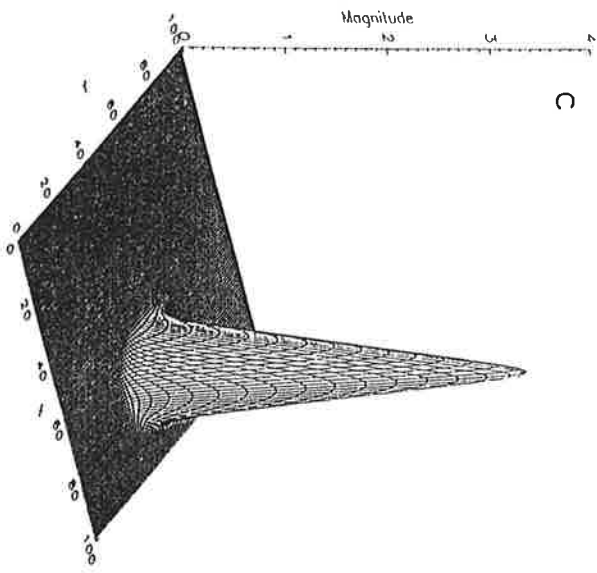


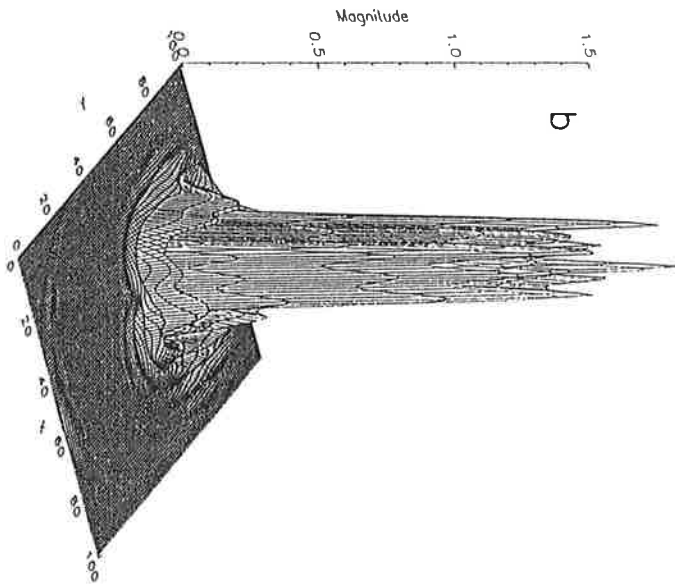
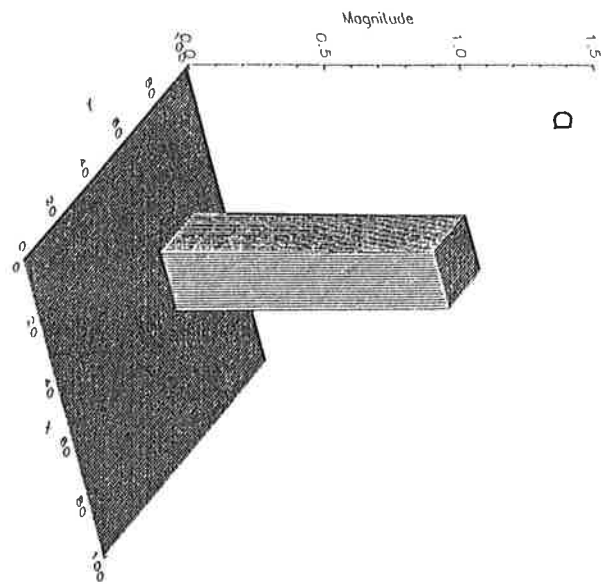
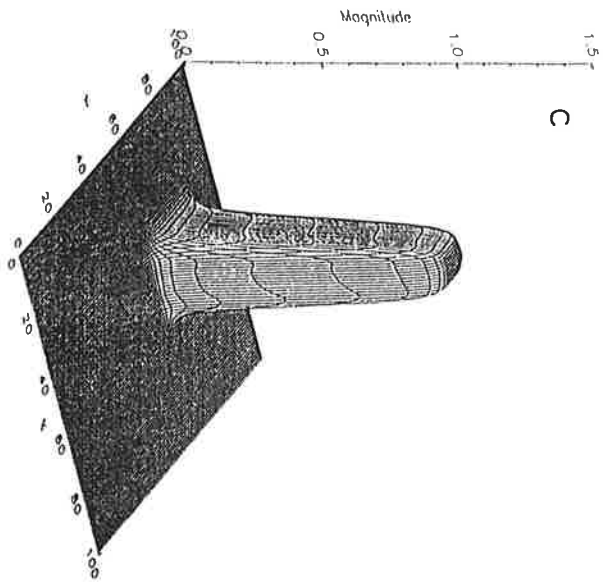
Exponential-Scheme



Combined-Scheme







A geometric approach to multidimensional advection: improving efficiency using economization of power series

Elías Valur Hólm

European Centre for Medium-Range Weather Forecasts
Reading, UK

March 19, 1998

Abstract

We will present one possible extension of the popular Godunov type advection algorithms to multidimensions with two-dimensional examples. The approach [5] is on flux form, and the fluxes are directed along the local flow direction, with the distribution of the advected variable within each cell approximated by a multidimensional polynomial. By construction, the method is mass-conservative and non-oscillatory. Since the basic algorithm is described elsewhere, we will focus on how the advection method can be made much more computer-time efficient using the economization of power series approach [7] to reduce the order of the multidimensional polynomial at the core of the algorithm without losing accuracy. The economization approach is simple to implement and can be used together with every advection algorithm requiring the evaluation of polynomials (for example the semi-Lagrangian approach). The economization approach is illustrated with two-dimensional advection of a passive scalar on the sphere. The experiment shows that by economization of a seventh order polynomial to third order, we can obtain the accuracy of the higher order method at the cost of the lower order method.

1 Introduction

Efficient polynomial approximations have had a revival for applications in the construction of accurate advection schemes. In Lagrangian and semi-Lagrangian advection schemes the value of the advected variable is determined from an interpolation to a point. The interpolation is often performed with polynomials, and for higher accuracy higher order polynomials are used. In flux-form or finite volume advection schemes, the fluxes are often approximated by an integration of a polynomial representing the variation of the advected variable within computational cells. The polynomial could be integrated over the cell boundary, or over the volume which flows through the boundary during a timestep. After performing the integration, the result is once again that interpolations to points need to be evaluated, now of the

primitive function. As above, the accuracy can be enhanced by using higher order polynomials. In the above mentioned advection schemes the efficiency can thus be increased by choosing more efficient representation of the variation of the advected variable within a cell, or in other words a better subcell resolution. For this purpose, it is worthwhile to study some of the classical results of practical approximations, as developed in the 1930–40's for efficient tablemaking of mathematical functions by hand- and mechanical calculators, for example [7, 8, 10, 11].

The purpose of this paper is to show how one particularly efficient technique, the *economization of power series* invented by Lanczos [7], can be used to increase the efficiency of finite volume advection schemes, with application to scalar advection on the sphere. But first we will start with a short sketch on the development of efficient polynomial approximations.

2 Some who's and why's of efficient polynomials

The quest for the best polynomial approximation of a given degree goes back to the 19th century. Notably Chebyshev found the best approximations in the sense that the maximum deviation from a given function is minimized over a given interval. These approximations are expressed as a series of Chebyshev polynomials (see Ortiz [10] for a short historical review and Rivlin [12] for the properties of the Chebyshev polynomials). Before the Second World War there were some large scale projects for constructing tables of mathematical functions, notably in the UK and USA [2]. The best known result of this effort are the tables in Abramowitz and Stegun [1]. In the construction of these tables mechanical desk calculators and hand calculations were used. It is obvious that efficient approximations can speed up table making by desk calculators considerably. In 1938 Lanczos [7] came up with two remarkable methods for efficient polynomial approximations, both based on the optimal properties of the Chebyshev polynomials. These methods were the *economization of power series*, which reduces the number of terms of a given power series without significantly reducing the accuracy, and the *tau-method*, which constructs a power series from linear differential or integral relations defining a function, where the resulting series is usually much more accurate than the corresponding Taylor series. These methods were used to derive some of the most efficient polynomial approximations of mathematical functions known. As a dramatic example, Lanczos [7] derives a seventh degree polynomial approximation to the function $\log(1+x)$ in the interval $0 \leq x \leq 1$, which has a maximum error less than 10^{-6} . The Taylor expansion of the same function needs one million terms to achieve the same accuracy. It is worth noting that Lanczos was impressed by the work performed by the mathematical tablemakers at The National Bureau of Standards, and he joined them for one year in 1943 [2]. There he was a source of inspiration for the staff, and contributed with a series of lectures among other things. Several methods were also derived for efficient interpolation in mathematical tables, including *throwback*, which reduces the work needed for accurate interpolations by replacing high order differences by modified low order differences (see [9] and the chapter on numerical analysis in [1], for example Everett's formula with throwback). With the advent of electronic computers by the end of the Second World War, there was a renewed in-

terest in polynomial approximations. With the new computers it became quicker to calculate mathematical functions from low order polynomial approximations whenever they were needed, instead of looking up the value in a mathematical table (Ortiz [10]). Again the methods of Lanczos and others could be successfully used. These computational aids and later developments are still used for the approximation of functions in every computer.

3 Unified view of interpolation in Lagrangian and finite-volume advection schemes

For the derivations in this paper we will consider the one-dimensional advection problem. This is no restriction, since the results translate to multidimensions through simple matrix multiplications [5]. In the one-dimensional advection problem we are given the values of the advected variable either as point values or as cell-average values, one value per computational cell.

In Lagrangian and semi-Lagrangian advection schemes the variable is usually interpreted as a point value. In this case we will consider the variable value given at the boundaries of the computational cells, that is

$$\psi_{i+1/2} = \psi(x'_{i+1/2}) \quad (1)$$

where $x'_{i+1/2}$ is the boundary between cell i and $i + 1$.

In the finite volume advection schemes the variable values are interpreted as cell averages of the advected variable $\psi(x')$ (note that the computational cells are shifted half a cell with respect to the above case),

$$\bar{\psi}_i = \frac{1}{x'_{i+1/2} - x'_{i-1/2}} \int_{x'_{i-1/2}}^{x'_{i+1/2}} \psi(x') dx' \quad (2)$$

However, in the finite volume advection schemes we are interested in the integral of fluxes, which means that we will be interpolating the primitive function of the advected variable. Its value is known exactly at cell boundaries,

$$\Psi_i = \int_0^{x'_{i+1/2}} \psi(x') dx' = \sum_{k=1}^i \bar{\psi}_k \quad (3)$$

where we $x' = 0$ is the left boundary of the domain.

A unified view of the subcell variation of the advected quantities in Lagrangian and finite-volume advection schemes is therefore to consider function values φ_i given at cell-boundaries,

$$\varphi_i = \begin{cases} \psi_{i+1/2} & \text{for semi-Lagrangian/Lagrangian case} \\ \Psi_i & \text{for flux-form/finite-volume case} \end{cases} \quad (4)$$

and construct polynomial approximations $P_i^n(x')$ which approximate the variation of $\varphi(x')$ within each computational cell. The boundary conditions for $P_i^n(x')$ are φ_{i-1} and φ_i . The order n of $P_i^n(x')$ can be increased by including more and more function values in the approximation.

When discussing polynomial approximations within cell i , it is suitable to transform the cell to the interval $[-1, 1]$, which coincides with the definition interval of the standard Chebyshev polynomials. Thus let

$$x = \frac{2x' - (x'_{i+1/2} + x'_{i-1/2})}{x'_{i+1/2} - x'_{i-1/2}} \quad (5)$$

Other intervals are of course easily introduced, however, one then needs to use the appropriately modified Chebyshev polynomials. We consider only approximations which use the information from the $n + 1$ nearest neighbouring cells centred around cell i ,

$$P_i^n(x) = \sum_{k=0}^n c_{i,k} x^k \quad (6)$$

The coefficients $c_{i,k}$ are determined from the function values,

$$c_{i,k} = \sum_{l=i-[\frac{n}{2}]-1}^{i+[\frac{n}{2}]} b_{k,l} \varphi_l \quad (7)$$

4 Economization of power series

We will now review some standard results on Chebyshev polynomials and the application to the economization of power series. These results are then used to derive a compact formula for the economized power series in terms of the given function values φ_i . The importance of the derivation lies in the end result, which is simple and can largely be precalculated once and for all.

In the economization of power series method we express the powers of x in the original polynomial $P_i^n(x)$, Eq. 6, in terms of Chebyshev polynomials $T_m(x)$, and then neglect all terms of order $n' + 1$ and onwards ($n' < n$), if this fulfills our accuracy criteria [7].

The expression of the powers of x in terms of Chebyshev polynomials $T_m(x)$ can be obtained by a simple calculation, or from Table 22.3 of [1]. We here use the general expression from Rivlin [12],

$$x^k = \frac{1}{2} A_{k,0} T_0(x) + \sum_{m=1}^k A_{k,m} T_m(x) \quad (8)$$

$$A_{k,m} = \begin{cases} 2^{1-k} \binom{k}{\frac{k-m}{2}} & m = k, k-2, \dots, k-2[\frac{k}{2}] \\ 0 & \text{otherwise} \end{cases} \quad (9)$$

For example,

$$\begin{array}{ll} 1 = T_0 & x = T_1 \\ x^2 = \frac{1}{2}(T_0 + T_2) & x^3 = \frac{1}{4}(3T_1 + T_3) \\ x^4 = \frac{1}{8}(3T_0 + 4T_2 + T_4) & x^5 = \frac{1}{16}(10T_1 + 5T_3 + T_5) \\ x^6 = \frac{1}{32}(10T_0 + 15T_2 + 6T_4 + T_6) & x^7 = \frac{1}{64}(35T_1 + 21T_3 + 7T_5 + T_7) \\ x^8 = \frac{1}{128}(35T_0 + 56T_2 + 28T_4 + 8T_6 + T_8) & x^9 = \frac{1}{256}(126T_1 + 84T_3 + 36T_5 + 9T_7 + T_9) \end{array}$$

It is easy to understand why one can approximate a given power of x by a lower order polynomial simply by deleting some of the highest order terms in the Chebyshev expansion. First we note that the coefficients of the Chebyshev expansion decrease rapidly as the order of the Chebyshev polynomial increases. Bearing in mind that the maximum amplitude of all Chebyshev polynomials is 1 within the approximation interval, the error will never be larger than the sum of the absolute value of the deleted coefficients. Furthermore, note that only even(odd) polynomials are used for even(odd) powers of x .

We now want to use the above result to express the original polynomial in terms of Chebyshev polynomials. Insertion of Eqs. 8–9 in Eq. 6 gives (see also [12] for this result)

$$P_i^n(x) = \sum_{k=0}^n c_{i,k} \left[\frac{1}{2} A_{k,0} T_0(x) + \sum_{m=1}^k A_{k,m} T_m(x) \right] = \frac{1}{2} C_{i,0} T_0(x) + \sum_{k=1}^n C_{i,k} T_k(x) \quad (10)$$

$$C_{i,k} = \sum_{m=0}^{\lfloor \frac{n-k}{2} \rfloor} A_{k+2m,k} c_{i,k+2m} = \sum_{m=0}^{\lfloor \frac{n-k}{2} \rfloor} 2^{1-(k+2m)} \binom{k+2m}{m} c_{i,k+2m} \quad (11)$$

Finally, we can insert the function values φ_i using Eq. 7

$$C_{i,k} = \sum_{m=0}^{\lfloor \frac{n-k}{2} \rfloor} [A_{k+2m,k} \sum_{l=i-\lfloor \frac{n}{2} \rfloor-1}^{i+\lfloor \frac{n}{2} \rfloor} b_{k,l} \varphi_l] = \sum_{l=i-\lfloor \frac{n}{2} \rfloor-1}^{i+\lfloor \frac{n}{2} \rfloor} B_{k,l} \varphi_l \quad (12)$$

$$B_{k,l} = \sum_{m=0}^{\lfloor \frac{n-k}{2} \rfloor} A_{k+2m,k} b_{k+2m,l} = \sum_{m=0}^{\lfloor \frac{n-k}{2} \rfloor} 2^{1-(k+2m)} \binom{k+2m}{m} b_{k+2m,l} \quad (13)$$

The result of Eq. 13 is very important, since it means that the coefficients $B_{k,l}$ can be precalculated once and for all, and can be used as an alternative to the coefficients $b_{k,l}$, if we want to express our polynomial in the form of a Chebyshev series. For example, the first few terms of $B_{k,l}$ would look as follow,

$$\begin{aligned} B_{0,l} &= \frac{1}{128} [256b_{0,l} + 128b_{2,l} + 96b_{4,l} + 80b_{6,l} + 70b_{8,l} + \dots] \\ B_{2,l} &= \frac{1}{128} [\quad \quad \quad 64b_{2,l} + 64b_{4,l} + 60b_{6,l} + 56b_{8,l} + \dots] \\ B_{4,l} &= \frac{1}{128} [\quad \quad \quad \quad \quad 16b_{4,l} + 24b_{6,l} + 28b_{8,l} + \dots] \\ B_{6,l} &= \frac{1}{128} [\quad \quad \quad \quad \quad \quad \quad 4b_{6,l} + 8b_{8,l} + \dots] \\ B_{8,l} &= \frac{1}{128} [\quad \quad \quad \quad \quad \quad \quad \quad \quad b_{8,l} + \dots] \end{aligned}$$

$$\begin{aligned} B_{1,l} &= \frac{1}{256} [256b_{1,l} + 192b_{3,l} + 160b_{5,l} + 140b_{7,l} + 126b_{9,l} + \dots] \\ B_{3,l} &= \frac{1}{256} [\quad \quad \quad 64b_{3,l} + 80b_{5,l} + 44b_{7,l} + 44b_{9,l} + \dots] \\ B_{5,l} &= \frac{1}{256} [\quad \quad \quad \quad \quad 16b_{5,l} + 28b_{7,l} + 32b_{9,l} + \dots] \\ B_{7,l} &= \frac{1}{256} [\quad \quad \quad \quad \quad \quad \quad 4b_{7,l} + 9b_{9,l} + \dots] \\ B_{9,l} &= \frac{1}{256} [\quad \quad \quad \quad \quad \quad \quad \quad \quad b_{9,l} + \dots] \end{aligned}$$

where of course only $n + 1$ coefficients would be calculated, and the summation in each coefficient would be performed up to n or $n - 1$, depending on if it was an odd or even coefficient. The calculation of the coefficients $B_{k,l}$ is not affected by the economization procedure.

The economization of the power series is now performed by deleting all terms of order greater than n' ($< n$) in the Chebyshev expression of the original polynomial, Eq. 10,

$$P_i^{n' \leftarrow n}(x) = \frac{1}{2} C_{i,0} T_0(x) + \sum_{k=1}^{n'} C_{i,k} T_k(x) \quad (14)$$

where we use the notation $P_i^{n' \leftarrow n}(x)$ for a polynomial which has been economized to order n' from the original order n . Thus the economization reduces the number of coefficients $C_{i,k}$ which need to be calculated, but the calculation of each coefficient is left unchanged. This means that information from the original stencil of function values, $\varphi_{i-\lfloor \frac{n}{2} \rfloor - 1}, \dots, \varphi_{i+\lfloor \frac{n}{2} \rfloor}$, is still used in each coefficient $C_{i,k}$.

The simplest way of evaluating the polynomial is to leave it on the Chebyshev form, and use the recursion relations for Chebyshev polynomials to evaluate $T_k(x)$ (see e.g. [1]),

$$T_k(x) = \begin{cases} 1 & k = 0 \\ x & k = 1 \\ 2xT_{k-1}(x) - T_{k-2}(x) & k \geq 2 \end{cases} \quad (15)$$

However, we can also transform the economized polynomial back to powers of x , using the expression for $T_k(x)$ given by Erdélyi et al. [3] for $k = 1, 2, \dots$,

$$T_k(x) = \sum_{m=0}^{\lfloor \frac{k}{2} \rfloor} a_{k,k-2m} x^{k-2m} = \sum_{m=0}^{\lfloor \frac{k}{2} \rfloor} \frac{2^{k-2m} k! (-1)^m (k-m-1)!}{2m! (k-2m)!} x^{k-2m} \quad (16)$$

For including $T_0(x)$ in the compact formulation below, define

$$a_{0,0} = \frac{1}{2} \quad (17)$$

Inserting these expressions in the economized polynomial, Eq. 14, we get

$$P_i^{n' \leftarrow n}(x) = \sum_{k=0}^{n'} C_{i,k} \sum_{m=0}^{\lfloor \frac{k}{2} \rfloor} a_{k,k-2m} x^{k-2m} = \sum_{k=0}^{n'} \left[\sum_{m=0}^{\lfloor \frac{n'-k}{2} \rfloor} C_{i,k+2m} a_{k+2m,k} \right] x^k \quad (18)$$

To find out what the coefficients are in terms of the original function values, we use Eq. 12,

$$P_i^{n' \leftarrow n}(x) = \sum_{k=0}^{n'} \left[\sum_{m=0}^{\lfloor \frac{n'-k}{2} \rfloor} \left(\sum_{l=i-\lfloor \frac{n}{2} \rfloor - 1}^{i+\lfloor \frac{n}{2} \rfloor} B_{k+2m,l} \varphi_l \right) a_{k+2m,k} \right] x^k = \sum_{k=0}^{n'} \left[\sum_{l=i-\lfloor \frac{n}{2} \rfloor - 1}^{i+\lfloor \frac{n}{2} \rfloor} \beta_{k,l} \varphi_l \right] x^k \quad (19)$$

$$\beta_{k,l} = \sum_{m=0}^{\lfloor \frac{n'-k}{2} \rfloor} B_{k+2m,l} a_{k+2m,k} \quad (20)$$

Here again the coefficients $\beta_{k,l}$ are precalculated once and for all.

4.1 Constraints on the economization

In finite volume advection schemes, the subcell distributions should be such that their integrated value over the cell coincides with the cell average. We have noted in experiments that failure to fulfill this criteria will introduce phase errors. For Lagrangian and semi-Lagrangian schemes, the subcell distribution should coincide with the given function values at the cell boundaries. These constraints can be summarized with the notation introduced in Eq. 4

$$P_i^n(-1) = \varphi_{i-1} \quad (21)$$

$$P_i^n(1) = \varphi_i \quad (22)$$

There is no guarantee that the economized polynomial $P_i^{n' \leftarrow n}(x)$ still fulfills Eqs. 21–22. However, it is possible to modify the economization to accommodate for this. We will not pursue the matter further here since it will not change the outcome of the main message of this paper, namely the gains in computational efficiency which can be made by using economization.

4.2 Computational cost of economization

We now compare the cost of a single interpolation with a polynomial economized from order n to n' with the cost of an interpolation using polynomials of n and n' . In the economized polynomial there are $n' + 1$ terms whose coefficients are calculated from a series containing $n + 1$ members, giving a total of $(n' + 1)(n + 1)$ floating point operations. This is to be compared with the costs $(n' + 1)^2$ and $(n + 1)^2$ of the original polynomials. If we let $\varrho = (n' + 1)/(n + 1)$, then the relative costs of the three alternatives is $1 : \varrho : \varrho^2$, where $\varrho \in [0, 1]$. The economization alternative is intermediate in cost.

In the application to advection schemes there is more than just the basic cost of one interpolation which counts. First, there might be several advected variables so that certain factors in the interpolation can be reused by different variables. Second, several interpolations might be required of each variable within a computational cell so that the polynomial coefficients can be reused. Let the number of variables be M and the number of interpolations per variable expected within each cell be L . The expressions for $P_i^{n' \leftarrow n}(x)$, Eq. 14 and Eq. 18, can be seen either as a series in the function values φ_l or the expansion functions x^k or $T_k(x)$.

If we use a series in the function values, the coefficients at each locations can be reused for the M variables, giving a floating point operation count of

$$N_\varphi = L(n + 1)(M + n' + 1)$$

If we use a series in the expansion functions, then we precalculate the coefficients for each polynomial and reuse them at the L locations within each cell, giving

$$N_x = M(n' + 1)(L + n + 1)$$

floating point operations. An analysis of different combinations of possibilities shows

- For $L = 1$, $N_\varphi < N_x$ when $M > 1$

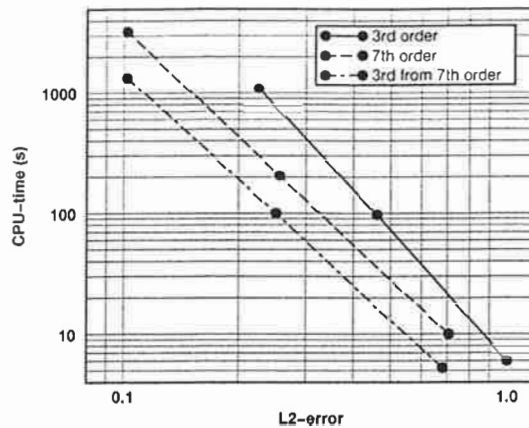


Figure 1: Computational efficiency of the economization approach. Shown are the computational costs as function of the error using the original third and seventh order polynomials and using the third order polynomial economized from the original seventh order polynomial.

- For large M , $N_\varphi < N_x$
- For $M = 1$, $N_x < N_\varphi$
- For large L , $N_x < N_\varphi$

The first case is typical of Lagrangian or semi-Lagrangian schemes, and the second case is typical of chemical transport models. The third case is typical of a model where all interpolation parameters are calculated anew for each variable, which should only be the case when computational costs are much less than storage costs. The fourth case is typical of some finite-volume schemes, but should really not occur but because of suboptimal programming.

5 Experiments

For testing the economization approach we will use the Godunov type finite volume method of [5] extended to spherical geometry (see [6]). The computational grid is regular in longitude and latitude. We will advect a passive scalar distribution in a constant cross-polar flow given by [13]. The velocity field is chosen so that it takes twelve days to advect the passive scalar once around the sphere. To make the test more demanding the flow is at an angle 0.45π relative the equator, so it is not parallel wit any gridlines. The initial condition, described in [5], consists of a cone, a dome, and a slotted cylinder of height 2.0, a sloping channel of depth 1.0, all superposed on a constant level of 1.0 (see Figs. 2– 3). The advection test is performed at three resolutions, 40×20 , 80×40 , and 160×80 , keeping the maximum CFL (Courant-Friedrichs-Lewy) number at 1.0 (i.e. the timestep is reduced in proportion to the gridsize).

We choose three subcell polynomial distributions for our tests: a third order polynomial, a seventh order polynomial, and a third order economized polynomial derived from the seventh order polynomial. In Fig. 1 we show the computational time

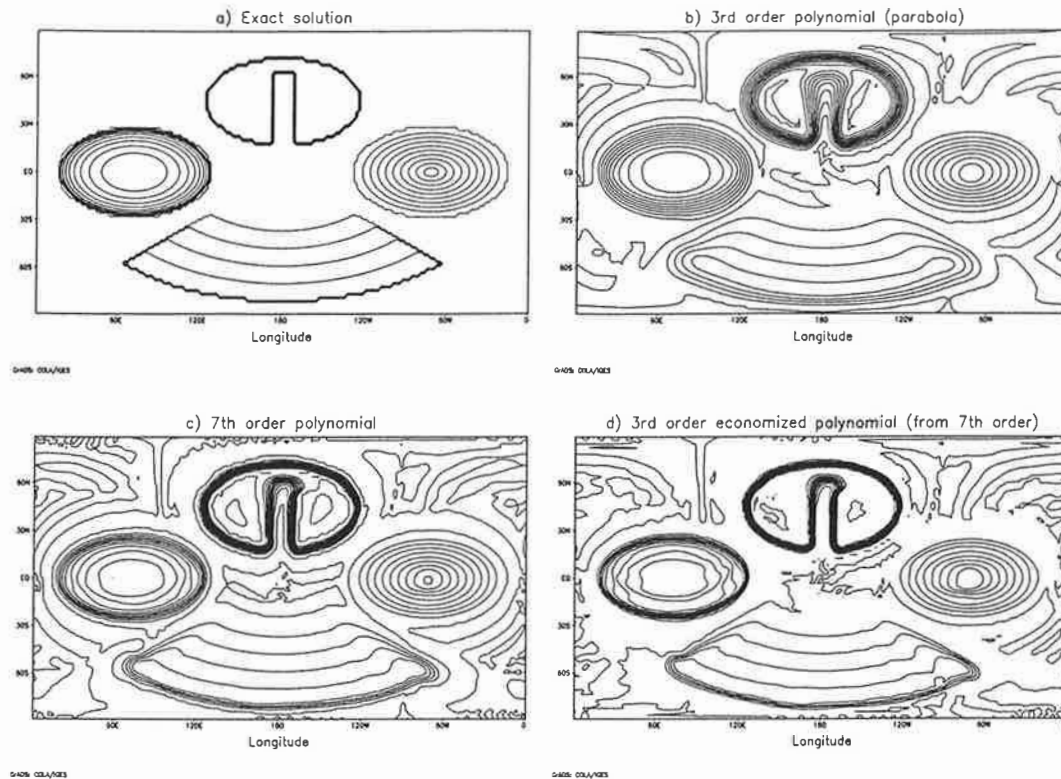


Figure 2: View of the final result after one rotation (day 12) for the different methods (160×80 resolution, maximum CFL number 1.0) The isoline interval is 0.2.

as a function of the accuracy of the different simulations. This figure shows that the economized polynomial method achieves the lowest error for a given computational cost, or equivalently, achieves a given accuracy at lowest computational cost. For the present methods we achieve the accuracy of the seventh order polynomials at the cost of the third order polynomials. The amount of saving will be different for different methods, but the message is that it is possible to achieve higher accuracy at lower cost for most advection schemes which use polynomials. In Figs. 2– 3 we show a comparison of the exact and the numerical solution after twelve days, corresponding to one rotation around the sphere at the highest resolution. We see that the seventh order and the third order economized polynomial results are very close. In particular the third order economized polynomial result has the sharpness of the seventh order polynomial result. There are some small scale deviations in the economized result, but these do not affect the accuracy.

6 Conclusions

We have shown how advection schemes which include evaluation of polynomials (e.g. Lagrangian, semi-Lagrangian and Godunov type finite volume advection schemes) can be made computationally more efficient by using the economization of power series approach of Lanczos [7]. In these types of advection schemes the advected quantity is estimated within each computational cell by a multidimensional polynomial. Higher accuracy is achieved by increasing the order of the polynomial. This

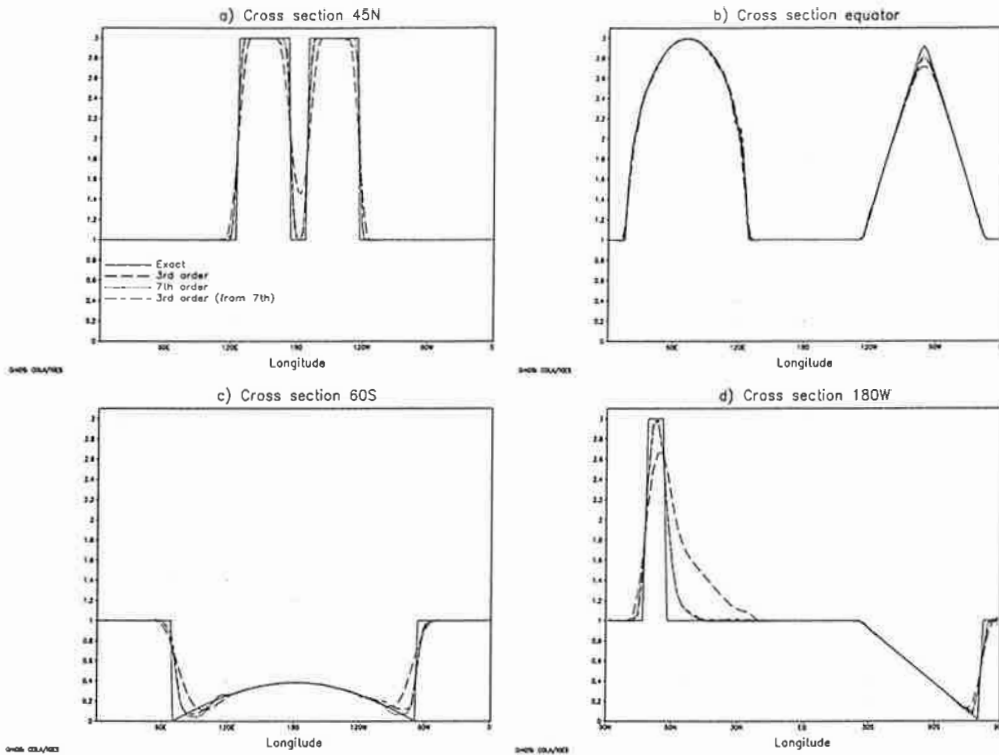


Figure 3: Cross section of the final result after one rotation (day 12) for the different methods (160×80 resolution, maximum CFL number 1.0).

increases the computational cost, especially in multidimensional applications. By replacing the high order polynomial by an economized lower order polynomial, almost the same accuracy can be achieved, but at a lower computational cost. If the polynomial is economized from order n to n' , the cost of a single one-dimensional polynomial evaluation is reduced by a factor $\rho = (n' + 1)/(n + 1)$. This will be especially important in multidimensional applications, where the computational cost can grow quicker with the polynomial degree than in one dimension (e.g. as n^2). By keeping n' low (linear, parabola, cubic), the cost can be kept low, and at the same time it is much easier to control features like unphysical wiggles with some of the polynomial preprocessing approaches which have been suggested in the literature (see e.g. [4]).

Although the present paper presents an application to a specific advection scheme, the results should be of wide application. The results shown here are first examples, and we will go on to extend the approach so that the economized polynomials will fulfill the same constraints as the original polynomials with respect to conserving the average within a computational cell (see Eqs. 21– 22).

References

- [1] M. Abramowitz and I. A. Stegun, editors. *Handbook of Mathematical Functions*. Dover Publications, 1965.

- [2] G. Blanch and I. Rhodes. Table-making at the National Bureau of Standards. In B. K. P. Scaife, editor, *Studies in Numerical Analysis*, pages 1–6. The Royal Irish Academy, Academic Press, 1974.
- [3] A. Erdélyi, W. Magnus, F. Oberhettinger, and F. G. Tricomi, editors. *Higher Transcendental Functions. Volume II*. Bateman Manuscript Project. McGraw-Hill Book Company, 1953.
- [4] A. Harten and S. Osher. Uniformly high-order accurate nonoscillatory schemes. I. *SIAM Journal on Numerical Analysis*, 24:279–309, 1987.
- [5] E. V. Hólm. A fully two-dimensional, nonoscillatory advection scheme for momentum and scalar transport equations. *Monthly Weather Review*, 123:536–552, 1995.
- [6] E. V. Hólm. On the assimilation of ozone into an atmospheric model. Scientific report 97–09, Koninklijk Nederlands Meteorologisch Instituut, 1997.
- [7] C. Lanczos. Trigonometric interpolation of empirical and analytical functions. *Journal of Mathematics and Physics*, 17:123–199, 1938.
- [8] C. Lanczos. Legendre versus Chebyshev polynomials. In J. J. H. Miller, editor, *Topics in Numerical Analysis*, pages 191–201. The Royal Irish Academy, Academic Press, 1973.
- [9] *Modern Computing Methods*. Number 16 in Notes on Applied Science. Her Majesty's Stationery Office, London, second edition, 1961.
- [10] E. L. Ortiz. Canonical polynomials in the Lanczos tau method. In B. K. P. Scaife, editor, *Studies in Numerical Analysis*, pages 73–93. The Royal Irish Academy, Academic Press, 1974.
- [11] J. R. Rice. *The Approximation of Functions. Volume 1: Linear Theory*. Computer Science and Information Processing. Addison-Wesley, 1964.
- [12] T. J. Rivlin. *The Chebyshev Polynomials*. John Wiley & Sons, 1974.
- [13] D. L. Williamson, J. B. Drake, J. J. Hack, R. G. Jacob, and P. N. Swarztrauber. A standard test set for numerical approximations to the shallow water equations in spherical geometry. *Journal of Computational Physics*, 102:211–224, 1992.

BOUNDED HIGHER-ORDER SCHEMES FOR CONVECTION-DOMINATED TRANSPORT

B.P. Leonard
The University of Akron

Convection-dominated transport involves some surprisingly challenging numerical difficulties. Classical ('central' difference) methods break down for reasons to be described. Popular 'remedies' (involving artificial diffusion) are far too inaccurate for practical purposes. Thus, if we confine ourselves to 'low' (i.e. first- or second-) order methods, we are faced with a choice between obviously unphysical numerical wiggles and less obvious (but no less disastrous) artificial smearing. Polynomial-based higher-order methods are more promising but still suffer from spurious numerical over/undershoots near strong changes in gradient. Fortunately, by making use of simple flux-limiter constraints, bounded higher-order (BHO) transport schemes offer an entirely satisfactory resolution of this dilemma. The first lecture (Part I) introduces some fundamental concepts, mostly based on simple one-dimensional problems. In Part II, we look at more advanced concepts involving the construction of genuinely multidimensional algorithms for convection-dominated transport.

PART I. FUNDAMENTAL CONCEPTS

A. Shortcomings of Conventional Methods

In order to understand the need for BHO schemes, we will first look at the reasons behind the failures of conventional numerical methods previously (and often still) used for computational fluid dynamics (CFD).

- **Problems with classical 'central' schemes.** So-called 'central' convection-diffusion schemes often exhibit spurious numerical oscillations (wiggles) or instability under high-convection conditions. Some insights into this (e.g., lack of stabilizing feedback sensitivity, etc.) will be discussed. 'Central' convection schemes are actually very unnatural—requiring the assumption of *downwind* weighting in the subcell structure; this is discussed more fully below. See References: [1,2,3]
- **'Remedy #1': explicit artificial diffusion.** For diffusion-dominated problems, central methods are quite successful. This has led to a philosophy of trying to make such methods 'work' for convection-dominated flows as well. One 'remedy' has been to explicitly add artificial diffusion and dissipation (with solution-dependent coefficients) to 'calm down' a potentially unstable method. [A CFD subculture has developed concerned with finding the 'best' forms of artificial diffusion!] Because 'central' methods are inappropriate for CFD to begin with, this philosophy is ill founded and results in a poor compromise, often involving both spurious wiggles *and* artificial smearing. [1,4]

- **'Remedy #2': implicit artificial diffusion.** Because of its inherent stability, first-order upwinding for convection has been very popular (used in combination with second-order-central diffusion terms). Unfortunately, the inescapable 'side effect'—massive inherent artificial diffusion—destroys any possibility of an accurate solution. The effective grid Reynolds (Péclet) number can never exceed 2. Numerical 'solutions' bear little resemblance to correct results. [1,4,5]
- **'Remedy #3': Hybrid and Power-Law schemes.** These well-known convection-diffusion schemes are based on so-called 'exponential differencing'. The latter gives an *exact* solution to a one-dimensional, linear, steady, source-free, two-point boundary-value problem governed by the constant-coefficient convection-diffusion equation. For physical grid Péclet numbers greater than 2 (Hybrid) or about 6 (Power-Law), these methods revert to first-order upwinding for convection with modelled physical diffusion terms ignored. Unfortunately, they are often used out of context (e.g., in multidimensional flows), thereby introducing the problems of artificial diffusion associated with first-order upwinding. So-called 'cross-wind' diffusion (when the flow is oblique or skew to the grid) is especially damaging. [1,4,5,6]

B. Finite-Volume BHO Convection-Diffusion Schemes

- **Flux-form finite-volume methods; subcell interpolation.** If the governing differential equation is integrated over a control volume and averaged over time-step Δt , we obtain an explicit, forward-in-time update equation for the cell-averaged transport variable. This requires an estimate of the time-averaged, surface-averaged fluxes flowing across control-volume faces. If these estimated (convective-plus-diffusive) fluxes are *unique to each face*, the method is conservative. We will discuss the concept of 'natural upwinding' in evaluating the fluxes. The actual form of an estimated flux depends on the assumed behavior of the subcell interpolation consistent with given cell-average data. [4,5,6,7]
- **One-dimensional sub-cell interpolants; piecewise polynomials.** A piecewise-constant subcell interpolant leads to first-order upwinding for convection with (physical) diffusion ignored. Piecewise-linear interpolants generate second-order methods. Downwind weighting corresponds to so-called 'central' differencing (strong phase lag); upwind weighting gives the second-order upwind method (strong phase lead)—this is upwind overkill! A velocity-direction-independent (VDI) linear interpolant results in Fromm's method (low phase error). A VDI piecewise-quadratic interpolant leads to the third-order QUICK scheme for steady flow and QUICKEST for unsteady flow. In general, VDI-based schemes have low phase error; higher-order VDI schemes are easily devised. We need to be very careful to distinguish between cell-average and nodal-point values. Similarly, there are subtle differences in truncation error between finite-difference and finite-volume formulations; the latter are generally a lot more accurate, [3,4,8]

- **BHO convection schemes for steady flow.** Polynomials are not appropriate for interpolating data involving discontinuities. Ideally, a high-accuracy *shape-preserving* VDI subcell interpolant would be optimal. Shape-preservation criteria are easily specified in one dimension using normalized variables. The normalized variable diagram (NVD) helps to categorize a number of well-known convection schemes. The shape-preserving universal limiter for steady flows is compared with the more restrictive total-variation-diminishing (TVD) limiter used in gasdynamics codes. Practical implementation (without IF statements) is achieved using the powerful Median function. [4,5,6,7,9,10]
- **Unsteady one-dimensional flow.** The explicit flux-integral method (FIM) can be used with various subcell interpolants. At third order (QUICKEST), there is a cross coupling between the effects of convection in estimating diffusion terms and vice versa. This can be clarified using a Taylor expansion of the complex amplitude ratio, G . For unsteady flows, the universal limiter has some additional (more restrictive) features—as does the TVD limiter. Contrary to ‘conventional wisdom’, explicit convection schemes *do not have any stability restrictions on Δt* —the so-called ‘CFL condition’ is irrelevant! Explicit large- Δt convection schemes, in conservative (or flux) form, are easy to devise in one dimension. [2,3,4,11]
- **Summary for Part I.** So-called ‘central’ convection schemes (of any order) are unnatural (being based on *downwind*-weighted subcell interpolants) and have very bad (lagging) phase error. They should *not* be used as a basis for CFD. Explicit or implicit artificial diffusion (involving spatial second derivatives) should be *totally shunned*. This eliminates all conventional CFD schemes, including second-order methods (with added artificial diffusion), first-order upwinding, and first/second-order methods such as Hybrid and Power-Law. Third-order (natural) upwinding—based on VDI quadratic subcell interpolation—is the rational basis for CFD; in particular, modelled physical diffusion is not corrupted; leading truncation error is a (dissipative) fourth spatial derivative. [Higher-order methods are progressively more computationally efficient; this is discussed in Part II.] Shape preservation is easily incorporated using the universal limiter. Contrary to common belief, explicit convection schemes *do not* have any stability restrictions on Δt . Bounded higher-order schemes are the appropriate way to tackle the unique challenges of highly convective transport.

PART II. ADVANCED CONCEPTS

A. Steady Multidimensional Flow

- **Control-volume formulation for steady multidimensional flow.** The effective face value (convection) and normal gradient (diffusion) are easily defined in terms of surface integrals involving subcell interpolants. As in one dimension, a number of well-known methods result from assuming various forms of subcell behavior. For first- and second-order methods, flux formulas have a coordinate-wise one-dimensional form normal to each face. At third order, transverse curvature terms appear if we work with node values—but not if we use cell averages. Higher-order VDI subcell interpolants should be explored, as computational efficiency increases monotonically with order: even though the operation count is higher, a coarser grid can be used leading to higher accuracy at reduced overall cost. Steady multidimensional flux limiters have the same form as their one-dimensional counterparts. [4,5,6,7,10]
- **Boundary conditions.** There is a popular misconception that higher-order methods imply intractably 'difficult' boundary-condition treatment. By using external pseudo-cells (pseudo-nodes), it is relatively straight forward to devise numerical boundary conditions *consistent* with the interior algorithm: simply extrapolate across the boundary, using all physical boundary information together with enough interior information to effect the subcell extrapolation to an appropriate degree of accuracy. Low-order boundary-condition treatment can seriously degrade the entire flow field, even when a high-order interior algorithm is used. Strongly varying boundary regions can sometimes be effectively handled using specially devised 'boundary-layer' functions, thereby reducing the need for expensive grid refinement. [1,4,6,7,12]

B. Unsteady Multidimensional Flow

- **The flux-integral method.** For highly convective flows, explicit fluxes through individual faces can be estimated by integrating over the area (2D) or volume (3D) defined by inflowing particle paths over time-step Δt . We assume the convecting velocity components are locally constant near each face; e.g., in 2D this leads to an integral over a flux-integral parallelogram. Given subcell information (consistent with cell-average data), approximate fluxes can thus be calculated. This process leads to a natural generalization of 1D formulas. As in 1D, VDI subcell interpolants correspond to algorithms with low phase error. Quadratic VDI interpolation leads to a uniformly third-order polynomial interpolation algorithm (UTOPIA) for convection and diffusion (including third-order convection-diffusion cross-coupling terms). This is the generalization of the 1D QUICKEST scheme and, in bounded form (UTOPIA limited), *should* form the basis of multidimensional CFD schemes. [4,11,13,14]

- **Unsteady multidimensional flux limiters.** For steady flow, 1D limiters can be successfully applied coordinate-wise in multidimensions. This is not the case in unsteady flow. The 1D unsteady universal limiter is not shape preserving in multidimensions; the TVD limiter can be shape preserving—but only under severe Δt restrictions (and it also results in gross distortion). Genuinely multidimensional unsteady flux limiters can be devised. This is a subject of recent research. [4,14,15]
- **Computational efficiency.** It is instructive to compare various transport schemes by testing them on a model problem (with a known exact analytical solution or highly accurate numerical or experimental results). Using a log-log scale, plot some measure of global error versus computational cost for each method, as the grid is refined over a wide range. This is called the ‘computational efficiency diagram’ (applicable to both steady and unsteady transport). We can then see at a glance which method has the lowest overall cost for a prescribed accuracy or which gives the best accuracy within a prescribed budget. As a general rule, computational efficiency increases monotonically with the formal order of the transport scheme, provided the results are well resolved over most of the flow domain. [4,7,17,18]
- **The operator-splitting dilemma.** For reasons to do with algorithmic complexity, the flux-integral method has Δt restrictions equivalent to requiring Courant numbers to be less than $O(1)$. Large- Δt explicit 1D schemes can be applied in multidimensions using operator splitting (sequential 1D updates in each coordinate direction). However, there are problems: if conservative (flux) form 1D schemes are used, the overall update is indeed globally conservative, but a serious ‘splitting error’ occurs: an initially constant transported scalar does not remain constant in general solenoidal convection fields—a kind of ‘numerical lumpiness’ is introduced; if ‘advective-form’ 1D schemes are used, constancy is preserved but the overall scheme is *not* conservative! This dilemma has very recently been resolved using the multidimensional advective-conservative hybrid operator (MACHO) method, conservative operator splitting for multidimensions with inherent constancy (COSMIC), and other related techniques. Strictly conservative and essentially shape-preserving results can be obtained (using an explicit forward-in-time update) without restrictions on the time step. [4,17,18,19]
- **Conclusions.** As in one dimension, third-order (natural) upwinding is the appropriate basis for multidimensional convection-dominated transport. Lower (first- or second-) order methods *should not be used*; neither should higher-order ‘central’ (necessarily even-order) methods. Computational efficiency increases monotonically with the formal order of the scheme. Multidimensional flux limiters can be applied to give highly accurate *bounded higher-order* transport schemes: inherent stability and efficiency with high accuracy in smoothly varying regions and sharp resolution of discontinuities without unphysical oscillations or artificial smearing. Conservative, constancy-preserving large- Δt explicit schemes (with essentially shape-preserving properties) can be constructed using a relatively minor modification of conventional operator-splitting techniques. Using bounded higher-order transport schemes of the type described, CFD can finally become a *reliable* predictive tool.

REFERENCES

1. B.P. Leonard, A Stable and Accurate Convective Modelling Procedure Based on Quadratic Upstream Interpolation. *Computer Methods in Applied Mechanics and Engineering*, **19**, 59–98, 1979.
2. B.P. Leonard, Note on the von Neumann Stability of Explicit One-Dimensional Advection Schemes. *Computer Methods in Applied Mechanics and Engineering*, **118**, 29–46, 1994.
3. B.P. Leonard, A.P. Lock, and M.K. MacVean, The NIRVANA Scheme Applied to One-Dimensional Advection. *International Journal of Numerical Methods for Heat and Fluid Flow*, **5**, 341–377, 1995.
4. B.P. Leonard, Bounded Higher-Order Upwind Multidimensional Finite-Volume Convection-Diffusion Algorithms. Chapter 1 in *Advances in Numerical Heat Transfer* (W.J. Minkowicz and E.M. Sparrow, eds.), Taylor and Francis, 1996.
5. B.P. Leonard, and J.E. Drummond, Why You Should Not Use ‘Hybrid’, ‘Power-Law’, and Related Exponential Schemes—There Are Much Better Alternatives. *International Journal for Numerical Methods in Fluids*, **20**, 421–442, 1995.
6. B.P. Leonard and Simin Mokhtari, Beyond First-Order Upwinding: The ULTRA-SHARP Alternative for Non-Oscillatory Steady-State Simulation of Convection. *International Journal for Numerical Methods in Engineering*, **30**, 729–766, 1990.
7. B.P. Leonard and Simin Mokhtari, ULTRA-SHARP Solution of the Smith-Hutton Problem. *International Journal of Numerical Methods for Heat and Fluid Flow*, **2**, 407–427, 1992.
8. B.P. Leonard, Order of Accuracy of QUICK and Related Convection-Diffusion Schemes, *Applied Mathematical Modelling*, **19**, 640–653, 1995.
9. P.H. Gaskell and A.K.C. Lau, Curvature-Compensated Convective Transport: SMART, a New Boundedness-Preserving Transport Algorithm. *International Journal for Numerical Methods in Fluids*, **8**, 617–641, 1988.
10. B.P. Leonard, Simple High-Accuracy Resolution Program for Convective Modelling of Discontinuities, *International Journal for Numerical Methods in Fluids*, **8**, 1291–1318, 1988.
11. B.P. Leonard, The ULTIMATE Conservative Difference Scheme Applied to Unsteady One-Dimensional Advection. *Computer Methods in Applied Mechanics and Engineering*, **88**, 17–74, 1991.
12. T. Hayase, J.A.C. Humphrey, and R. Greif. A Consistently Formulated QUICK Scheme for Fast and Stable Convergence Using Finite-Volume Iterative Calculation Procedures. *Journal of Computational Physics*, **98**, 108–118, 1992.
13. B.P. Leonard, M.K. MacVean, and A.P. Lock, The Flux Integral Method for Multidimensional Convection and Diffusion. *Applied Mathematical Modelling*, **19**, 333–342, 1995.
14. B.P. Leonard, M.K. MacVean, and A.P. Lock, Positivity-Preserving Numerical Schemes for Multidimensional Advection, NASA TM 106055, ICOMP-93-05, NASA Lewis Research Center, Cleveland, OH, 1993.
15. J. Thuburn, Multidimensional Flux-Limited Advection Schemes. *Journal of Computational Physics*, **123**, 74–83, 1996.
16. B.P. Leonard and M.K. MacVean, Grid-Refinement Study of a Benchmark Problem Using the Flux-Integral Method. In *Quantification of Uncertainty in Computational Fluid Dynamics* (R.W. Johnson and E.D. Hughes, eds.) 45–50, ASME New York, 1995.
17. B.P. Leonard, A.P. Lock, and M.K. MacVean, Conservative Explicit Unrestricted-Time-Step Multidimensional Constancy-Preserving Advection Schemes. *Monthly Weather Review*, **124**, 2588–2606, 1996.
18. S.J. Lin and R.B. Rood, Multidimensional Flux-Form Semi-Lagrangian Transport Schemes. *Monthly Weather Review*, **124**, 2046–2070, 1996.
19. B.P. Leonard, A.P. Lock, and M.K. MacVean, Extended Numerical Integration for Genuinely Multi-dimensional Advective Transport Insuring Conservation. In *Numerical Methods in Laminar and Turbulent Flow*, Vol. 9 (C. Taylor and P. Durbetaki, eds.), 1–12, Pineridge Press, 1995.
20. P.J. Roache, A Flux-Based Modified Method of Characteristics. *International Journal of Numerical Methods in Fluids*, **15**, 1259–1275, 1992.
21. C.J. Freitas, Editorial Policy on Reporting Numerical Uncertainty. *ASME Journal of Fluids Engineering*, **115**, 339–340, 1993.

The Flux-Form Semi-Lagrangian Transport Scheme and its Applications in Atmospheric Models

S.-J. Lin

Joint Center for Earth Systems Technology

University of Maryland Baltimore County and NASA-GSFC, USA

1. Introduction

It is generally agreed that for constituent transport (advection) upstream-biased schemes, Eulerian or semi-Lagrangian, are superior to traditional spectral or center differencing schemes (Rood 1987, Tremback et al. 1987, Allen et al. 1991, Williamson and Rasch 1989, Lin et al. 1994, and Lin and Rood 1996). Although non-conservative, semi-Lagrangian schemes based on the advective form of the conservation law are very popular due to their clear computational advantage on the sphere (Staniforth and Côté 1991). Eulerian upstream-biased schemes, on the other hand, are generally based on the flux form of the conservation law and are therefore inherently conservative. Unfortunately, among other problems, the pole singularity poses too severe a stability restriction on Eulerian flux-form schemes. Rasch (1994) proposed the use of a spherical reduced grid to counter this "pole-Courant number problem". Other approaches of easing the severe time step restriction associated with the pole singularity include the use of a polar filter and the so-called operator (in time and/or in space) splitting, as has been successfully used by Allen et al. (1991) and Lin et al. (1994). With time splitting, different time steps can be taken at different latitudes to satisfy local Courant-Friedrichs-Lewy (CFL) stability condition.

A undesirable consequence of the operator splitting approach is that the continuity equation of the constituent can become inconsistent with the underlying continuity equation of the background air. This error is often called "splitting error". Ideally, the flux form constituent continuity equation should degenerate to the flux form continuity equation of the air itself for an initially constant constituent mixing ratio field; deformational error could be generated otherwise. This problem is most severe when the continuity equation of the

background fluid is non-hyperbolic (e.g., incompressible flow or hydrostatic flow using pressure coordinate in the vertical direction). In the continuing quest for an optimal transport scheme on the sphere, Lin and Rood (1996) presented solutions to the aforementioned problems by extending the 1D Eulerian flux-form transport schemes to semi-Lagrangian and to multidimensions. Important attributes of Lin and Rood's Flux-Form Semi-Lagrangian (FFSL) scheme are as follows:

- 1) Mass conserving (local and global).
- 2) Multi-dimensional Algorithm with freedom to choose underlying 1D schemes (e.g., PPM, collela and Woodward, 1984).
- 3) Monotonicity preserving in 1D; relatively easy to enforce a Multidimensional Flux-Corrected Transport Algorithm (MFCT, Zalesak, 1979).
- 4) Stable for Courant number > 1 .
- 5) "Quasi-linear" in the following sense:

$$p^n = \alpha q^n + \beta \quad \Rightarrow \quad p^{n+1} = \alpha q^{n+1} + \beta$$

where p and q are mixing ratio-like quantities, and α and β are arbitrary constants.

Lin and Rood's multidimensional FFSL scheme is reviewed in section 2. In section 3, the "reverse engineering" procedure for applying the FFSL transport scheme to a complete dynamical framework is introduced (see Lin and Rood 1997 for details). Some related modeling works are discussed in section 4.

2. The multidimensional FFSL scheme on the sphere - a brief review

The multidimensional FFSL scheme is derived from a direction-split perspective using strictly 1D operators. A procedure is then applied to remove the directional bias and the dominant (first-order) error resulting from the splitting approach. We will only highlight the development of the 2D FFSL transport scheme. Detailed derivation as well as error and stability analyses are given in Lin and Rood (1996). The conservation law (the transport equation) for a density-like field Q (e.g., in the context of the shallow water equations, Q may represent the depth of the fluid and/or the absolute vorticity) is

$$\frac{\partial}{\partial t} Q + \nabla \cdot (\mathbf{V} Q) = 0 \tag{2.1}$$

where $\mathbf{V} = (u, v)$ is the horizontal vector velocity. To model Eq. 2.1, we define F and G as the 1D flux-form operators for updating Q for one time step in the zonal (λ) and meridional (θ) direction, respectively. The 1D operators are assumed only to be 1D finite-volume scheme, but no explicit form of the 1-D operator is assumed a priori. Adopting the following standard difference δ and average $(\bar{\quad})$ notations,

$$\delta_{\sigma} q = q\left(\sigma + \frac{\Delta\sigma}{2}\right) - q\left(\sigma - \frac{\Delta\sigma}{2}\right) \quad (2.2)$$

$$\overline{q}^{\sigma} = \frac{1}{2} \left[q\left(\sigma + \frac{\Delta\sigma}{2}\right) + q\left(\sigma - \frac{\Delta\sigma}{2}\right) \right] \quad (2.3)$$

F and G can be written as follows:

$$F(u^*, \Delta t; Q^n) = - \frac{\Delta t}{A \Delta \lambda \cos \theta} \delta_{\lambda} \left[X(u^*, \Delta t; Q^n) \right] \quad (2.4)$$

$$G(v^*, \Delta t; Q^n) = - \frac{\Delta t}{A \Delta \theta \cos \theta} \delta_{\theta} \left[\cos \theta Y(v^*, \Delta t; Q^n) \right] \quad (2.5)$$

where A is the radius of the sphere, λ the longitude, and θ the latitude. X and Y , the time-averaged fluxes of Q in the zonal and meridional direction, respectively, are defined as

$$X(u^*, \Delta t; Q^n) = \frac{1}{\Delta t} \int_t^{t+\Delta t} u Q dt - hot \quad (2.6)$$

$$Y(v^*, \Delta t; Q^n) = \frac{1}{\Delta t} \int_t^{t+\Delta t} v Q dt - hot \quad (2.7)$$

where “*hot*” stands for the “higher order terms”. To approximate the “time-averaged flux” X (or Y) across the boundaries of the grid cell, a properly defined time-averaged (or time-centered) winds, (u^*, v^*) , and the cell-averaged field at time-level n , Q^n , are required. The fluxes are then used for updating the cell-averaged fields to the next time level. As illustrated in Fig. 1, the advective winds and the cell-averaged Q field (the “mass”) are defined on the C-grid. For convenience, we will omit, in the rest of this section, the dependence of the F and G operators on (u^*, v^*) and Δt .

Cross-derivative terms that are essential to a scheme’s stability in multidimensions are automatically included by applying the 1D operators sequentially. However, the sequential splitting process introduces a “splitting error” term, which is usually directionally asymmetric. The transport scheme is therefore directionally biased. The first step to achieving the desired multidimensionality is to remove directional biases by averaging two anti-symmetric operator-split algorithms (F followed by G , or G followed by F). The resulting directional bias free algorithm is

$$Q^{n+1} = Q^n + F [Q^n + \frac{1}{2} G (Q^n)] + G [Q^n + \frac{1}{2} F(Q^n)] \quad (2.8)$$

Scheme (2.8) still suffers from the “deformational error”. An immediate consequence of this error is that a constant Q field will not remain constant in a non-divergent flow. Furthermore, it can be verified that linear correlation between constituents will not be preserved by the above algorithm. To address these problems, the second step is to replace F and G inside the square brackets in (2.8), the contributions from the cross-stream directions, with their *advective-form* counter part f and g , respectively, to arrive at the following form of the 2D FFSL scheme:

$$Q^{n+1} = Q^n + F [Q^n + \frac{1}{2} g (v_a^*, \Delta t; Q^n)] + G [Q^n + \frac{1}{2} f (u_a^*, \Delta t; Q^n)] \quad (2.9)$$

where

$$u_a^* = \overline{u^*}^\lambda, \quad v_a^* = \overline{v^*}^\theta$$

Remark: In principle, one can use the traditional advective-form semi-Lagrangian scheme to approximate f and g . In practice, it is more convenient to simply use the following “deformation compensation technique”:

$$\begin{aligned} f(Q^n) &= F(Q^n) - Q^n F(Q=1) \\ &= F(Q^n) + Q^n C_{def}^\lambda \end{aligned}$$

where C_{def}^λ is the “deformational Courant number” (or the Lipschitz number).

Scheme 2.9 is free of the deformational error, and preserves linear constituent correlation exactly even when a monotonicity constraint is enforced. In the context of the shallow water system, transport of the fluid depth (h) and the absolute vorticity (Ω) by Scheme 2.9 ensures that h and Ω are better correlated during the time marching, which in turn ensures that the Potential Vorticity ($PV = \Omega/h$), a very important dynamical quantity, is better simulated.

The generalization of the scheme 2.9 to large time step (Courant number greater than one), which only involves slight modification to the 1D operators, is described in Lin and Rood (1996). Equation 2.9 will be used in the next section to discretize the transport equations for the “mass” (h) and the “absolute vorticity” (Ω) in the shallow water system of equations.

Lin and Rood (1996) presented some 1D and 2D examples of the FFSL scheme. It is noted here that the PPM based 2D FFSL scheme (FFSL-3) is computationally very efficient on the sphere. It is only about 2.2 times more expensive than the first order “super donor cell” scheme (FFSL-1, see Table 6, Lin and Rood 1996). However, the FFSL-3 scheme is not strictly monotonic because the 1D PPM monotonicity constraint is applied independently in the two spatial directions. Monotonicity in multidimensions can be enforced by a semi-Lagrangian generalization of Zalesak’s MFCT algorithm.

3. The FFSL discretization of the shallow water equations on the sphere

The mass conservation law for a shallow layer of “water” is

$$\frac{\partial}{\partial t} h + \nabla \cdot (\mathbf{V} h) = 0 \quad (3.1)$$

where h represents the depth of the fluid (the “mass” in the shallow water system). The vector invariant form of the momentum equation in the spherical coordinates can be written concisely in component form as follows.

$$\frac{\partial}{\partial t} u = \Omega v - \frac{1}{A \cos \theta} \frac{\partial}{\partial \lambda} [\kappa + \Phi] \quad (3.2)$$

$$\frac{\partial}{\partial t} v = -\Omega u - \frac{1}{A} \frac{\partial}{\partial \theta} [\kappa + \Phi], \quad (3.3)$$

where

$\Phi = \Phi_s + gh$, the free surface geopotential (g is the gravitational acceleration),

$\Phi_s =$ the surface geopotential,

$\Omega = 2\omega \sin \theta + \nabla \times \mathbf{V}$, the absolute vorticity,

$\omega =$ angular velocity of the earth,

$\kappa = \frac{1}{2} \mathbf{V} \cdot \mathbf{V}$, the kinetic energy.

A significant advantage of this form of the momentum equation is that the metric terms, which are singular at the poles, are absorbed into the definition of the relative vorticity, which is well defined (i.e., non-singular) at the poles. A disadvantage of this form is that the numerical form of the kinetic energy κ needs to be carefully formulated to minimize inconsistency between $\nabla \kappa$ and the absolute vorticity fluxes. This inconsistency manifests

itself as a spurious momentum source and could result in what is called “Hollingsworth-Källberg instability” (Hollingsworth et al. 1983).

The conservation law for the absolute vorticity can be readily obtained by taking curl of the vector momentum equation [i.e., $\nabla \times (3.2, 3.3)$]

$$\frac{\partial}{\partial t} \Omega + \nabla \cdot (\mathbf{V} \Omega) = 0. \quad (3.4)$$

The divergence ($\eta = \nabla \cdot \mathbf{V}$) equation is obtained by applying the divergence operator to the same vector equation. If the vorticity-divergence form is chosen, a way must be found to invert the pair (Ω, η) back to (u, v) each time step for the time integration to proceed. The spectral transform method is ideally suited for this purpose because the inversion is nearly trivial. Due to the continuous differentiability of the basis functions used in the spectral transform method, there is no theoretical advantage for the spectral method to choose the vorticity-divergence form over the usual or the vector-invariant form of the momentum equations described above. There is, however, advantage for choosing the vorticity-divergence form when local discretization methods are used (The “Z grid”, Randall 1994). Part of the advantage can be explained by the fact that the transport of the (absolute or relative) vorticity, a higher order conservative scalar, is being modeled directly. To retain this advantage while avoid inverting an elliptic equation, the idea introduced by Sadourny (1975) and Arakawa and Lamb (1981, AL hereafter) can be generalized to discretize the vector-invariant form of the momentum equations. AL’s method amounts to a subtle second order center-in-space discretization to (3.1), (3.2), and (3.3). Some design constraints are enforced to ensure that, after taking curl of the center differenced form of (3.2) and (3.3), the resulting vorticity equation is reduced to the celebrated “Arakawa Jacobian” for vorticity advection (Arakawa 1966) when the flow is non-divergent. The approach developed here in some ways mirrors that of AL’s, but in other ways is a complete opposite to their approach. The fundamental departures from their approach are outlined next.

The first and the most important difference is in the transport scheme itself and in the way absolute vorticity is transported in a more general divergent flow. AL’s method is a center-differenced scheme and therefore it is possible to conserve both the total energy and potential enstrophy, in the point-wise sense. A subgrid scale mixing parameterization is generally required for realistic flows. In our approach, we seek to build the subgrid mixing process into the grid-scale transport process by using a physically motivated upstream-biased monotonicity-preserving finite-volume scheme — the multidimensional FFSL

scheme. It is applied explicitly to the transport of the fluid depth h and implicitly to the absolute vorticity Ω . The discretized h and Ω are considered as cell-averaged values, not point-wise values. Because the implied subgrid distribution is forced to be monotonic, no additional damping (subgrid scale mixing) mechanism is needed. The same scheme is used for transporting h and Ω , regardless of the divergence of the flow. Functional relations between h and Ω can therefore be better preserved. In AL's approach, the equation for the fluid depth (Eq. 3.1) is center differenced in a straightforward manner while (3.2) and (3.3) are center differenced, in a more sophisticated way, to achieve the goal of vorticity transport by the Arakawa Jacobian for nondivergent flow. Therefore, the transport scheme for h and Ω in AL's approach will be, in general, different. As a consequence, initial functional relationship between these two variables will be lost during the course of time integration. It is our view that the lost of the functional relation will have some negative impacts on the predictability of the flow.

To achieve the goal of transporting h and Ω in exactly the same manner, a basic requirement is that they be defined at the same point. Since our prognostic variables are h and (u, v) , instead of h and (Ω, η) , the D-grid arrangement (see Fig. 1) is the best choice. It is known that any grid, other than the C grid or the Z grid (Randall 1994), generates two-grid-interval gravity wave noises. We avoided this problem by computing the time-centered advective winds (u^*, v^*) directly on the C grid. We shall consider (u^*, v^*) as given and defer the discussion on how they are computed after the discretization of the governing equations on the D grid are presented.

It is observed that if the first term on the right hand side (r.h.s.) of 3.2 and 3.3, at the numerical level, is interpreted as the time-averaged latitudinal and longitudinal flux of the absolute vorticity, respectively, a consistently discretized absolute vorticity equation can be formed by taking curl, numerically, of these two discretized component equations. Directly from Eq. (2.9), the discretized transport equation for h and Ω are simply as follows.

$$h^{n+1} = h^n + F(u^*, \Delta t; h^\theta) + G(v^*, \Delta t; h^\lambda) \quad (3.5)$$

$$\Omega^{n+1} = \Omega^n + F(u^*, \Delta t; \Omega^\theta) + G(v^*, \Delta t; \Omega^\lambda) \quad (3.6)$$

where

$$(\)^\theta = (\)^n + \frac{1}{2} g [\overline{v^*}, \Delta t; (\)^n], \text{ and } (\)^\lambda = (\)^n + \frac{1}{2} f [\overline{u^*}, \Delta t; (\)^n]$$

It is stressed here that we will not actually update Ω^n to Ω^{n+1} . Instead, only the absolute vorticity fluxes will be used for the discretization of the r.h.s of Eq. 3.2 and 3.3. To complete the discretization of (3.2) and (3.3), the pressure gradient terms are discretized with the explicit "forward-backward scheme" (Mesinger and Arakawa 1976), which is stable and second order accurate if it is combined with a *forward-in-time* advection scheme such as the one used here. The final form of the momentum equations are

$$u^{n+1} = u^n + \Delta t \left\{ Y(v^*, \Delta t; \Omega^\lambda) - \frac{1}{A\Delta\lambda \cos \theta} \delta_\lambda \left[\kappa^* + \overline{\Phi^{n+1}^\lambda}^\theta \right] \right\} \quad (3.7)$$

$$v^{n+1} = v^n - \Delta t \left\{ X(u^*, \Delta t; \Omega^\theta) + \frac{1}{A\Delta\theta} \delta_\theta \left[\kappa^* + \overline{\Phi^{n+1}^\lambda}^\theta \right] \right\}, \quad (3.8)$$

where κ , the upstream-biased "kinetic energy" defined at the four corners of the cell (the hollow circles in Fig. 1), is formulated as

$$\kappa^* = \frac{1}{2} \left\{ X(u^*, \Delta t; u^n) + Y(v^*, \Delta t; v^n) \right\} \quad (3.9)$$

The above form of κ minimizes the inconsistency in the momentum equation and thus avoided the "Hollingsworth-Källberg instability". It is noted that (3.6) can be recovered by taking "curl" of the two components, (3.7) and (3.8), of the vector momentum equation. The time-centered winds $\mathbf{V}^* = (u^*, v^*)$ on the C grid are computed by advancing the advective winds at time level n on the C grid (obtained by spatial averaging) for a half time step. For clarity, we describe next the complete cycle of the time marching.

Assuming the time integration starts from time-level n , before updating the prognostic variables on the D grid for a full time step to time-level $n+1$, the time-centered advective winds (u^*, v^*) on the C grid are computed (cf., 3.7 and 3.8) as follows.

$$h^* = h^n + F(u_c^n, \frac{\Delta t}{2}; h^{\theta/2}) + G(v_c^n, \frac{\Delta t}{2}; h^{\lambda/2}) \quad (3.10)$$

$$u^* = u_c^n + \frac{\Delta t}{2} \left\{ Y(v^n, \frac{\Delta t}{2}; \Omega_c^{\lambda/2}) - \frac{1}{A\Delta\lambda \cos \theta} \delta_\lambda [\kappa^{**} + \Phi^*] \right\}, \quad (3.11)$$

$$v^* = v_c^n - \frac{\Delta t}{2} \left\{ X(u^n, \frac{\Delta t}{2}; \Omega_c^{\theta/2}) + \frac{1}{A\Delta\theta} \delta_\theta [\kappa^{**} + \Phi^*] \right\}, \quad (3.12)$$

where

$$\begin{aligned}
 h^{\lambda/2} &= h^n + \frac{1}{2} f(u_a^n, \frac{\Delta t}{2}, h^n), & h^{\theta/2} &= h^n + \frac{1}{2} g(v_a^n, \frac{\Delta t}{2}, h^n), \\
 \Omega_c^{\lambda/2} &= \Omega_c^n + \frac{1}{2} f(u_b^n, \frac{\Delta t}{2}, \Omega_c^n), & \Omega_c^{\theta/2} &= \Omega_c^n + \frac{1}{2} g(v_b^n, \frac{\Delta t}{2}, \Omega_c^n), \\
 u_b^n &= \overline{u^n}^\lambda, & v_b^n &= \overline{v^n}^\theta, \\
 u_c^n &= \overline{u_b^n}^\theta, & v_c^n &= \overline{v_b^n}^\lambda, \\
 u_a^n &= \overline{u_c^n}^\lambda, & v_a^n &= \overline{v_c^n}^\theta, \\
 \Omega_c^n &= 2\omega \sin \theta + \nabla \times \mathbf{V}_c^n,
 \end{aligned}$$

and κ^{**} , the upwind-biased kinetic energy defined at the mass point, is computed as

$$\kappa^{**} = \frac{1}{2} \left[X(u_a^n, \frac{\Delta t}{2}, u_c^n) + Y(v_a^n, \frac{\Delta t}{2}, v_c^n) \right] \quad (3.13)$$

After (u^*, v^*) are obtained, prognostic variables h^n and (u^n, v^n) are updated using Eq. 3.5, 3.7, and 3.8.

It is noted that the ‘‘divergence’’ of the advective winds (u^*, v^*) and the ‘‘curl’’ of the prognostic winds (u^n, v^n) , the relative vorticity, as well as the ‘‘mass’’ are defined at the same point. Therefore, as far as linear behavior of the system is concerned, this two-grid (C and D) system is essentially the same as Randall’s Z grid. Due to the use of the two-step procedure, there is no need to invert the vorticity and divergence, which is a great computational advantage.

The algorithm described above can be easily applied to a regional model if appropriate boundary conditions are supplied. There is formally no time step restriction associated with the advective processes. There is, however, a stability condition imposed by the gravity-wave processes, which are treated explicitly. For our intended application on the whole sphere, a polar filter is therefore recommended for computational efficiency. The purpose of the polar filter is to stabilize the short-in-length (and high-in-frequency) gravity waves that are being unnecessarily and unidirectionally resolved at very high latitudes in the zonal

direction. Numerical examples of the above algorithm can be found in Lin and Rood (1997).

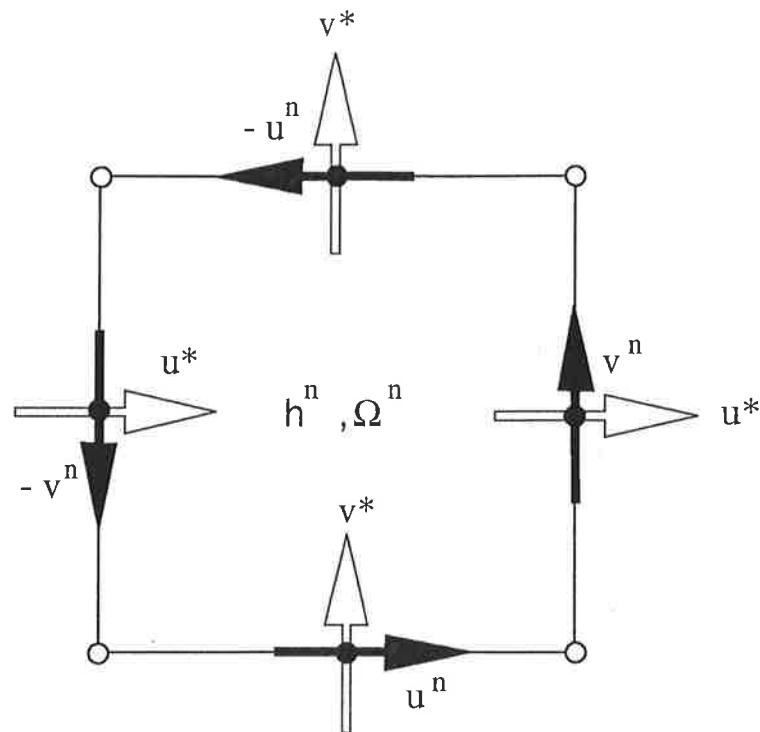


Fig. 1. Schematics of the two-grid system: the combined “CD grid”. The time-centered advective winds (u^* , v^*) (the hollow arrows) are staggered as in the C grid whereas the prognostic winds (u^n , v^n) (the solid arrows) are staggered as in the D grid. The cell-averaged relative vorticity is computed by the Stokes theorem.

4. Concluding Remarks

The Flux-Form semi-Lagrangian methodology for the shallow water equations can be easily extended to the hydrostatic primitive equations using a traditional hybrid sigma-P vertical coordinate (Lin 1997). We have recently developed a “Lagrangian Control-Volume” vertical coordinate for the 3D hydrostatic system, which is the basis of a dynamical core for the proposed next generation Goddard Earth Observing System General Circulation Model (GEOS-GCM).

References

- Allen, D. J., A. R. Douglass, R. B. Rood and P. D. Guthrie, 1991: Application of a monotonic upstream-biased transport scheme to three-dimensional constituent transport calculations. *Mon. Wea. Rev.*, **119**, 2456-2464.
- Arakawa, A., 1966: Computational design for long-term numerical integration of the equations of fluid motions: Two-dimensional incompressible flow. Part I. *J. Comput. Phys.*, **1**, 119-143.
- Arakawa, A., and V. R. Lamb, 1981: A potential enstrophy and energy conserving scheme for the shallow water equations. *Mon. Wea. Rev.*, **109**, 18-36.
- Colella, P., and P. R. Woodward, 1984: The piecewise parabolic method (PPM) for gas-dynamical simulations. *J. Comput. Phys.*, **54**, 174-201.
- Lin, S.-J., W. C. Chao, Y. C. Sud, and G. K. Walker, 1994: A class of the van Leer-type transport schemes and its applications to the moisture transport in a general circulation model. *Mon. Wea. Rev.*, **122**, 1575-1593.
- Lin, S.-J., and R. B. Rood, 1996: Multidimensional flux-form semi-Lagrangian transport schemes. *Mon. Wea. Rev.*, **124**, 2046-2070.
- Lin, S.-J., and R. B. Rood, 1997: An explicit flux-form semi-Lagrangian shallow water model on the sphere. To appear in *Quart. J. Roy. Met. Soc.*
- Lin, S.-J., 1997: A finite-volume integration method for computing pressure gradient forces in general vertical coordinates. To appear in *Q. J. Roy. Met. Soc.*
- Randall, D. A., 1994: Geostrophic adjustment and the finite-difference shallow-water equations. *Mon. Wea. Rev.*, **122**, 1371-1377.
- Rasch, P. J., 1994: Conservative shape-preserving two-dimensional transport on a spherical reduced grid. *Mon. Wea. Rev.*, **122**, 1337-1350.
- Rood, R., 1987: Numerical advection algorithms and their role in atmospheric transport and chemistry models. *Rev. Geophys.*, **25**, 71-100.
- Sadourny, R., 1975: The dynamics of finite difference methods of the shallow water equations. *J. Atmos. Sci.*, **32**, 680-689.
- Staniforth, A., and J. Côté, 1991: Semi-Lagrangian integration schemes for atmospheric models -- A review. *Mon. Wea. Rev.*, **119**, 2206-2223.
- Tremback, C. J., J. Powell, W. R. Cotton, and R. A. Pielke, 1987: The forward-in-time upstream advection scheme: Extension to higher orders. *Mon. Wea. Rev.*, **115**, 540-555.
- Williamson, D. L., and P. J. Rasch, 1989: Two-dimensional semi-Lagrangian transport with shape preserving interpolation. *Mon. Wea. Rev.*, **117**, 102-129.
- Zalesak, S. T., 1979: Fully multidimensional flux-corrected transport algorithms for fluid. *J. Comput. Phys.*, **31**, 335-362.

Recent Development in Transport Methods at NCAR

Philip. J. Rasch
National Center for Atmospheric Research¹
P.O. Box 3000-80307
Boulder CO 80307
(303)-497-1368 (office) (303)-4971324 (fax)
email: pjr@ncar.ucar.edu

and

Mark Lawrence
Max Planck Institute für Chemie
Postfach 3060
55020 Mainz, Germany
email: lawrence@mpch-mainz.mpg.de

Printed: February 20, 1998

¹The National Center for Atmospheric Research is sponsored by the National Science Foundation

1 Introduction

Numerical methods used for the transport of trace constituents are an important component of general circulation and chemical transport methods. But, in spite of the simplicity of the equations expressing this transport, solving the equations pose a formidable task, because we insist that the numerical solutions be accurate, and also satisfy a number of constraints Rasch and Williamson [1990a]. Some of the more important these constraints, in addition to accuracy are:

1. The solutions should be cost effective, that is, memory and computational costs should be sufficiently small that practical problems may be solved;
2. The solutions should be local, that is, the solution at any point should not be strongly influenced by what is going on far away from that point;
3. The solutions should be transportive, that is information should tend to propagate primarily *downwind*;
4. The solutions should be monotonic, that is, in the absence of divergence, the numerical method should not introduce new extrema in the solution, since the continuous form of the equations would not. It is this property that maintains the positive nature of the species mixing ratios or densities in a tracer simulation.
5. The solutions should be conservative, that is, some of the integral constraints expressed in the continuous equations should have an analogue in the discrete system. In the context of tracer transport problems we usually require that the mass within a volume be conserved, or that the change in mass within one volume have a corresponding compensating change in other volumes.

The solutions of transport equations in a spherical geometry pose other particular problems. The singularities at the pole and associated convergence of the longitudinal coordinate create what has become known as the 'pole problem'. We will not discuss most aspects of the pole problem, but one manifestation of it is that solutions on (approximately) regular latitude by longitude grids suffer by having very small cells in the vicinity of the pole. Many numerical methods require that the information be restricted to propagate some fraction of a cell distance in one time step, the so-call 'Courant-Friedrichs-Lewy', or CFL condition. This CFL restriction is often expressed in terms of a CFL number $C = u\Delta t/\Delta x < \text{constant } O(1)$, where u is the velocity, Δt the time step and Δx the cell width. When this time step restriction is exceeded, the solutions become unstable, and rapidly useless. Therefore, for methods suffering from CFL conditions, very small time steps are required with (approximately) regular spherical grids. One of the first techniques to overcome this restriction in meteorology was the 'semi-Lagrangian' technique of Robert [1982]. This technique has much more robust stability properties, and it is often cited as having no limit on the length of the time step. In fact the technique also has a stability restriction, expressible as a restriction on the Lipschitz number ($\|\frac{\partial u}{\partial x}\Delta t\| \leq 1$).

In practice this is equivalent to requiring that trajectories of parcels solved for within the semi-lagrangian method not be allowed to cross in one time step. In constant flow of course trajectories cannot cross, and thus for this special case there is no time step limitation other than that imposed by a need for reasonable accuracy. In the early 1990s, Rasch and Williamson [1990b] and Williamson and Rasch [1989] introduced a class of *shape preserving* semi-Lagrangian transport (SLT) methods that added the monotonicity property in the above list of desirable properties to this numerical method.

Monotonic versions of semi-Lagrangian transport (SLT) have proved to be a useful numerical framework for treating the advection process in GCMs and CTMs over the last decade. They are used in many applications around the world, due to their robust stability properties, lack of over- and undershoot, and local nature. Nevertheless, SLT schemes are not perfect. SLT methods are not inherently conservative (constraint 5 above), because they effectively sample different points in a fluid (with different parcel properties), and from the use of an advective form, rather than a flux form of the evolution equations. These methods also can have problems in the vicinity of the upper and lower boundaries in atmospheric models, because they require the velocity fields (and associated trajectory calculation) to be very consistent with the tracer field as the boundary is approached. The boundary condition formulation, and the lack of a strict conservation constraint sometimes interact with each other to form particularly troubling problems. The manifestation of these problems is discussed in some detail in Feichter (1998, this volume). To partially alleviate the conservation problems Williamson and Rasch [1989], and Rasch et al. [1995] have proposed ad-hoc conservation corrections to the solution that improve the solutions behavior, but they are not completely successful.

Finally, we have repeatedly encountered problems in the representation of transport at low resolution in the vicinity of the tropopause, where the atmosphere makes a transition from a relatively well mixed turbulent fluid to a stably stratified one. One important example of this problem occurs for the transport of trace species with a similar distribution to ozone, and this constitutes our test problem below.

Recently, another class of numerical methods have appeared that also have very robust stability properties. These are discussed in Leveque [1993], Lin and Rood [1996], Leonard et al. [1996a] from three very different (and each very useful) perspectives for one dimensional advection problems. Extensions to these one-dimensional methods have also been proposed that make them useful for multi-dimensional problems. These techniques also have a stability restriction very similar to that of the SLT method. But they have the advantage of being strictly conservative. This gain is not without penalty however. For large Courant numbers the schemes are no longer strictly monotonic. In practice the amount of overshoot or undershoot they introduce is very small and it is hoped to be tolerable. They are also somewhat more expensive (at least in our implementation) than SLT methods.

In this note we compare the solutions found by the two numerical methods for a prototypical problem that has been found to be particularly difficult for SLT methods, the simulation of an Ozone-like tracer with extremely steep gradients at the tropopause. This test problem was developed during the evaluation of our chemical transport model MATCH (Model for Atmospheric Transport and CHemistry) (Rasch et al 1997) with a photochemical module developed as a rather simple representation of ozone chemistry in the pristine troposphere [Lawrence, 1996]. It has since also manifested itself during the development of a more comprehensive CTM called MOZART that consists of MATCH with additional complex photochemistry, deposition and emission modules [Brasseur et al., 1996].

In section 2 we describe our form of the class of flux form methods mentioned above. In section 3 we describe the test problem, and in section 4 we show the results of simulations with the SLT scheme and our new method. Section 5 summarizes our conclusions about the new methods.

2 New fluxform method

We have developed a numerical method combining ideas gleaned from the formalisms of Leonard et al. [1995b], Lin and Rood [1996], Leonard et al. [1996b], Purnell [1976], Collela and Woodward, 1984; Hyman et. al. 1992; Leonard et al. [1995a], and others to construct a multi-dimensional flux form (conservative) scheme that is shape preserving. We will only describe the methodology schematically in this paper. More

detail will be provided in an upcoming paper.

The scheme works in the context of a tracer density $\tilde{\rho} = \rho m$, where ρ is an air density, and m a tracer mixing ratio. The conservation equation for the tracer density is

$$\frac{\partial \tilde{\rho}}{\partial t} = -\nabla \cdot \tilde{\rho} V$$

The multi-dimensional scheme is constructed by a sequence of one-dimensional updates. We first outline the one-dimensional scheme, and then describe its multi-dimensional extension.

2.1 The one-dimensional scheme

The one-dimensional updates solve the conservation equation

$$\frac{\partial \tilde{\rho}}{\partial t} = -\frac{\partial \tilde{\rho} u}{\partial a} \quad (1)$$

where a is the x , y or z coordinate.

The solution to equation (1) is inspired by Leonard et al. [1995a]. First an ‘integral’ or ‘primitive’ function Ψ is constructed

$$\Psi(a) = \int_0^a \tilde{\rho}(a') da' \quad (2)$$

The integral is calculated by assuming that $\tilde{\rho}_i$ represents the mean value within a cell, so the exact discrete integral at the cell walls $a_{i+1/2}$ is:

$$\Psi(\rho, a_{i+1/2}) = \Psi(\rho, a_{i-1/2}) + \tilde{\rho}_i \Delta a_i \quad (3)$$

where $\Psi(a_{1/2}) = 0$. Then the departure point for a particle arriving at each cell wall is defined as

$$a_{i+1/2}^{dp} = a_{i+1/2} - v_{i+1/2} \Delta t \quad (4)$$

The flux of mass through a cell wall is then just

$$F(\rho)_{i+1/2} = \Psi(a_{i+1/2}^{dp}) - \Psi(a_{i+1/2}) \quad (5)$$

and the discrete solution to (2) is

$$\tilde{\rho}^n = \tilde{\rho}^o - (F(\rho)_{i+1/2} - F(\rho)_{i-1/2}) / \Delta a_i \quad (6)$$

Since the a^{dp} 's are not located at a gridpoint, an interpolation is required. We use a *quasi-monotone uniformly 4th order accurate cubic interpolant*, that in principle provides no loss of accuracy at extrema (Huynh, 1991) of the integral function Ψ . This results in a C^1 continuous representation for Ψ whose derivative provides a 3rd order accurate representation to $\tilde{\rho}$. Because the integral values $\Psi_{i+1/2}$ are monotonic, no special treatment near extrema is required (there are no extrema). This formalism results in a 1-D conservative robust, positive definite solution valid for a non-uniform grid.

Although the interpolant for Ψ is monotonic, the solutions using this interpolant are merely positive definite. The addition of Leonard's ‘universal limiter’ makes the 1-D scheme strictly monotonic.

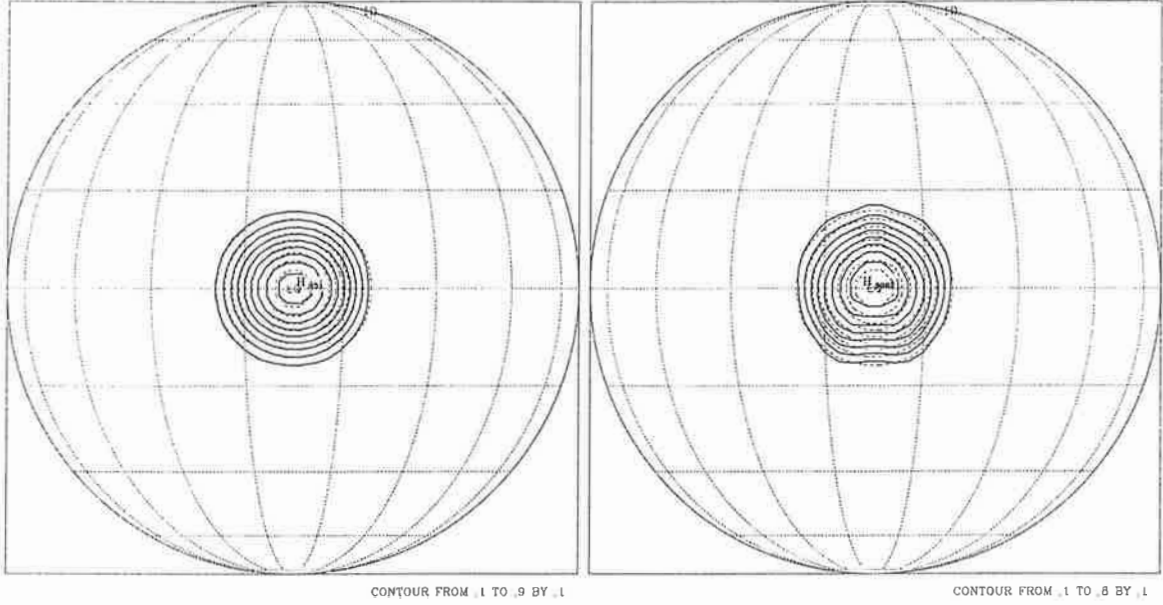


Figure 1: Solutions to the solid body rotation over the pole test. The solution has been integrated for 256 time steps.

2.2 Extensions to multi-dimensions

Again we have borrowed unabashedly from previous work, in this case the previous studies of Easter(1993), Lin and Rood (1996), Leonard et al. [1996a] and Li and Chang (1996). The horizontal transport is obtained by toggling eastwest and north south updates every other time step. We will refer to the 2 coordinates as coordinate a or b to keep them generic. The horizontal transport proceeds in three steps.

Step 1: We calculate the fluxes in direction a using (5). We also calculate an *advective* update to the density that represents the solution to the *advection equation*

$$\frac{\partial \tilde{\rho}}{\partial t} = -u \frac{\partial \tilde{\rho}}{\partial a}.$$

Note that in this case we are neglecting the divergence term in the evolution equation. We call the solution to this equation the *provisional advective update*, and solve this equation using the discretization

$$\tilde{\rho}^* = \tilde{\rho}^o - (F(\rho)_{i+1/2} - F(\rho)_{i-1/2})/\Delta a_i + \Delta t \rho^o (u_{i+1/2} - u_{i-1/2})/\Delta a$$

Step 2: We then calculate the fluxes in the other direction b , this time using the *provisional advective densities* $\tilde{\rho}^*$. We call these fluxes $G(\tilde{\rho}^*)$.

Step 3: Finally we update the horizontal solution with

$$\tilde{\rho}_{i,j}^n \Delta a_i \Delta b_j = \tilde{\rho}_{i,j}^o \Delta a_i \Delta b_j - (F(\rho^o)_{i+1/2} - F(\rho^o)_{i-1/2}) - (G(\tilde{\rho}^*)_{j+1/2} - F(\tilde{\rho}^*)_{j-1/2})$$

where i and j are indices in direction a and b respectively. As noted in other studies, because of the operator splitting and the large time step solution the result is shape preserving, but not strictly monotonic. In

practice all of the problems occur near the pole, and some special treatment is inevitably required. Lin has used a polar cap. Li and Chang have used extended grid zones near the pole. Here, we have used a simple one dimensional running mean filter in the zonal direction, and this seems sufficient to provide a monotonic solution. An example of the quality of the solution can be seen in the simple solid body rotation test of a cone over the pole and along the equator (figure 1). The test is performed on a standard spectral gaussian grid. Each test returns the cone to its starting point in 256 time steps. For the rotation over the pole, the Lipschitz number is ≈ 0.9997 for the 128x64 grid. The deformation number is very close to that point where the solution will become unstable. The accuracy of the solutions seen here is quite similar to that shown for Lin and Rood's and Li and Chang's solution. The rotation along the equator is performed very accurately. The tests of rotation over the pole is somewhat less accurate but still quite good.

3 The test problem

Because we have noted difficulties with SLT at the tropopause we have attempted to construct a test problem that reveals problems rapidly, and simply. Briefly, the test problem begins with the specification of initial conditions for a tracer that looks something like ozone. The tracer is small near the surface, and increases slowly to the vicinity of the tropopause. There, it jumps by a factor of 30 over 5 km, then continues to increase linearly to above 40 km. The initial conditions for the tracer are shown in figure 2. It is uniform in latitude and longitude. This test was performed in a chemical transport model (CTM) called the Model for Atmospheric transport and Chemistry (MATCH, [Rasch et al., 1997]). The test was performed using meteorological data from the NCAR CCM [Kiehl et al., 1997]. In order to isolate sensitivities to vertical resolution we have replaced the standard vertical SLT transport with the new vertical advection algorithm, and left the horizontal advection alone. The tracer is advected for 10 days in MATCH in a variety of configurations. First, the tracer is advected at the (low) nominal resolution of our CTM (in our case 18 levels spaced approximately 4 km apart near the tropopause, with a top about 35km). This is the nominal vertical resolution used for the CCM3. It is not ideal for a reasonable representation of cross-tropopause transport. Then the tracer integrations are repeated at a sequence of higher resolutions. *Each time the wind field is interpolated to the higher resolution in the vicinity of the tropopause by inserting a set of levels in between the original nominal resolution levels and linearly interpolating them.* In this way the tracer field is allowed to evolve at higher resolutions, in a wind field which is essentially unchanged. The sequence of higher resolutions gradually reduces the spatial discretization error to smaller and smaller amplitudes, and the 'true' (i.e. convergent solution) becomes evident. The highest vertical resolution is near that used at NCAR in problems involving interactions between the stratosphere and troposphere [Boville, 1995, Rasch et al., 1995, e.g.].

4 Results

In figures (3) and (4) we show the solution to the test problem at day 10 for two numerical methods for a sequence of three increases to the numerical resolution, from approximately 5km, to 2.5 km, to 1.25km, using respectively 18, 24 and 46 levels. The tick marks on the left side of figure (2) show the distribution of layers for the standard 18 level model used in configurations of CCM2, and CCM3 designed for tropospheric problems. The numerical method used in the left columns of figures (3) and (4) use the standard semi-Lagrangian numerical method we have developed and used for years in MATCH and CCM. The right column of those figures uses the new numerical method that is described above.

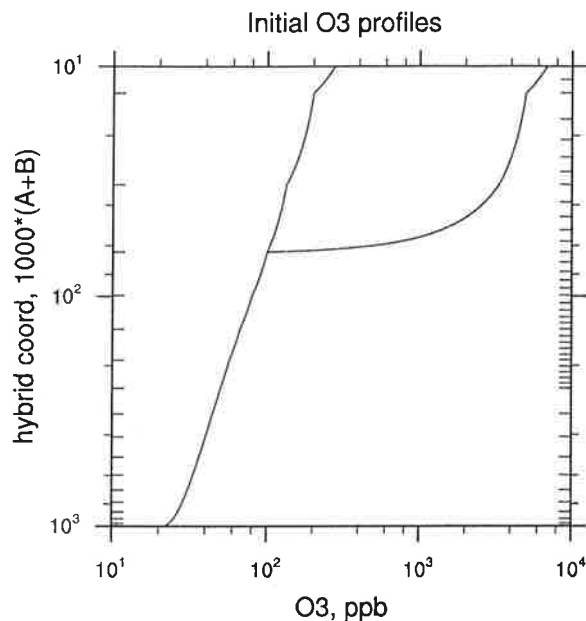


Figure 2: The initial conditions for the pseudo-ozone tests. Tic marks on left show the level structure for the 18 level model. Tics on right show the level structure for the 46 layer model.

Figure 3 shows the solution at about 100 hPa, just below the tropopause in the tropics, and above it in extratropical and polar regions. The top row of the figure shows that the solutions for the two numerical methods look very different at low resolution. As the resolution is increased to 25 layers (middle row), the simulations begin to converge, and by 46 layers, they are virtually identical. It is reassuring to see that both methods do converge to the (presumably) correct solution by a 1.25 km layer spacing, although it is distressing that the semi-Lagrangian solution is clearly converging much more slowly. The new vertical advection scheme looks virtually the same at all three vertical resolutions, suggesting that it has converged to the correct solution much more rapidly than the SLT scheme.

The picture is somewhat different 5 km higher, at about 65 hPa, above the tropopause in our models, and right at the discontinuity in the initial conditions (figure 4). Neither numerical method has converged at the 5km or 2.5km resolution. Interestingly, the SLT scheme seems to be converging to the correct solution slightly more rapidly. The downward transport in the extratropical vortices is present at 25 levels in the SLT scheme and much weaker in the new scheme. When one reaches 1.25km resolution one does see evidence that the two numerical methods are converging towards the same solution, but even then, significant differences are evident. To be the same, one would probably want to go to approximately 0.5km resolution in the vertical in order to feel comfortable that these solutions were not strongly affected by the numerics.

O3, day 10, eta=.099, IC = 80ppb

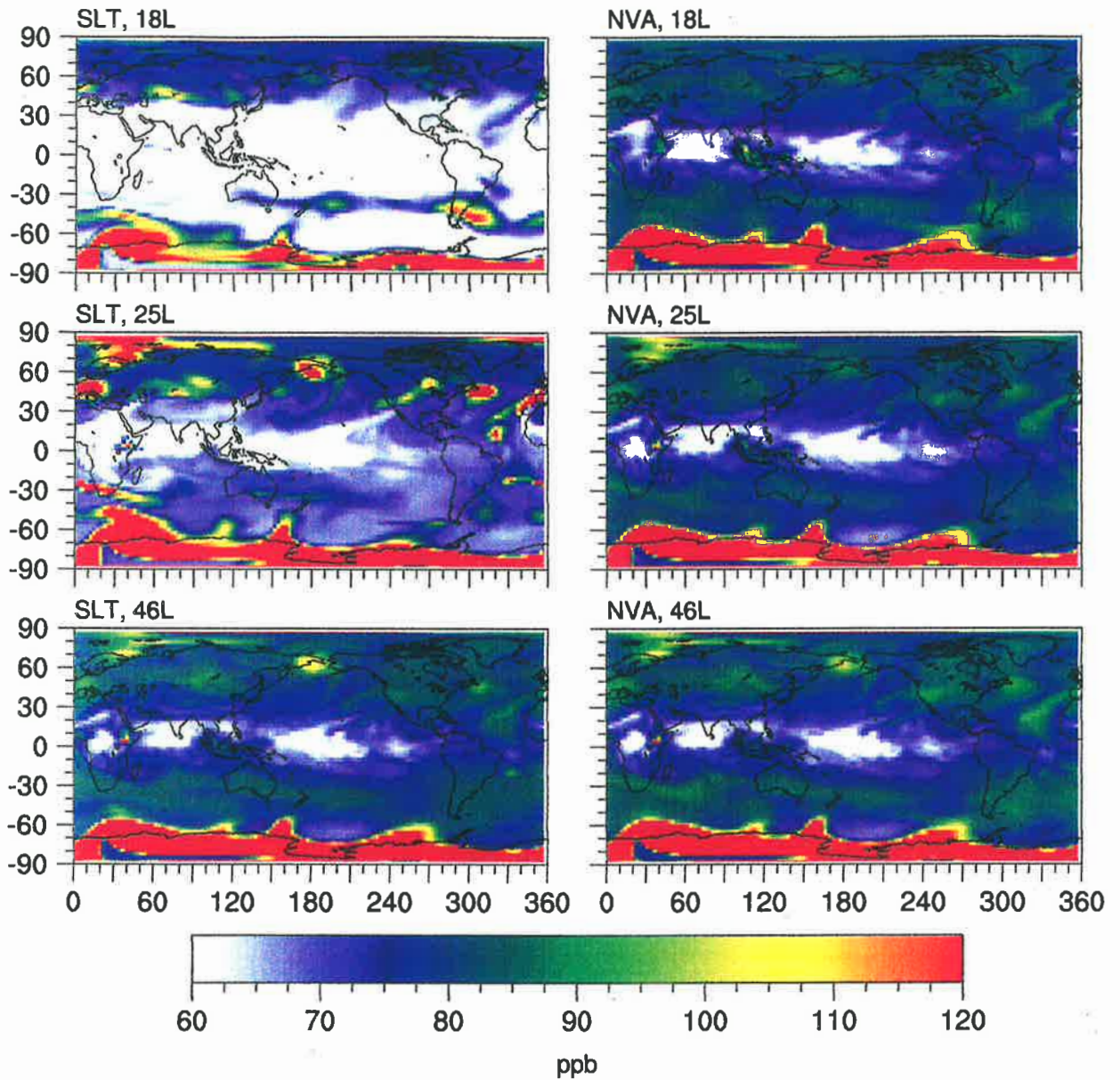


Figure 3: The mixing ratio of pseudo-ozone after 10 days at approximately 100 hPa. Left column shows the traditional semi-lagrangian transport. Right column shows the new flux form transport scheme. Upper panels show the solutions using an 18 level model. Middle panel show the solutions using 25 levels, and lower panels show the solution using 46 levels.

O3, day 10, eta=.064, IC = 100ppb

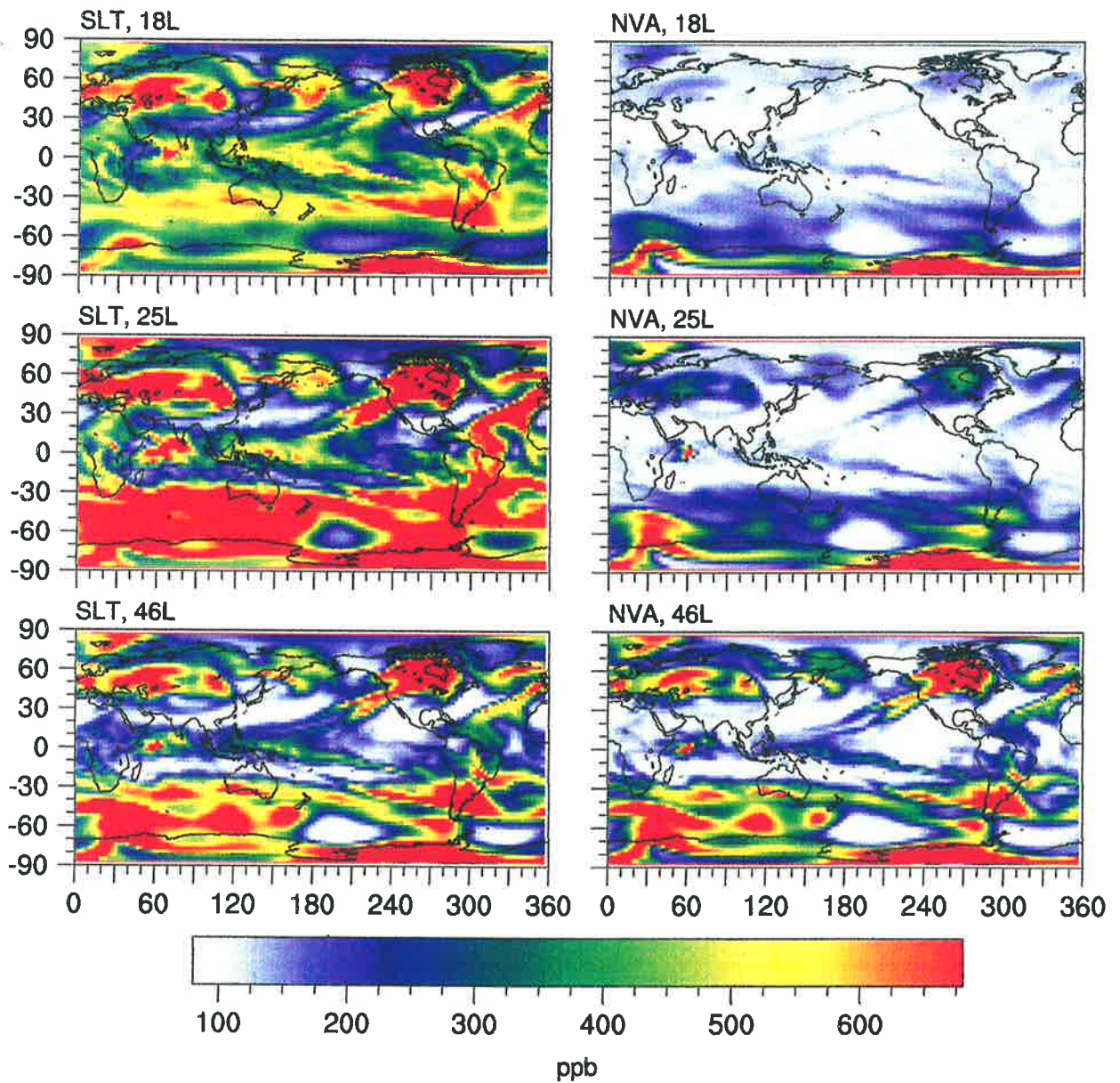


Figure 4: As in figure 3, except at approximately 65 Hpa.

5 Summary

We have introduced a new conservative advection algorithm, and compared its behavior to the popular semi-lagrangian transport (SLT) algorithm. For the test problem with an analytic solution, the new advection algorithm is perhaps a factor of 2 to 3 times more accurate. For the more realistic problem of a tracer similar to ozone the results are mixed. There are situations where the new advection algorithm is clearly superior, and situations where the new advection algorithm seems somewhat inferior. These two tests reveal differences in the advection algorithms when used in a 'horizontal transport only' comparison and a 'vertical transport only' comparison. We have also examined the model behavior for a much broader class of practical problems where both the horizontal and vertical transport is replaced, but all other processes are held identical within the model. These comparisons will be made elsewhere, but we can say that the chief advantages of the new scheme tend to be:

- It is strictly conservative, and it is possible connect the fluxes across regions to mass changes within the domain. This eases significantly improves ones ability to interpret the model results.
- Unlike the SLT method, it is natural to specify the numerical solution in terms of a no flux boundary condition and the solutions using new and SLT schemes can look quite different in the vicinity of the boundaries.

It is also worth noting however that in situations within the free atmosphere where the solutions differ, the only method that provides confidence in the result is to increase the resolution. And we also note here that the solutions tend to look the most different when there are no other processes (ie sources or sinks) entering the problem. When other processes are important the simulations become nearly indistinguishable.

References

- B. A. Boville. Middle atmosphere version of ccm2 (maccm2): Annual cycle and interannual variability. *J. Geophys. Res.*, 100:9017-9039, 1995.
- G. P. Brasseur, D. A. Hauglustaine, and S. Walters. Chemical compounds in the remote pacific troposphere: Comparison between MLOPEX measurements and chemical transport model calculations. *J. Geophys. Res.*, 101:14795-14813., 1996.
- J. T. Kiehl, J. J. Hack, and J. W. Hurrell. The energy budget of the NCAR Community Climate Model (CCM3). *J. Clim.*, 1997. submitted.
- M. G. Lawrence. *Photochemistry in the tropical pacific troposphere: Studies with a global 3D chemistry meteorology model*. Ph.D. thesis, Georgia Institute of Technology., Atlanta, GA., 1996.
- B. P. Leonard, A. P. Lock, and M. K. MacVean. The NIRVANA scheme applied to one-dimensional advection. *Int. J. Numer. Methods Heat Fluid Flow*, 5:341-377, 1995a.
- B. P. Leonard, A. P. Lock, and M. K. MacVean. Conservative explicit unrestricted-time-step multidimensional constancy-preserving advection schemes. *Mon. Weather Rev.*, 124:2588-2606, 1996a.
- B. P. Leonard, A. P. Lock, and M. K. MacVean. Conservative explicit unrestricted-time-step multidimensional constancy preserving advection schemes. *Mon. Weather Rev.*, 124:2588-2606, 1996b.

- B. P. Leonard, M. K. MacVean, and A. P. Lock. The flux integral method for multidimensional convection and diffusion. *Appl. Math. Modelling*, 19:333-342, 1995b.
- R. J. Leveque. High-resolution conservative algorithms for advection in incompressible flow. Technical Report 93-03, University of Washington, Seattle, WA., 1993.
- S.-J. Lin and R. Rood. Multi-dimensional flux-form semi-lagrangian transport schemes. *Mon. Weather Rev.*, 124:2046-2070, 1996.
- D. K. Purnell. Solution of the advective equation by upstream interpolation with a cubic spline. *Mon. Weather Rev.*, 104:42-48, 1976.
- P. J. Rasch, B. A. Boville, and G. P. Brasseur. A three-dimensional general circulation model with coupled chemistry for the middle atmosphere. *J. Geophys. Res.*, 100:9041-9071, 1995.
- P. J. Rasch, N. M. Mahowald, and B. E. Eaton. Representations of transport, convection and the hydrologic cycle in chemical transport models: Implications for the modeling of short lived and soluble species. *J. Geophys. Res.*, 1997. this issue.
- P. J. Rasch and D. L. Williamson. Computational aspects of moisture transport in global models of the atmosphere. *Q. J. R. Meteorol. Soc.*, 116:1071-1090, 1990a.
- P. J. Rasch and D. L. Williamson. On shape-preserving interpolation and semi-lagrangian transport. *SIAM J. Sci. Stat. Comput.*, 11:656-687, 1990b.
- A. Robert. A semi-lagrangian and semi-implicit numerical integration scheme for the primitive meteorological equations. *J. Meteorol. Soc. Jpn.*, 60:319-325, 1982.
- D. L. Williamson and P. J. Rasch. Two-dimensional semi-lagrangian transport with shape preserving interpolation. *Mon. Weather Rev.*, 117:102-129, 1989.

Design of a semi-implicit cell-integrated semi-Lagrangian model

by

Bennert Machenhauer and Markus Olk

Max Planck Institute for Meteorology, Hamburg, Germany

Abstract

In a cell-integrated semi-Lagrangian (CISL) transport scheme considered here trajectories are constructed backward in time from the corner points of a grid cell, thereby defining the extent of the cell at a previous time. The predictive variables being advected are considered to be averaged values over the cell rather than point values. The determination of the averaged values over the irregular cells at the previous time level is called a remapping. By choosing integral invariants (e.g. mass, angular momentum, total energy) as the predicted variables and an explicit time scheme the application of the CISL scheme gives a model which conserves exactly these invariants in a locally consistent way.

A full set of baroclinic model equations, based on the primitive ones, for such a model was set up in Machenhauer (1994). This system would conserve exactly mass, total energy, angular momentum, entropy, humidity and last but not least important any passive tracer (e.g. chemical constituents) included in the model. In a subsequent paper Machenhauer and Olk (1996) investigated the numerical stability of simple one-dimensional shallow water model versions for which they also designed and tested two versions with semi-implicit time extrapolation. The two versions conserved exactly mass and momentum or mass and total energy, respectively.

Computational expensive remapping procedures have so far been a limiting factor for the use of CISL schemes. In the paper Machenhauer and Olk (1997) a new efficient 2D remapping procedure was designed and also formulations on the sphere were presented for a set of shallow water equations.

In Machenhauer (1994) a procedure for a consistent semi-Lagrangian time extrapolation of the hydrostatic continuity equation was proposed. It was building on a tracking backward the 3D cells which were assumed to move with vertical walls. It resulted in an implicit system of coupled linear equations in surface pressure, one equation for each horizontal grid point, which would be computational expensive to solve. A much less expensive time extrapolation has been designed. The new one is building on tracking backward only the horizontal grid cells, still assumed to move with vertical walls, and extrapolating forward in time the vertical grid intervals of pressure. Application of the hydrostatic equation then determine the vertical pressure interval of the grid cells at the new time level. The time extrapolation of the continuity equation is the basis for the extrapolation of all the prognostic variables.

So far the horizontal transport on the sphere of a passive scalar has been coded in the framework of the ECMWF IFS code and is being tested using monotonous parabolic distributions within each cell. Plans for the future are presented.

1 Introduction

The accuracy of atmospheric numerical models has steadily improved with enhanced resolution and improvements in physical parameterization schemes. This increase of accuracy, which has taken place for the relatively high resolution weather prediction models as well as for the lower resolution climate models, has been made possible due to the steadily growing computer power but also due to the introduction of more efficient numerical techniques. One such numerical technique was the semi-implicit time stepping scheme, which was introduced by André Robert (Robert, 1969, Kwizak and Robert, 1971) and is used now in most atmospheric models to eliminate the Courant-Friedrichs-Levy (CFL) time step restriction due to gravity waves. In semi-implicit models typically a six time larger time step than in the former explicit models can be used without loss of accuracy. The time step in the usual Eulerian semi-implicit models is limited only by the advective CFL restriction. Another important new technique, also introduced in meteorological applications by Robert (1981, 1982), is a semi-Lagrangian treatment of advection offering a potential further increased efficiency by elimination of the advective CFL time-step restriction. In principle, the time step in a combined semi-implicit semi-Lagrangian model can be chosen based on accuracy considerations. As developers of physical parameterizations are uncomfortable applying their schemes over time steps exceeding one hour (Williamson and Olson, 1994), this may put an upper bound to the time steps which can be used in practice. Significant computational savings can however be obtained in many applications, even within this limit.

The semi-Lagrangian advection offers additional advantages beyond the longer time-step. It gives minimal phase error, minimizes computational dispersion, can handle sharp discontinuities and furthermore desirable properties such as monotonicity or, more generally, shape preservation may be incorporated.

A disadvantage is that the smallest scales resolved may be damped more by semi-Lagrangian methods than by some Eulerian methods. However, this seems not to be a serious issue as it can be counteracted by a reduction or elimination of horizontal diffusion. A more serious disadvantage of semi-Lagrangian schemes today is that they do not formally conserve integral invariants as total mass or total energy. This may not be a problem in weather forecasting applications. For long simulations in climate applications, however, lack of conservation might have serious consequences. The total mass, in particular, has been found to drift significantly if no corrections are applied during longer integrations. Moorthi et al. (1994) report that the global mean surface pressure increased monotonously over a seventeen-month integration period. The rate of increase varied and at the end of this seventeen-month period it had increased 34 hPa from its initial value. In another case, reported by Machenhauer (1994), a three-month test integration with an early version of the ECMWF operational semi-implicit semi-Lagrangian model resulted in a systematic loss of mass corresponding to 4.5 hPa. Obviously in these cases errors in the prediction equation for surface pressure are accumulating. The mechanisms leading to these errors are not known and we can detect only the error in the global mean surface pressure field. Therefore, we know nothing about the three dimensional structure of the errors in the mass field. It seems likely, however, that the accumulating large errors in the mean surface pressure are accompanied by pressure errors locally which are even larger and which may be systematically correlated with the pressure pattern. If such a correlation exists the internal dynamics of

the model may be affected significantly. We do not know if this is the case, but it seems possible, and if it is the case the non-conservation is a symptom of some, perhaps more serious systematic errors.

Conservation of total mass may be obtained by a "mass-fixer" which after each time step restores the mean surface pressure to its initial value. Such a mass-fixer was tested by Moorthi et al. (1994) who repeated the above mentioned seventeen-month integration restoring after each time step the mean surface pressure by multiplying everywhere the preliminary calculated surface pressure by a constant factor equal to the ratio between the initial mean value and the preliminary mean value. This mass-fixer is similar to that used by (Williamson and Olson, 1994), except that they allow for variations in the total mass due to variations of water vapour. By this form of the mass-fixer the horizontal pressure gradient is not affected by a restoration and the effect on the internal dynamics is therefore minimized. When comparing seasonally averaged fields from the above mentioned seventeen-month integrations with and without mass restoration Moorthi et al. (1994) found no significant differences. Thus, with this type of mass-fixer the restoration does not seem to affect significantly the simulated climate. This result is not so surprising as the fixer as mentioned above was designed to have minimal effect on the dynamics. However, the restoration each time step with the same factor everywhere is of course completely arbitrary and most likely the geographical distribution of the corrections is wrong.

Recently Gravel and Staniforth (1993) have presented an alternative mass-fix procedure where the restoration of the mean pressure is made only in some specially selected points. They argue that the interpolation is likely to introduce the errors that cause the lack of conservation in areas of strong gradients and that the points where they make the corrections are exactly such points. A great deal of arbitrariness is, however, still present in their procedure with regard firstly to the magnitude of correction in each point (kind of equipartition among the points chosen) and secondly by choosing not to do any mass restoring corrections in those points in which the preliminary correction to fulfil monotonicity goes in the "wrong" direction.

2 The cell- integrated semi-Lagrangian scheme

In the present report we will advocate for a different approach towards incorporating conservation principles within the semi-Lagrangian framework. Namely to use special forms of the meteorological equations and special numerical schemes designed to conserve integral invariants exactly. Such a system based upon the full set of primitive equations was set up in Machenhauer (1994). Each of the prognostic equations in the system was written on the form

$$\frac{d}{dt}(X\delta M) = F_X + \delta M S_X \quad (1)$$

where δM is the mass of an infinitesimal particle moving with the flow, X is unity or the mean value over the particle of a conservative variable, F_X is a flux and/or pressure terms working at the surface of the parcel and S_X is a source term working inside the parcel. When X is unity ($X \equiv 1$), equation (1) is the continuity equation for which both right hand terms are zero. In the remaining equations of the system, X is specific total energy, specific angular momentum, specific entrophy, specific humidity or specific liquid water. In the discrete form of (1) grid point

values of X are assumed to be mean values over the surrounding grid cell. As the moving parcel in (1) we consider the air which at the end of a time step is ending up in a grid cell. It is tracked back in time using trajectories from the corner points of the grid cell. With a consistent evaluation of the flux terms F_X in neighboring grid cells and a conservative remapping of X at the previous time level the integral invariants valid for (2.1) are maintained also for the discrete form of the system. A model based on equations of the form (2.1) and in the finite-difference form as indicated above will be called a cell-integrated semi-Lagrangian (CISL) model.

After the initial design of the CISL system considered here it was realized that a somewhat similar system had been developed for the Navier-Stokes equations by Hirt et al. (1974) and had been applied to hydrodynamical problems. More similar in all respects to the cell-integrated scheme proposed here are the 2D advection schemes introduced and tested by Rancic (1992) and Laprise and Plante (1995). Although we did not know their works when our scheme was initially developed, the cell-integrated model system we propose may be considered as an extension to the complete 3D system of the meteorological equations of the scheme developed by Rancic (1992) and the similar one developed independently by Laprise and Plante (1995).

3 Linear stability and semi-implicit time-stepping

In Machenhauer (1994) we speculated that perhaps due to the conservation properties of a CISL model it might be absolutely stable even with an explicit time-stepping scheme. In Machenhauer and Olk (1996), however, experiments with simple one-dimensional versions showed that even such a model becomes unstable when the time step exceeds the critical value determined by the CFL criterion for gravity waves. The most unstable short waves are found to grow in amplitude even though total mass and total momentum or total mass and total energy are conserved exactly. When the amplitude has become large the trajectories begin to cross in some points which at once causes a break down of the conservation properties and subsequently leads to an "explosion".

In order for a CISL model to be able to compete with traditional semi-Lagrangian models it is essential that either a split-explicit or a semi-implicit time-stepping scheme can be introduced in the cell-integrated system. We have tried to develop a split-explicit version of the cell-integrated model which conserves mass and momentum or mass and total energy. It turned out, however, that it was not possible to design such a model without relaxing the requirement of exact conservation of these quantities. This is because when splitting the system of equations in an advective and an adjustment part each of these subsystems does not conserve total momentum or total energy, respectively. Without abandonment of the exact conservation properties this leaves us with the semi-implicit scheme as the other known possibility of an efficient time-stepping. From the start it was not obvious how the CISL scheme could be combined with the semi-implicit time stepping as firstly the divergence has been eliminated and appears indirectly in the trajectory positions and secondly because some of the prognostic variables are non-linear in the basic variables. For both one-dimensional energy conserving and momentum conserving versions, these difficulties were overcome in Machenhauer and Olk (1997) and semi-implicit models were established which maintain the conservation properties. In the one-dimensional model only two quantities, mass and an additional one, can be conserved exactly. In three dimensions, beside the mass of various forms of water variables and passive tracers,

four quantities can be conserved and the obvious choice is mass, angular momentum, total energy and entropy, as was done in Machenhauer et al. (1994). However, it seems not possible to chose total energy as one of the predictive variables when we want to use the semi-implicit scheme. This is due to the fact that we cannot linearize the expression for kinetic energy in two dimensions as we could in one dimension. We consequently have to choose an alternative third equation instead of (3). In the model we plan to set up we have intend to use the v-component of the momentum equation in vector form instead. The form of the momentum equation we will use is (the shallow water version for simplicity)

$$\frac{d}{dt}((Uhi\vec{i} + vhj\vec{j})\delta A) = -\delta A \nabla \frac{1}{2}gh^2 \quad (2)$$

in which the Coriolis term is included into the advective part. Here $U = u + 2a\Omega\cos\phi$, u , i , v and j are velocity components and unit vectors pointing towards the east and the north, respectively, and h is the height of the shallow water. (2.2) has been derived from the vector form of the momentum equation proposed by Rochas (1990) and Temperton (1994). We will use only the v-component which is derived from the discrete version of (2) (taking into account, of course, the changes of the orientation of the local coordinate system as one moves along the trajectories (Ritchie, 1988)).

4 An efficient remapping scheme

Computational expensive remapping procedures have so fat been a limiting factor for the use of the CISL scheme. In the paper Machenhauer and Oik (1997) a new efficient 2D remapping procedure were designed and also formulations on the sphere were presented for a set of shallow water equations.

We shall briefly sketch this new remapping procedure. Consider as an example the shallow water continuity equation. The Lagrangian form is

$$\frac{d}{dt}(h\delta A) = 0 \quad (3)$$

Where h is again the height of the fluid, which apart from a constant factor, the density, is equal to the mass in a column of unit cross section area. δA is the cross section area of a fluid column or a cell we follow and thus $h\delta A$ is proportional to the mass of the cell.

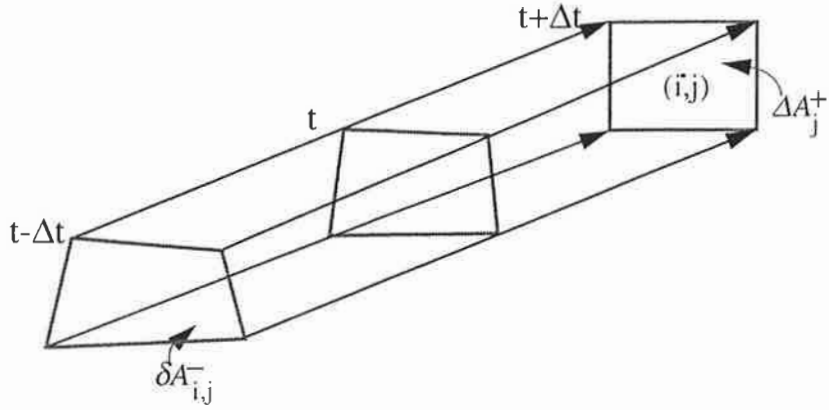


Figure 1: Illustration of the backward tracking of a grid cell in the CISL scheme.

As illustrated in Figure 1 we use a three-time-level scheme with time step Δt and determine the departure points at $t-\Delta t$ of trajectories which end up at the corner points of the grid cells. The trajectories are assumed to be great circles and are determined using the winds at time level t and the usual iterative procedure.

In the case of explicit time stepping we get the following discrete form of equation (3):

$$h_{i,j}^+ \Delta A_j = \overline{h_{i,j}^-} \delta A_{i,j}^- \quad (4)$$

The superscripts “+” and “-” denote the time levels $t+\Delta t$ and $t-\Delta t$, respectively. $\overline{h_{i,j}^-} \delta A_{i,j}^-$ denotes the integral of h at time level $t-\Delta t$ over the (i,j) -cell area, $\delta A_{i,j}^-$ (see Fig. 2.1):

$$\overline{h_{i,j}^-} \delta A_{i,j}^- = a^2 \int_{\delta A_{i,j}^-} \int h^- \cos \varphi d\varphi d\lambda = a^2 \int_{\delta A_{i,j}^-} \int h^- d\lambda d\mu \quad (5)$$

λ and φ are longitude and latitude, respectively, and $\mu = \sin(\varphi)$. We use the λ - μ coordinate system for the evaluation of such integrals because of the simple cartesian-coordinate-like expression we obtain for the integrals and assume that the sides in the quadrangle of area $\delta A_{i,j}^-$ are straight lines in this coordinate system.

At time level $t-\Delta t$ we have given the area mean values $\overline{h_{i,j}^-}$ in each of the “regular” grid cells (see Fig. 2.1). In order to evaluate the integral in (5) over grid cells in the irregular grid we may define analytical two-dimensional functions $\psi_{i,j}(\lambda, \mu)$ in each regular cell. Each function must have the correct mean value i.e. it must satisfy

$$\overline{h_{i,j}^-} = \frac{1}{\Delta A_j} \int_{\Delta A_j} \int \psi_{i,j}(\lambda, \mu) d\lambda d\mu \quad (6)$$

The simplest possibility is to assume piecewise constants for $\psi_{i,j}$, that is, $\psi_{i,j}(\lambda, \mu) = h_{i,j}^-$. This would imply discontinuities at the cell boundaries and rather severe damping during the integration, especially of small scales. To reduce the damping the assumption of a higher order polynomial than the piecewise constant one is necessary. Piecewise bipolarabolic functions were considered by Rancic (1992) to be a good compromise between the desired properties and the computational cost to determine them in each cell. The nine coefficients determining each such function were determined in such a way that (6) is satisfied and so that interpolated values at the cell corner points and side mid points were fitted exactly. The calculation of the coefficients for all the cells followed by the remapping, i.e. the determination of the integrals in (5), turns out to be very time consuming. In his comparison with a usual semi-Lagrangian cubic interpolation scheme Rancic (1992) found for pure advection that the cell integrated scheme with the bipolarabolic functions gave slightly better results, but needed 2.5 times more computer time. Obviously a more efficient method should be found if the CISL scheme should be competitive; as far as possible without scarifying the good performance with bipolarabolic representations. Such an alternative method were presented in Machenhauer and Olk (1996) and since then we have introduced an even simpler version which we shall describe briefly.

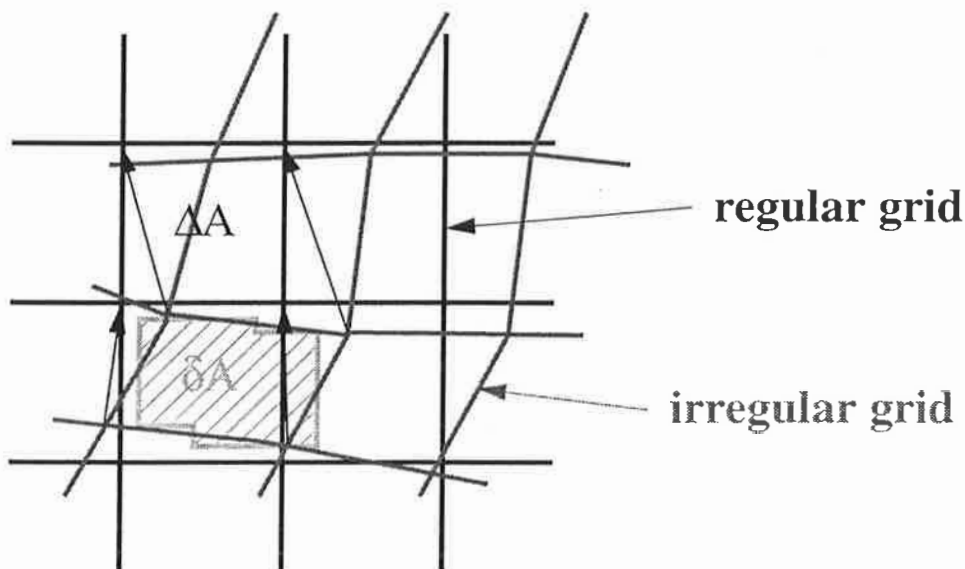


Figure 2: Illustration of the remapping procedure showing an irregular grid cell at $t-\Delta t$ which at $t+\Delta t$ ends up in a regular grid cell.

The departure cell is at first approximated by a figure with the same area but with sides parallel to the coordinate axis as indicated by hatched area in Figure 2. Then the accumulated mass from the Greenwich meridian ($\lambda=0$) to each of the sides parallel to the meridians are computed assuming parabolic (one-dimensional) variations within each (regular) grid cell in each coordinate direction. The integrated mass (5) is then determined as the sum of the accumulated masses of the western sides minus the sum of the accumulated masses of the eastern sides. Each of the accumulated masses contributing to one area $\delta A_{i,j}^-$ is contributing to a neighbor area with the reversed sign. For each regular cell both one-dimensional parabolic functions has a mean value equal to the mean value (6) of the cell.

5 Extensions to three dimensions

We turn now to three dimensions. In Machenhauer (1994) a procedure for a consistent semi-Lagrangian time extrapolation of the hydrostatic continuity equation was proposed. It was building on a tracking backward the 3D cells which were assumed to move with vertical walls. It resulted in an implicit system of coupled linear equations in surface pressure, one equation for each horizontal grid cell, which would be computational expensive to solve. We have now designed a much less expensive time extrapolation.

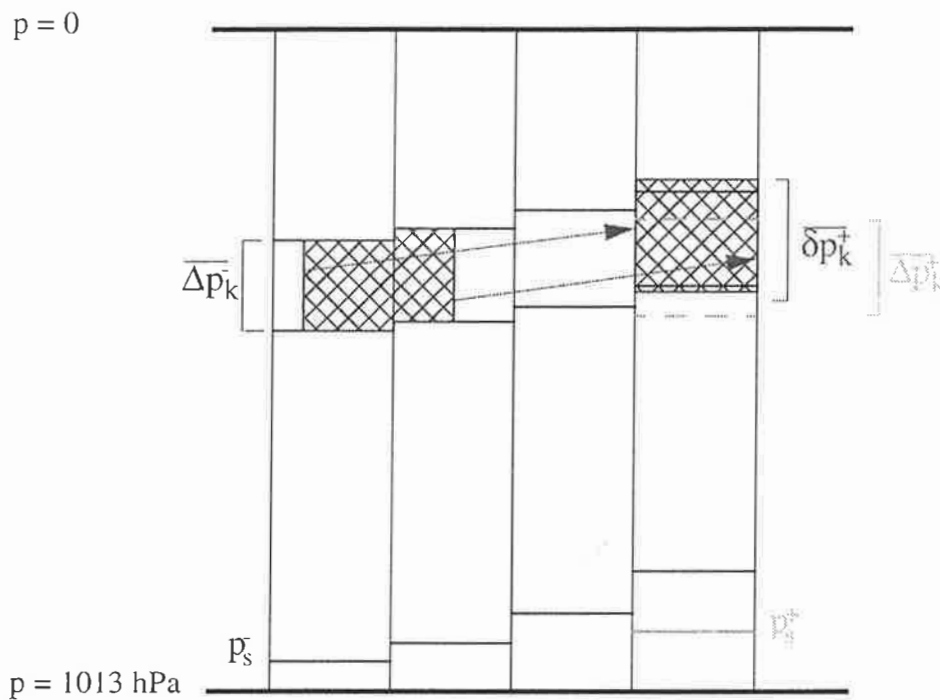


Figure 3: Illustration of new procedure used in the integration of the continuity equation.

In the old formulation the discrete form of the continuity equation were

$$\Delta p_k^+ \Delta A^+ = \overline{\delta p_k^-} \delta A_k^- \quad (7)$$

Here p is pressure and k denote the number of an arbitrary level in the hybrid sigma-pressure vertical coordinate system.

$$\Delta p_k^+ = \Delta A_k + \Delta B_k p_s^+ \quad (8)$$

The A's and B's are constants defining the levels. The new formulation is building on tracking backward only the horizontal grid cells, still assumed to move horizontally with vertical walls with the velocities at level k and time t , but extrapolating forward in time the vertical grid intervals of pressure. Thus instead of (7) the new formulation is

$$\overline{\delta p_k^+ \Delta A^+} = \overline{\Delta p_k^- \delta A_k^-} \quad (9)$$

The procedure is illustrated in Figure 3.

Summing up the pressure increments obtained at all levels then determine the surface pressure at $t+\Delta t$.

$$p_s^+ = \sum_{k=1}^{NLEV} \delta p_k^+ \quad (10)$$

The vertical pressure intervals of the grid cells at the new time level is then determined by (8). The time extrapolation of the continuity equation is the basis for the extrapolation of all the other prognostic variables which beside the horizontal remapping from the irregular to the regular grid cells at $t-\Delta t$ also require a vertical remapping at $t+\Delta t$ to the vertical pressure intervals of the grid cells determined by the continuity equation.

6 Outlook

So far the horizontal transport on the sphere of a passive scalar has been coded in the framework of the ECMWF IFS code and is being tested using monotonous parabolic functions within each cell. The preliminary results look promising and we plan to intensify the implementation of the CISL scheme for a full 3D baroclinic primitive equation system as outlined above.

References

- Bermejo, R. and A. Staniforth, 1992: The conversion of semi-Lagrangian advection schemes to quasi-monotone schemes. *Mon. Wea. Rev.*, **120**, 2622-2632.
- Gravel, S. and A. Staniforth, 1994: A Mass-Conserving Semi-Lagrangian Scheme for the Shallow-Water Equations. *Mon. Wea. Rev.*, **122**, 243-248.
- Hirt, C. W., Amsden, A. A. and J. L. Cook, 1974: An arbitrary Lagrangian-Eulerian Computing Method for all Flow Speeds. *J. Comput. Phys.*, **14**, 227-253.
- Kwizak, M. and A. J. Robert, 1971: A semi-implicit scheme for grid point atmospheric models of the primitive meteorological equations. *Mon. Wea. Rev.*, **99**, 32-36.
- Laprise, R. and A. Plante, 1995: SLIC: A semi-Lagrangian integrated-by-cell mass conserving numerical transport scheme. *Mon. Wea. Rev.*, **123**(2), 553-565.
- Machenhauer, B., 1994: A note on a Mass-, Energy- and Entrophy Conserving Semi-Lagrangian and Explicit Integration Scheme for the Primitive Meteorological Equations. MPI Workshop on Semi-Lagrangian Methods, Hamburg 8-9 Oct. 1992. MPI Report **146**, 73-102.
- Machenhauer, B. and M. Oik, 1996: On the development of a cell-integrated semi-Lagrangian shallow water model on the sphere. ECMWF Workshop on Semi-Lagrangian Methods, 6-8

- November 1995. Workshop Proceedings, 213-228.
- Machenhauer, B. and M. Olk, 1998: The implementation of the semi-implicit scheme in cell-integrated semi-Lagrangian models. The Andre J. Robert Memorial Volume. Numerical methods in Atmospheric and Oceanic Modelling (C. Lin, R. Laprise, H. Ritchie, Eds.). CMOS / NRC Research Press, Ottawa, Canada, 103-126.
- Moorthi, S., R.W. Higgins and J.R. Bates, 1994: A Global Multilevel Atmospheric Model Using a Vector Semi-Lagrangian Finite Difference Scheme. Part 2: Version with Physics. Submitted to Mon. Wea. Rev.
- Priestly, A., 1993: A quasi-conservative version of the semi-Lagrangian advection scheme. Mon. Wea. Rev., **121**, 621-629.
- Rancic, M., 1992: Semi-Lagrangian piecewise Biparabolic Scheme for Two-Dimensional Horizontal Advection of a Passive Scalar. Mon. Wea. Rev., **120**, 1394-1406.
- Robert, A., 1969: The integration of a spectral model of the atmosphere by the implicit method. Proc. of WMO/IUGG Symp. on NWP, Tokyo, Japan Meteorological Agency, VII.19-VII.24.
- Robert, A., 1981: A stable numerical integration scheme for the primitive meteorological equations. Atmos. Ocean., **19**, 35-46.
- Robert, A., 1982: A semi-Lagrangian and semi-implicit numerical integration scheme for the primitive meteorological equations. J. Meteor. Soc of Japan., **60**, 319-325.
- Smolarkiewicz, P.K., and J.A. Pudykiewicz, 1992: A Class of semi-Lagrangian Approximations for Fluids. J.Atmos.Sci., **49**, 2082-2096.
- Williamson, D. L. and J. G. Olson, 1994: Climate Simulations With a Semi-Lagrangian Version of the NCAR Community Climate Model. Mon. Wea. Rev., **122**, 1594-1610.

A Finite Difference Approximation For Convective Transports Which Maintains Positive Tracer Concentrations

Sabine BRINKOP and Robert SAUSEN

DLR, Institut für Physik der Atmosphäre, Oberpfaffenhofen, 82234 Weßling, Germany

Abstract

We have modified the mass-flux convection scheme of Tiedtke (1989) in order to ensure positive tracer concentrations during the course of a model integration. The transport equations in updraught, downdraught and the environment now take the form of an upwind scheme instead of a central-difference scheme. The model with the new numerics is tested against the standard scheme in a one-column (1-D) and a (3-D) climate model. From the 1-D results we find that for certain initial conditions the standard scheme may keep or even increase maxima in tracer concentration profiles in convective situations. The standard scheme is not able to smooth out maxima and minima in each case. All shortcomings are eliminated when the new numerical formulation is used. The model with the new numerics has been tested against the standard scheme in several 3-D climate model simulations which differ with respect to the location of the tracer source. Typical difference patterns associate with the prescribed tracer source can be noticed from the results. In the case of a strong surface source, the upward transport away from the surface tends to be reduced with the new scheme compared to the standard scheme. However, in the case of atmospheric tracer sources at an upper tropospheric level the upward transport above the source and downward below it are both enhanced. A student-t test confirms that these difference patterns are highly significant (99%).

1. Introduction

Cumulus convection is a major process in determining the temperature and moisture vertical profiles of the atmosphere through condensation and the corresponding diabatic heating. Accordingly, convective processes must be adequately represented in large-scale models of the atmosphere. In the framework of environmental tracer studies it is important to include convective tracer transports in the respective parameterizations. This has been done, in the case of the general circulation model (GCM) ECHAM, which has been developed as a sophisticated tool of climate research (Roeckner et al., 1992). Convection is parameterized by a state-of-the-art mass-flux scheme (Tiedtke, 1989). This parameterization can also be found in the weather prediction models of the German Weather Service (Cress et al., 1995) and the Forecast Model of the European Centre

of Medium Range Weather Forecasts (ECMWF). A convection scheme should guarantee non-negative concentrations. This is of particular importance for humidity and for tracer studies. Unfortunately, this constraint is not fulfilled for all possible conditions by the Tiedtke scheme. The main problem shows up in cases of convective activity connected with strong vertical tracer gradients, when more mass can be moved away from a grid box than is available. This results in a numerically modified tracer distribution that is clearly unwarranted. Apart from this basically numerical feature, subsequent physical effects like the interaction of tracers with radiation or chemistry may be expected to enhance this error dramatically. We have modified the mass-flux scheme of Tiedtke, such that tracer concentrations remain non-negative throughout a model integration.

2. Development of an Alternative Numerical Scheme

A detailed analysis of the numerics of the mass-flux scheme revealed several sources of potential negative tracer concentrations. The main source is due to the discretization of the tracer variables. In the operational versions of ECHAM a tracer concentration \overline{X}_k is defined as a prognostic variable on full levels (middle of a layer, index k). However, in the numerical scheme for the calculation of convective transports \overline{X}_k is interpolated from full levels to half levels (index $(k + \frac{1}{2})$) according to

$$X_{k+\frac{1}{2}} = \frac{1}{2} (\overline{X}_k + \overline{X}_{k+1}) \quad (1)$$

The prognostic variables temperature T and humidity q are extrapolated to the half levels according to Equation (25) of Tiedtke (1989). This deviates from the treatment of variables outside the convection routine. The modifications in the convection routine refer to tracers only. Thus, tracers are left on full levels in the new scheme (Brinkop and Sausen, 1997). In the original model the transport equations are discretized as centered-finite differences in updraught, downdraught and the environment. Now they take the form of upwind schemes. The calculation of tracer mass fluxes below cloud base also has been changed. The technical details are described in Brinkop and Sausen (1996).

3. Testing the new numerical scheme

In order to test the new numerical scheme of the mass-flux parameterization we performed a variety of numerical simulations with the ECHAM3 model (Roeckner et al., 1992) applying the (1-D) and the (3-D) version.

3.1 Mass conservation

First it was checked whether the mass conservation constraint is fulfilled during a model integration period. It can be expected that tracer mass increases during a model integration if negative tracer concentrations calculated by the convection scheme are set to zero by the semi-Lagrangian advection scheme. We run the 3-D model over 15 time steps from a critical initial tracer distribution without sources and sinks. The initial tracer

distribution is prescribed globally at 1000hPa in one layer only. By analyzing the differences between initial and final total tracer mass we found that with the new formulation the tracer mass remains constant during a model integration whereas with the standard formulation the mass increases by 12 %. As indicated by a larger number of similar simulations, the magnitude of the mass increase depends on the altitude where the initial tracer is located. Strong tracer gradients in the boundary layer seem to be most critical in generating large negative tracer concentrations and hence creating additional tracer mass.

3.2 Simulations with the one-column version

The 1-D simulations were used to study in detail how an initially prescribed tracer distribution is modified after 15 timesteps (10 hours simulated time). Only one type of convection (deep convection or shallow convection) is present throughout the simulation period. Several initial tracer distributions critical to the development of negative tracer concentrations were chosen. No sources or sinks of tracer mass were allowed. Several cases with deep or shallow convection of different strength were selected and analysed. Generally, it can be expected that during convective events sharp gradients of tracer concentration are smoothed out towards a more homogeneous distribution over the height of convection. The standard scheme, however, increases the tracer concentration gradient (Figure 1a) instead of mixing the tracer mass as it can be seen for the simulation with the modified numerics (Figure 1b). Additionally, the results of the standard scheme show negative tracer values. Some general features are evident for the final tracer profiles: The standard convection scheme is not effective in smoothing out maxima in the tracer concentration profile. Often the maxima are kept or even increased in magnitude. This is in part due to the fact that the calculated local maxima can only be seen as smoothed out by the convection scheme (Figure 2). All these difficulties are eliminated with the new numerical formulation of the tracer transport in the convection scheme.

3.3 Permanent July simulations with the 3-d climate model

In this section the results of two simulations with the ECHAM model with different sources of tracer mass are presented. The model was integrated from a balanced climate state over 26 month in perpetual July mode. Only the last 20 months were chosen for comparison between the standard and the modified model version. In experiment SL the tracer sources are prescribed at all surface points while in experiment AL they are prescribed in the free atmosphere at 326 hPa. The sources are uniformly distributed over the respective model level. The half-lifetime of tracers of 3.83 days is assumed globally, recalling the life time of a standard tracer like radon. In both the SL and the AL case a comparison of zonal mean tracer distributions simulated by the revised scheme and the original scheme reaches differences up to 10%. Both cases produce a quite characteristic difference pattern. In the SL case (Figure 3) the new scheme transports less tracer mass into the free atmosphere than the standard scheme. Instead, more tracer mass remains in the lowest model layers. The typical difference pattern for AL (Figure 4) shows a completely different structure. Here, the new scheme transports more tracer mass downwards

than the standard scheme, which is an effect of the new discretisation of tracer variables on full model levels. Additionally, more tracer mass can also be found above the source, leading to a distinct dipole structure. Applying a student t-test it can be proved that all these differences have not a random character but are statistically significant. The 99% significance level (shaded area in Figures 1 and 2) is reached for almost the whole region affected by the difference patterns just described.

4. Conclusion

We have modified the mass-flux convection scheme of Tiedtke (1989) in order to ensure positive tracer concentrations during the course of a model integration. Tracer concentrations now remain on full levels in the convection scheme as it is already discretised in the rest of the model. We do not conclude that the result of former tracer simulations with the frequently used standard scheme have been proven worthless by the results of this paper. The resulting distributions remain rather similar at all. Nevertheless, due to the significance and robustness of the difference pattern in connection with a prescribed source in the 3-d simulations it can be expected that the results of former tracer studies will significantly change. This might become very important in simulations, where the tracer interacts with other physics as for instance radiation or chemistry. Most importantly, regarding chemical species as tracers, the mass is conserved without additional correction terms. So far only the numerics of the tracer transport have been corrected. It is intended also to correct the heat and moisture transport and corresponding variables to get a consistent modification of the numerics in the convection routine.

Acknowledgment

This work was partly sponsored by BMBF.

References

- Brinkop, S., R. Sausen (1996): A modified mass-flux scheme for convection which maintains positive tracer concentrations, DLR Institut für Physik der Atmosphäre, Oberpfaffenhofen, Germany, Report No 67, 25pp, ISSN 0943-4771.
- Brinkop, S., R. Sausen (1997): A Finite Difference Approximation for Convective Transports Which Maintains Positive Tracer Concentrations. *Contr.Atmos.Phys.*, (70), 245-248.
- Cress, A., D. Majewski, R. Podzun, V. Renner (1995): Simulation of European climate with a limited area model. Part I: Observed boundary conditions, *Contr.Atmos.Phys.*, 68(2), 161-178.
- Roeckner, E., K.Arpe, L. Bengtsson, S. Brinkop, L. Dümenil, M. Esch, E. Kirk, F. Lunkeit, M. Ponater, B. Rockel, R. Sausen, U. Schlese, S. Schubert, M. Windelband (1992): Simulation of the present-day climate with the ECHAM model: Impact on model physics and resolution. Max-Planck-Institut für Meteorologie, Hamburg, Report Nr. 93.
- Tiedtke, M. (1989): A comprehensive mass-flux scheme for cumulus parameterization in large-scale models. *Mon.Wea.Rev.*, 117,1779-1800.

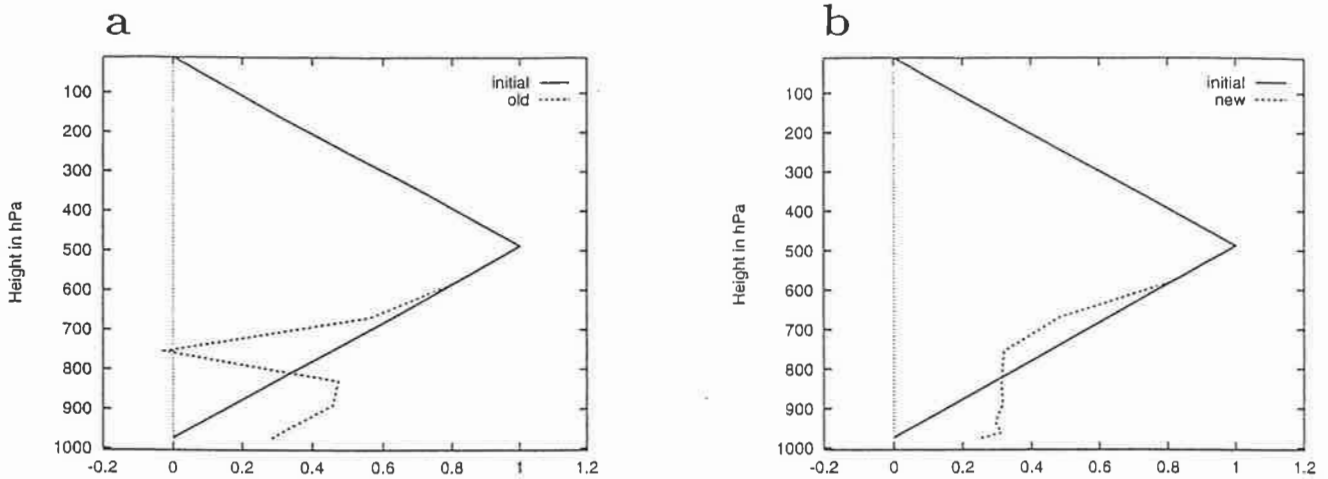


Figure 1: (a) Initial (full line) and final (dashed line) tracer concentration profile (after 10 hours) normalized with the maximum tracer concentration of the initial profile. This is a case of shallow convection simulated with the standard convection scheme. (b) As Figure 1(a) but with modified numerics.

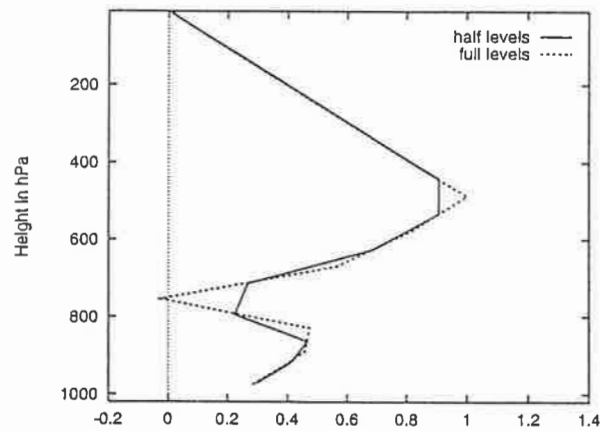
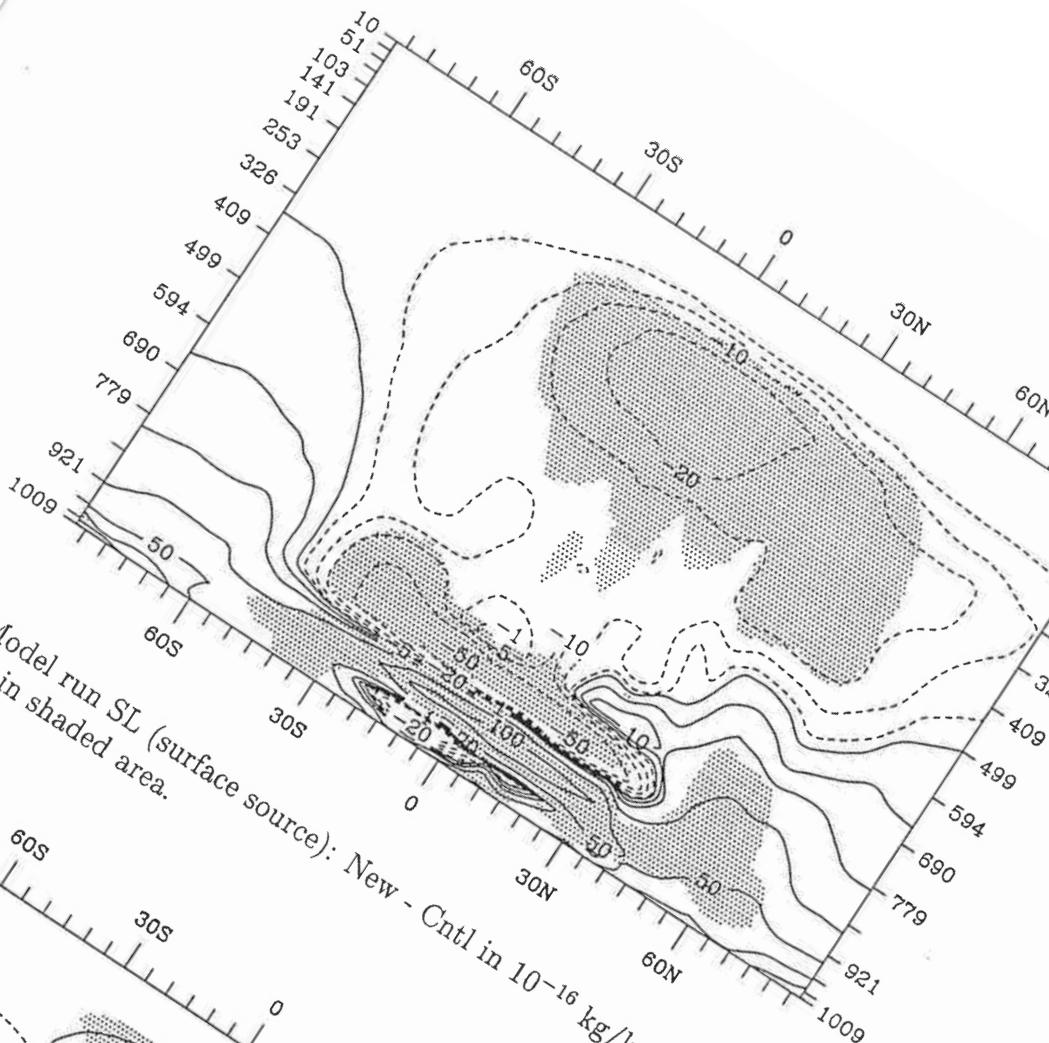
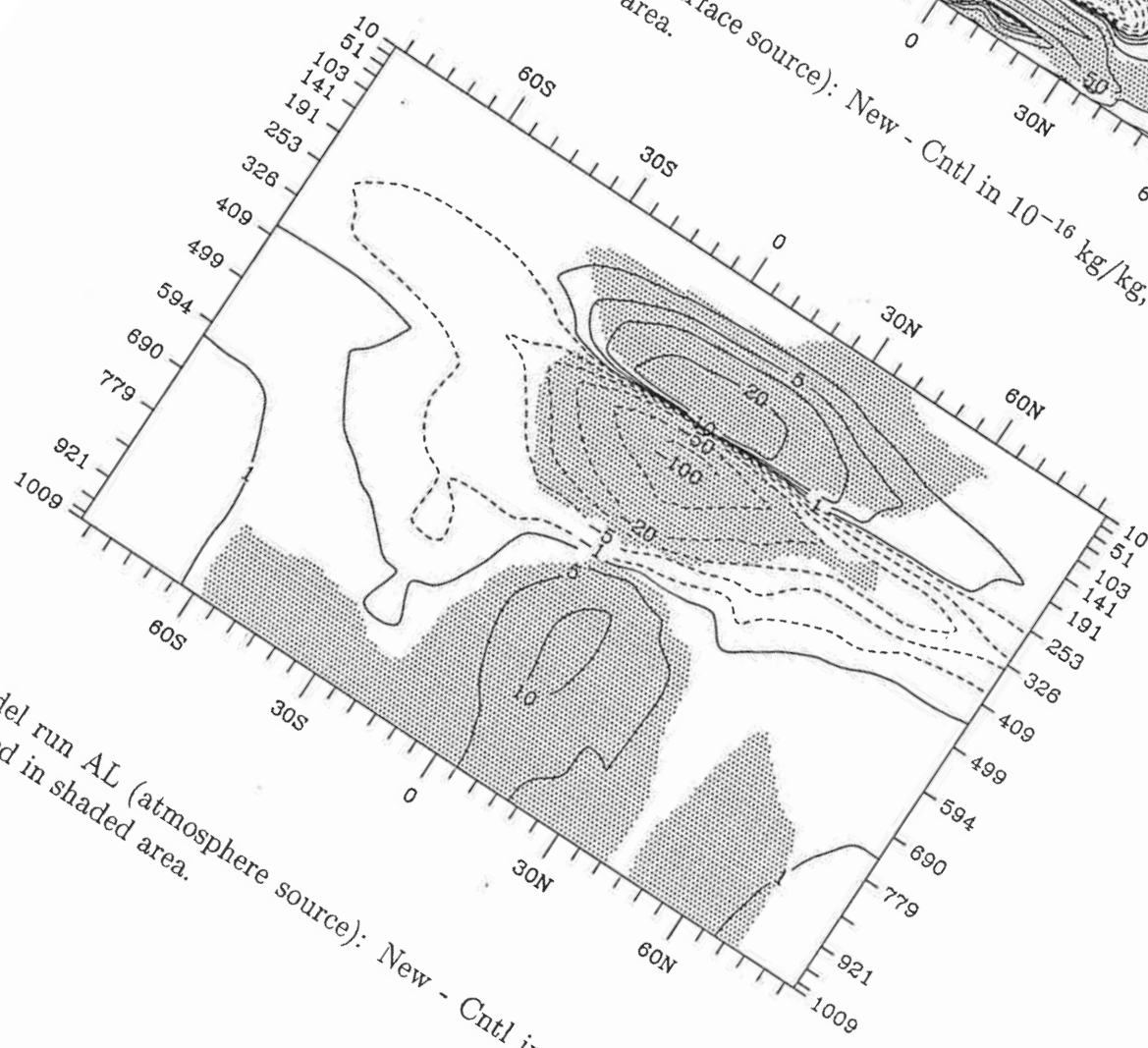


Figure 2: As Figure 1(a) but 2 final tracer concentration profiles: Full line: Tracer concentration on half levels as it is interpolated and used by the convection scheme. Dashed line: Tracer concentration on full levels as it is seen by the other routines of the model.

Figure 3: Model run SL (surface source): New - Cntl in 10^{-16} kg/kg, significance level of 99% reached in shaded area.



Model run AL (atmosphere source): New - Cntl in 10^{-12} kg/kg, significance level of 99% reached in shaded area.



Coupling of a Semi Langrangian Transport Scheme to the Berlin TSM GCM

P. Braesicke and U. Langematz

20.6.97

Introduction

The semi-Langrangian transport scheme developed by Boettcher (1996) has been coupled to the Berlin TSM GCM (Langematz and Pawson, 1997). The scheme calculates the displacement vector α using the equations:

$$\begin{aligned}
 q(\mathbf{x}, t + \Delta t) &= q(\mathbf{x} - \alpha, t) \\
 \alpha_{\frac{1}{2}} = \mathbf{x}(t + \Delta t) &- \frac{\Delta t}{2} \mathbf{v}(\mathbf{x}, t + \Delta t) \\
 &+ \frac{(\Delta t/2)^2}{2} \frac{D\mathbf{v}(\mathbf{x}, t + \Delta t)}{Dt} \\
 \alpha &= \mathbf{x}(t + \Delta t) - \mathbf{v}\left(\mathbf{x} - \alpha_{\frac{1}{2}}, t + \frac{\Delta t}{2}\right) \Delta t
 \end{aligned}$$

where q is the advected quantity and Δt is the time step for the transport calculation. The interpolations in λ , ϕ and z are performed using smoothed exponential splines. The smoothing function is derived by investigating the local curvature of the tracer field. The transport model is evaluated every n 'th time step. Figure 1 summarizes the different time scales of the model, assuming a one month integration, where the transport is calculated every six hours.

A first application

An arbitrary January integration was performed with the Berlin TSM GCM. The initialization was for 0 GMT on 1. January. The initial tracer distribution was zonally stratified, with the

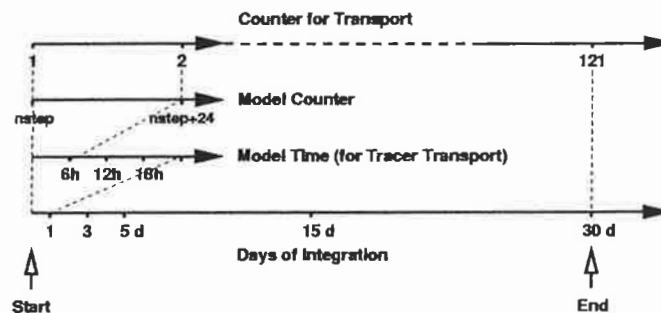


Figure 1: Summary of the different model time scales.

lowest values at the South Pole and the highest at the North Pole. Only the situation after 32 time steps (~ 8 d) will be discussed here.

Figure 2 shows a comparison between the tracer distribution and Ertel's potential vorticity (PV). On the left-hand side polar stereographic projections between 20 and 40°N at about ~ 20 km are presented. The top panel shows PV (shaded) on the 475 K isentropic surface with the 50 hPa geopotential height (isolines), the bottom panel shows the tracer distribution (shaded) near 20 km and the same geopotential height field. Comparing the PV and tracer distributions to the east of Greenwich, it is obvious that the low values of PV are in good agreement with the tongue of lower tracer concentrations; but the tongue is much more confined than the PV pattern. The right hand side of figure 2 shows latitude-altitude cross sections (with low latitudes to the right) at Greenwich, displaying wind (shaded) together with temperature (isolines) at the top and PV (shaded) together with the tracer distribution (isolines) at the bottom. There is no evidence of a corresponding disturbance in the wind and temperature fields at this location and time. But the tracer distribution displays again the confined tongue of low tracer concentrations between 20 and 25 km. The PV also shows some meridional displacement of low values to the north near 500 K. This kind of (northward) meridional displacement agrees qualitatively with some kind of observations (e.g. Danielsen et al., 1991).

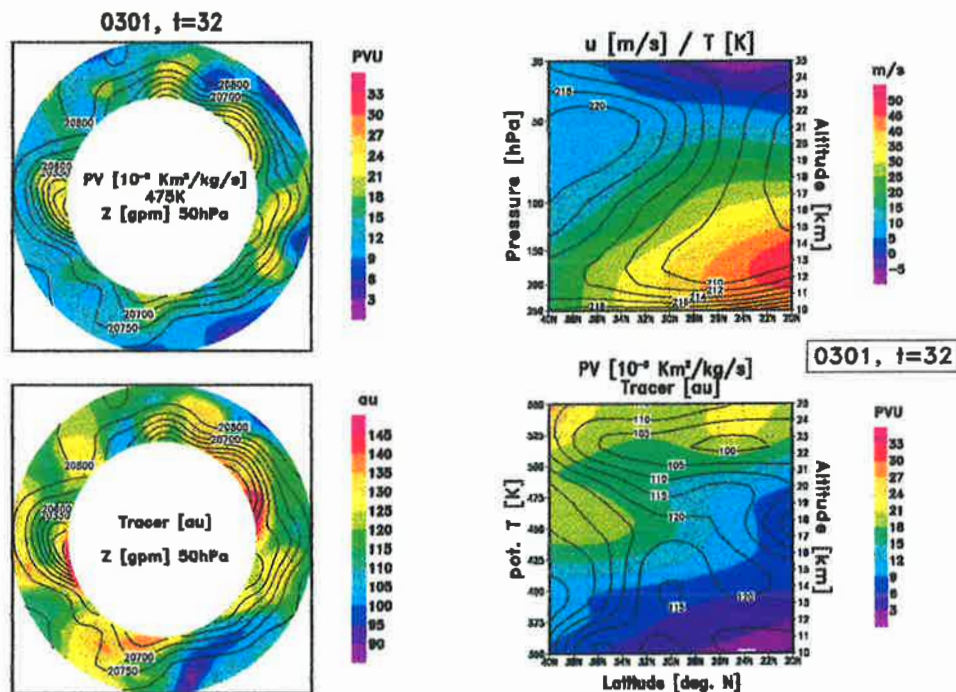


Figure 2: Left panel: Polar stereographic projections between 20 and 40°N of three meteorological quantities (Greenwich to the bottom). Top: Ertel's potential vorticity (PV, shaded) on the 475 K isentropic surface and geopotential height (isolines) at 50 hPa. Bottom: Tracer distribution (shaded) at ~ 20 km altitude and geopotential height (isolines) at 50 hPa. Right panel: Latitude altitude cross section between 20 and 40°N at Greenwich using different measures of altitude. Top: zonal wind (shaded) and temperature (isolines). Bottom: Ertel's potential vorticity (PV, shaded) and tracer distribution (isolines). The potential temperature scale refers to PV and the geometric height to the passive tracer.

Summary

Since the PV is more diffusive than the tracer transport, the meridional (northward) transport of air can be identified clearly by using a passive tracer. This assumption is only fulfilled for short time periods, where no mixing takes place. Generally the distributions of PV and tracer are in good agreement. The obtained results are qualitatively in good agreement with observations (e.g. Danielsen et al., 1991).

Literature

Boettcher, M., 1996: A semi-Lagrangian advection scheme with modified exponential splines, *Mon. Wea. Rev.*, **124**, No 4, 716-729.

Danielsen, E. F., R. S. Hipskind, W. L. Starr, J. F. Vedder, S. E. Gaines, D. Kley and K. K. Kelly, 1991: Irreversible transport in the stratosphere by internal waves of short vertical wavelength, *Journal Geophys. Res.*, **96**, 17433-17452.

Langematz, U. and S. Pawson, 1997: The Berlin Troposphere-Stratosphere-Mesosphere GCM: Climatology and forcing mechanisms, *Quart. J. Roy. Meteorol. Soc.*, **123**, 1075-1097.